Order-Disorder Phenomena in Polyelectrolyte Tissues

Thesis

ORDER-DISORDER PHENOMENA IN POLYELECTROLYTE TISSUES

Thesis submitted for the Degree of Doctor of Philosophy in the Discipline of Biophysics

By

Justyn Wiktor Regini BSc, MSc

The Open University

Oxford Research Unit

Date of submission : 8th July 1994

Date of award : 4th January 1995

JULY 1994

In memory of my grandparents,

Wiktor & Zofia Regini and Esau & Chora Anderson

ABSTRACT

Three polyelectrolyte-based tissues, muscle, cornea and lens have been investigated using microelectrode and low angle X-ray diffraction techniques. It has been found that with increasing temperature the net fixed charge in the A- and I-bands in muscle falls, in both the relaxed and rigor states. In the rigor state a definite temperature transition between 27.5 - 30 ^{0}C has been established. The sharpness of the off meridional peaks of the 365 Å actin layer line of rigor muscle increases with increasing temperature at low ionic strength. In relaxed muscle previous reports show that the myosin layer-lines disappear with decreasing temperature. We have shown that.the net charge decreases with increasing temperature, as these two phenomena occur within the same temperature range, it is probable that they are connected. All these effects are explained in terms of ion binding models.

Previous reports have shown that there is an anomalous negative temperature coefficient of Donnan swelling theory in cornea. We have shown that the net fixed charge decreases linearly with increasing temperature in corneal stroma. This is explained in terms of an ion binding model, which accounts for the negative temperature coefficient.

In calf lens no change in the measured Donnan potentials is observed below the critical temperature for the onset of the cold cataract phenomenon. This is probably due to the low concentration of the cryoprotein responsible for this effect.

Micromolar concentrations of ATP and PPi have been shown to decrease the fixed negative charge on the myosin molecule in previous work. We have shown that in muscle at zero overlap the lattice spacing and X-ray equatorial intensities are at a maximum at micromolar concentrations of PPi. This effect is interpreted in terms of a change of the electrical regime within the muscle lattice.

LIST OF CONTENTS

CHAPTER 1 INTRODUCTION

CHAPTER 2 METHODS

LIST OF FIGURES AND TABLES

ACKNOWLEDGEMENTS

I would like to thank my supervisor, Prof. Gerald Elliott for his continual guidance and support in my research. I would also like to thank Prof. Jack Lowy and Prof. Roy Worthington who have taken part in many useful discussions during the course of this work, and Dr Else Bartels for her help with the microelectrode techniquies. I must also thank Wim Bras of the Daresbury laboratory for his help with the data processing programs and general support.

I am also indebted to Mr Paul Healy of Luton University for advice with the statistical analysis and to many colleagues and staff at the Oxford research unit. These include Ted Beaver, David Sommervile, Jason Shackleton and Alan Knight for their technical assistance; and to my fellow research students for their input and interest in my work.

Finally I would like to thank my family for their continued support throughout the course of my studies in higher education, without which the completion of these studies would not have been possible.

CHAPTER 1

INTRODUCTION

1.1 POLYELECTROLYTES AND ELECTRICAL DOUBLE-LAYERS IN BIOLOGICAL SYSTEMS

The idea of the electrical double-layer was first described by Gouy, Chapman, and Debye & Huckel; this early work was reviewed by Verwey & Overbeek (1948).

A polyelectrolyte is a macromolecular compound containing many ionizable groups within the same molecule. Within the field of physical chemistry the term is usually used for soluble substances, however ion-exchage resins and fibrous proteins are considered insoluble polyelectrolytes (Sharp, 1988). In their structure biological macromolecules contain a number of amino acids with ionizable side groups (basic groups are lysine, pK 10.53, arginine, pK 12.48 and histidine, pK 6.5; acidic groups are aspartate, pK 3.86 and glutamate, pK 4.25). In solution at physiological pH (pH 7.0-7.5) many fibrous proteins therefore bear a net electrical charge. Polyelectrolytes exhibit various interesting phenomena due to their dual character as highly charged electrolytes and flexible chain molecules.

In solution polyelectrolytes are dissociated into polyvalent macroions and a large number of small ions of opposite charge (counter-ions). Verwey & Overbeek (1948) describe an electrical double-layer by saying "...each particle charge is screened off by an equivalent swarm of counter-ions surrounding the particle. Hence, if we consider one particle separately, immersed in the liquid, it is surrounded by an electrical double-layer. One layer is formed by the charge in the surface of the particles. Though in reality it is a

charge consisting of point charges, it is customary to consider it, as a first approximation, as a homogeneous surface charge spread over the surface of the particles. The second layer is formed by the oppositely-charged ions in the solution....".

In a matrix of charged macromolecules and in the absence of physical cross-links, the stability of the matrix (or lattice) is maintained by the balance between long-range attractive forces and electrostatic repulsive forces. Van der Waals forces are the long-range attractive forces. These are weak intermolecular and interatomic forces that are electrostatic in origin. If two molecules have permanent dipole moments and are in random thermal motion then some of their relative orientations cause repulsion and some attraction. On average there will be a net attraction. Thus the attractive force between two large macromolecules will be significant.

The opposite repulsive force arises simply because similarly-charged molecules repel each other, through the interaction of their oppositely oriented electrical double-layers. The extent of this repulsive force is dependant on two factors, the amount of charge on the molecules and the ionic strength of the surrounding medium.

The amount of charge on each molecule is primarily dependant on the pH of the bathing medium. A high pH gives rise to a higher negative charge as more side groups of the amino acids become ionized. The isoelectric point of any polyelectrolyte is the pH value at which the molecule becomes electrically neutral as the negative and positive charges of the amino acids are balanced. At physiological pH the surface potential on such molecules or macromolecular assemblies may be of the order of a few tens of millivolts, a magnitude which is comparable with the membrane potential of the cell.

However, as the ionic strength of the solution is increased the increasing population of ions in solution serves as a barrier to the operation of the repulsive force, reducing its effectiveness. This is known as the screening effect, which was first demonstrated experimentally by Bernal & Fankuchen (1941) in their studies of tobacco mosaic virus (TMV).

1.2 POLYELECTROLYTE TISSUES IN THIS STUDY

In this study three biological polyelectrolyte systems are investigated, striated skeletal muscle, bovine corneal stroma and calf lens

1.2.1 MUSCLE

Striated skeletal muscle consists of groups of muscle fibres, which in turn are comprised of bundles of myofibrils. Each myofibril is comprised mainly of the contractile proteins myosin and actin. There are also a number of structural or other proteins which include the C-protein, and the regulatory proteins tropomyosin and three troponins C, I and T. The myofibrils contain sets of thick and thin filaments. The thick filaments are comprised mainly of myosin and the thin filaments mainly of actin, both of which are arranged in a highly ordered lattice which is the basis of the fundamental repeat unit, the sarcomere (Figure 1.1)

A myosin molecule has two globular heads with an average diameter or 90 Å and a flexible tail about 1500 Å (Slater & Lowey, 1967); it has a molecular weight of about 478, 000 daltons (D) (Harrington 1979). The enzyme papain cleaves myosin into two head sections, called subfragment 1 or S1, each with a molecular weight of about 115 kD, and a tail section called myosin rod, with a molecular weight of about 220 kD. The enzyme trypsin splits the molecule at a different site, the hinge region part way down the tail, this yields two fragments, heavy meromyosim (HMM) which includes the two S1 heads, and light meromyosim (LMM).

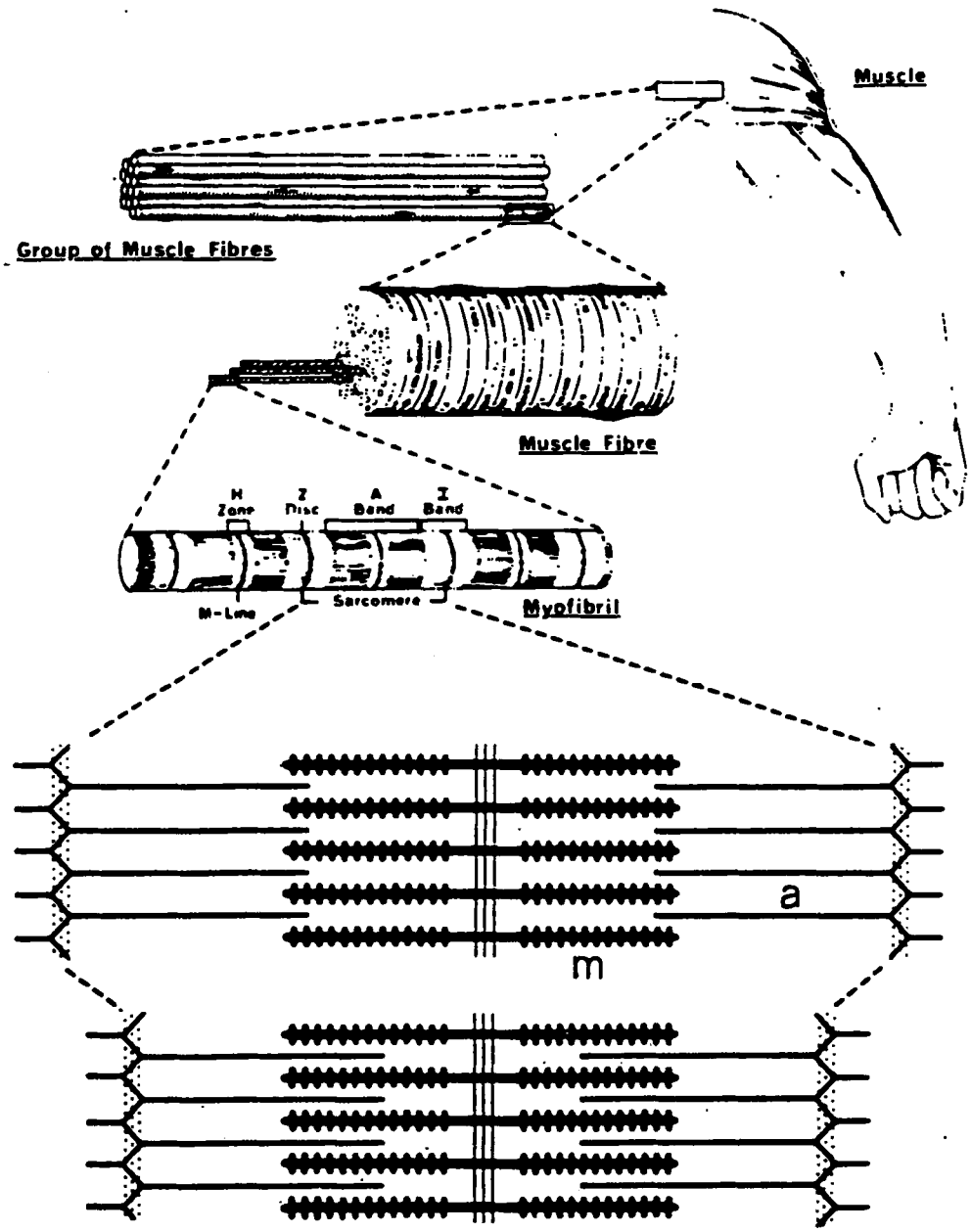

Figure 1.1 Summary of the structure of skeletal muscle. a = actin based thin filaments, m = myosin based thick filaments. (After Bloom & Fawcett, 1975)

Actin is a polypeptide chain in a globular conformation (G-actin). In physiological salt conditions, it associates into filaments (F-actin) (Asakura et al. , 1963). In the thin filament F-actin is complexed with the regulatory proteins tropomyosin and the troponins.

It is believed that shortening is produced by the two sets of filaments sliding past each other. The sliding filament model was first suggested by two groups of workers at the same time back in the 1950's (Huxley & Niedergerke, 1954, and Huxley & Hanson, 1954) The model is extensively reviewed in the literature, for a good example see the monograph of Bagshaw (1993), and will not be considered here. However, the actual physicochemical mechanism by which tension is generated is as yet unknown. In the field of muscle physiology the electrical regime within the muscle lattice is often overlooked and models based on the electrical properties of the contractile proteins have not been widely accepted.

From X-ray diffraction studies of the equatorial patterns of glycerinated rabbit muscle, Rome (1967) showed that the interfilament spacing varied as a function of both pH and ionic strength. Thus the whole muscle lattice was able to shrink or swell as the amount of fixed charge on the proteins was varied. From these findings she inferred that there must be electrical repulsive forces between the filaments. Millman & Irving (1988) showed that the muscle lattice could be compressed osmotically by the use of large polymers which did not penetrate the muscle lattice, they interpret their results using electrical double-layer theory (a more detailed discussion of Millman & Irving, 1988, is given in section 4.4.1).

The above examples of studies of the operation of electrical forces in muscle are isolated investigations, and all depend on indirect measurements of charge characteristics, or on estimates of charge derived from other observed parameters. A contributing factor to the neglect of the muscle protein charge characteristics, compared to the mass of data of muscle biochemistry and protein structure, is probably due the difficulty of making direct measurements of protein charge under given conditions.

Shortly after Rome's work on muscle filaments, Collins and Edwards (1971)

developed a method of measuring Donnan potentials using microelectrodes. The development of this technique allowed Naylor (1977) and Naylor et al. (1985) to advance Rome's work. More recently, a mechanism was developed by Bartels & Elliott (1985) which facilitated the accurate microelectrode impalement of the A- and I-bands of muscle fibres, separately, allowing direct measurement of the charge in each. A detailed account of the findings of Bartels & Elliott is given in sections 3.1.2 and 4.2.

From X-ray diffraction studies it has been observed that the muscle lattice becomes disordered when the muscle goes either into contraction or the rigor state. The meridional pattern shows that myosin layer-lines, which are believed to be due to the helical order of the S1 myosin heads around the filament backbone, disappear. Clearly, order-disorder transitions are important when considering models of muscle contraction. It has been shown that it is possible to induce such disordering by a variety of methods. Wray (1987) and Lowy et al. (1991) observed that the visibility of the myosin layer lines decreased with decreasing temperature in relaxed muscle. Yagi (1992) reported that on addition of the chemical reagent N-ethlymalimide (NEM) the visibility of the myosin layer-lines also decreased. More detailed description and discussion of these temperature and chemically-induced disorder transitions are given in sections 4.2.2 and 4.3.

1.2.2 CORNEA

The cornea is the main refracting structure of the eye and is a transparent, avascular and membranous tissue. Most of the focussing in the eyeball takes place at the corneal surface. Cornea consists of five layers, which lie parallel to the surface of the cornea. Figure 1.2 shows these layers which from top to bottom are as follows.

The epithelium, which comprises about 10% of the thickness of the cornea and is made up of a number of different types of cells. These are a single layer of basal cells which are attached to the basement membrane by hemidesmosomes. Above these lie three layers of winged cells, then two layers of surface cells.

Bowman's layer is an acellular layer composed of collagen and contributes to 2% of the thickness of the cornea. Its role is to ensure that swelling occurs in a posterior direction by restraining the cornea anteriorly. It is able to achieve this as it is highly resistant to mechanical deformation (Buckley, 1987).

The stroma, which is that part of the cornea of interest to this study, makes up 85% of the thickness of the cornea and is composed of lamellae parallel to the surface of the cornea. There are about 200 of these lamellae, each of which is comprised of collagen fibrils alined in the same direction along the lamella. The fibrils are of uniform diameter and regular spacing. The fibrils of adjacent stromal lamellae are oriented at large angles to each other. The fibrils are embedded in a matrix which consists mainly of proteoglycans. Glycosaminoglycans are long, unbranched polysaccharide chains composed of repeating disaccharide units. One of the two sugar residues in the repeating disaccharide is always an amino sugar (N-acetylglucosamine or N-acetylgalactosamine). Proteoglycan molecules consist of a protein core to which glycosaminoglycans are covalently linked. When dry, 90 to 95% by weight of the cornea is attributed to type 1 collagen, the rest of the dry weight is due to glycosaminoglycans and proteoglycans .The stroma is populated by keratocytes which are involved in proteoglycan synthesis and secondary collagen fibrillogenesis.

Descemet's membrane represents 3% of the thickness of the cornea and is located between the endothelial cells and the stroma. The membrane is composed of type iv and viii collagen.

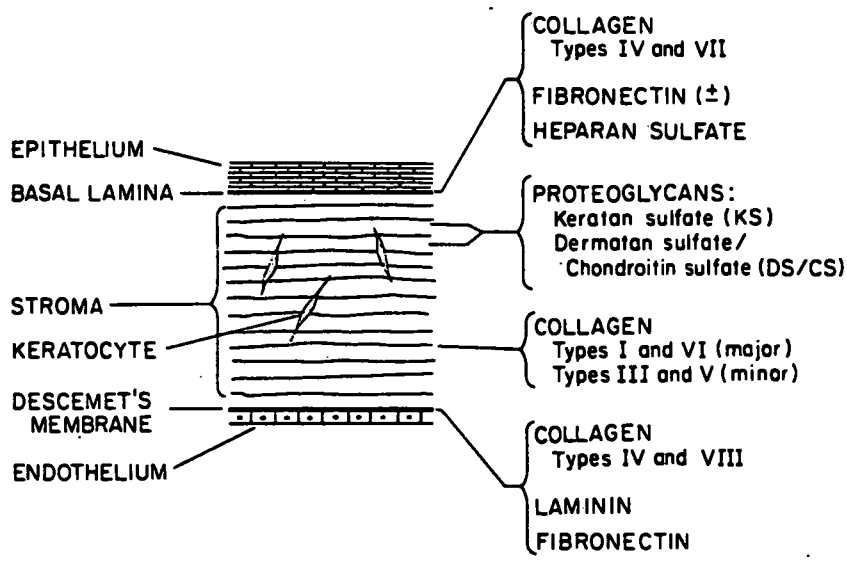

Figure 1.2 The structure of the cornea (After Berman, 1991)

The endothelium is a single layer of hexagonally shaped cells below the Desemet's membrane. Its function is to maintain corneal hydration and transparency by pumping ions and fluid out of the stroma.

A striking phenomenon of the corneal stroma is its ability to swell to many times its original weight when the cellular layers lining the cornea are scraped in vivo and also when placed in aqueous solution in vitro. This swelling clearly involves a disordering effect. The origin of the diving force for swelling, the swelling pressure, has been the subject of much debate over the years. Unlike the field of muscle research electrical models to account for the swelling pressure have gained acceptance. The early work of Elliott (1968) and Hodson (1971) proposed that the swelling pressure could be explained in terms of electrical double-layer and Donnan-osmotic theory. Evidence for this was reported in a comprehensive study by Elliott et al. (1980) who found that increasing the pH of the bathing medium, and thus increasing the fixed charge of the stromal matrix, resulted in an increase both in the rate of swelling and the hydration reached in a given time. They also found a general decrease in swelling with increasing ionic strength, which was explained in terms of the screening effect (section 1.2.1). An objection to the Donnan-osmotic model for the swelling pressure came from Hara & Maurice (1972). Donnan swelling theory predicts that the temperature coefficient of pressure change $\alpha'_p = (\Delta P/P)/\Delta T$ is positive. The authors found that the swelling pressure fell if the temperature was raised from 22 to 37 ^{0}C and was observed to rise when the temperature was reduced from 22 to 3 ^{0}C. Hara & Maurice (1972) argued that the swelling pressure could not be interpreted in terms of Donnan theory alone as α'_p from their observation would be anomalously negative. Further discussion on models of cornea structure and swelling pressure are given in sections 4.2 and 4.2.3.

1.2.3 LENS

The crystalline lens, with its unusually high concentration of proteins, called crystallins, and unique arrangement of structural fibres, provides the large index of refraction and the ability to change shape necessary in the process of accommodation, to focus images on the retina. The fibres are cells that lack nuclei, mitochondria and other organelles that might compromise lens transparency. Figure 1.3 shows a schematic diagram of a mammalian lens. The lens is an avascular transparent tissue enveloped in a membrane called the lens capsule. It is comprised of two types of cell; epithelial cells on the anterior surface underlying the capsule, and fibre cells that make up the rest of the lens and comprise the major component of the tissue. Starting in the embryo and continuing throughout life, the epithelial cells undergo mitosis at the equator and differentiate into elongated fibre cells. This process is characterised by a large accumulation of soluble crystallins, lipids, and other components for insertion into the rapidly elongating fibre cell plasma membrane. The mature fibre cell consists of two major components, the structural soluble and insoluble crystallins and cytoskeletal components (Berman, 1991).

New fibre cells are laid down as concentric layers on previously formed embryonic fibres. As a result , the nucleus contains the oldest cells, and the cortex the newest ones. There is little or no turnover of protein in the lens nucleus, most if not all of the protein synthesis occurs in the epithelium and in developing fibre cells in the peripheral cortex (Berman, 1991).

Mammalian lenses contain primarily three groups of crystallins which are; α-crystallins 700-1,200 kD, β-crystallins 50-300 kD and γ(i-iv)-crystallins 20 kD (Siezen et al., 1985). Their relative proportions vary with age and location within the lens as a result of both differential synthesis during development and selective degradation and

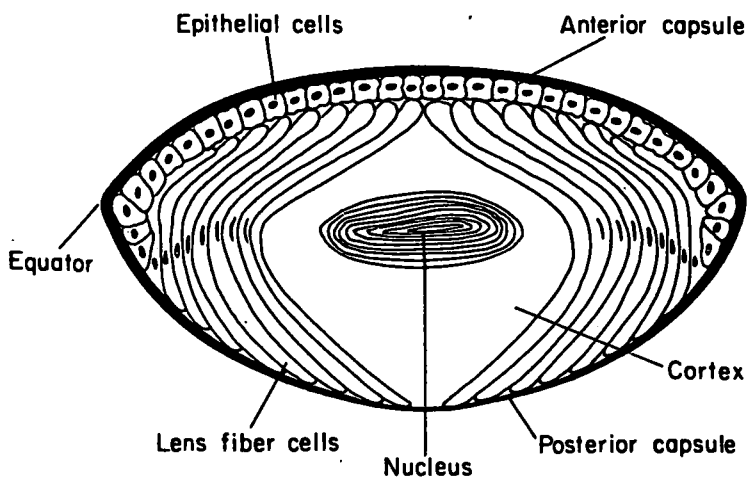

Figure 1.3 The structure of the mammalian lens (After Berman, 1991)

insolubilization with aging (Papaconstantiou, 1965, Slingsby & Croft, 1973, and Slingsby & Miller, 1983). The nucleus of the lens is highly enriched in γ-crystallins, with are monomeric, basic proteins with many charged sulfhydryl groups (Bjork, 1970).

In most young mammalian lenses the cold cataract phenomenon is observed. A temperature dependent reversible opacification can be induced in the nucleus of these immature lenses. This temperature disordering effect has been modelled as a reversible phase-separation phenomenon by workers such as Clark & Benedek (1980), Clark et al. (1982) and Benedek et. al (1979). As the temperature is decreased below the point at which the cataract appears (T_{cat}), the cytoplasm separates into protein-rich and protein-poor domains. The spatial variations in the refractive index associated with these domains scatter incident light very effectively, thus producing opacification.

1.3 AIMS OF THIS STUDY

The aim of this study is to try and identify those physical parameters which characterise order-disorder transitions in the three polyelectrolyte systems of muscle, cornea and lens, using microelectrode and X-ray diffraction techniques. In particular, the objective of this investigation is to try and see if such disorder transitions occur due to changes in the net fixed electrical charge on the constituent proteins of these tissues.

In the field of physical chemistry, in which non-biological polyelectrolytes are often studied, it has long been known that polyelectrolytes are able to convert chemical energy into mechanical work. In his monograph on polyelectrolytes Oosawa (1971) says "...Biological systems such as muscle, membranes, and protoplasm in general may be regarded as organized polyelectrolytes. Some of their properties can be understood from this standpoint.....The theory of polyelectrolytes must be extended in this direction.". Elliott et al. (1985) expand on this by saying " A direct physical approach to any working mechanism of microscopic dimensions should include 1) the distribution of matter, and importantly 2) the distribution of electrical charge. Some understanding of these two distributions would provide an essential step in defining a working mechanism in physical terms. While the experimental paradigm in the biological sciences usually includes substantial effort to define the distribution of matter in systems which may have been simplified, in solution for example, the distribution of electrical charge is often overlooked or ignored in kinetic schemes, largely because of the technical difficulties in obtaining a reliable index of charge patterns at high spatial and temporal resolution. Even in contracting muscle, where finite changes in the distribution of contractile material occur on a measurable time scale, very little effort has been made to analyse the mechanism in the physical terms of charge density and distribution".

CHAPTER 2

METHODS

2.1 SPECIMEN PREPARATION

2.1.1 GLYCERINATED RABBIT MUSCLE

Experiments were carried out on the psoas muscle of New Zealand white rabbits. The rabbits were usually killed by injection of barbiturates at Oxford University Park Farm, and the muscles were dissected about 15 minutes after death. Some rabbit muscle was dissected and stretched immediately after death at Oxford University Physiology Department in order to obtain long sarcomeres. Fibre bundles, 2- 3 mm in diameter and as long as possible (50 - 70 mm), were dissected from the main portion of the psoas and tied at each end to a perspex rod. The length of the muscle in the body when the rabbit was laid on its back with its hind legs stretched was taken as the " rest length " of this muscle (Hanson & Huxley, 1955 ; Elliott , Lowy & Worthington, 1963). Several fibre bundles at " rest length " were obtained in this way. Some bundles were allowed to shorten and others stretched before tying to the perspex rods, thus giving a range of sarcomere lengths (s) from 2.0 μm to 3.7 μm.

Two methods of glycerination were used. The first method was similar to that described by Szent-Gyorgyi (1951). The fibre bundles were immersed in the glycerol solution (Table 2.1) immediately after dissection and stored for 24 hours at 0 ^{0}C, changing the solution every 8 hours. The muscle was then placed in the freezer at -20 ^{0}C and stored for at least 3 weeks before use. Preparations not used within six months were discarded.

The second method of glycerol extraction was similar to that of Rome (1972). To ensure the rapid breakdown of the membranes and extraction of the internal cellular constituents, the fibre bundles, immediately after dissection, were osmotically shocked by alternating them at 0 ^{0}C between the glycerol solution and the standard salt solution (Table 2.1) for a period of 3 hours, 0.5 hour being spent in each solution. Following a period of 24 hours in glycerol at 0 ^{0}C the preparations were placed in fresh glycerol solution and stored at -20 ^{0}C until required. The advantage with these preparations is that they are able to be used within 2 days of excision from the rabbit.

	KCl (mM)	$MgCl_2$ (mM)	EGTA (mM)	Buffer (mM)
Standard salt solution	100	1		Phosphate 10
50% Glycerol solution by volume + (50% Glycerol) by volume	100	2	4	Phosphate 10

Table 2.1 Solutions used for glycerination. All solutions adjusted to pH 7.0 with KOH

2.1.2 CHEMICALLY SKINNED FROG MUSCLE

Frogs (*Rana Temporia*) were obtained (Blades Biological Ltd., Surrey, England) and killed by decapitation and pithing, after stunning. The method of dissection and preparation solutions used were similar to those of Yagi (1992). The sartorius muscle of the frog was dissected whole with a small piece of bone attached to the distal end, threads

were tied to the tendon and the bone. The muscles were then placed in a relaxing solution with a high ATP concentration (Table 2.1) for 5 minutes (the high ATP concentration was used to ensure relaxation of the whole muscle, after Yagi, 1992). The preparations were then placed in the skinning solution (Table 2.1). After 1 hour the solution was changed for a relaxing solution without the saponin, in which the preparations were washed for 30 minutes. The muscles were then transferred directly to the experimental solutions.

	KCl (mM)	$MgCl_2$ (mM)	EGTA (mM)	Na_2ATP (mM)	Buffer (mM)	Saponin
Relaxing solution	140	1	3	10	10 Immidazole	
Skinning solution	140	1	3	10	10 Immidazole	50 $\mu g\ ml^{-1}$

Table 2.2 Solutions used for chemical skinning. All solutions adjusted to pH 7.0 with KOH

2.1.3. BOVINE CORNEA

Adult bovine eyes were obtained immediately after death from a local abattoir (Reading, England) and stored at -20 ^{0}C until needed. The dissection methods were similar to that of Goodfellow (1975), corneas were dissected from the whole eyes whilst still frozen, all sclera was carefully removed from the edges On thawing the anterior and posterior surfaces of the cornea were scraped with a scalpel to remove the epithelium and endothelium. The stroma was then cut into six evenly sized strips thus exposing the lamellae. The strips were then glycerinated following the methods of Szent-Gyorgyi (1951) and stored at -20 ^{0}C for a period of up to six months (See section 2.1.1).

2.1.4. CALF LENS

Frozen "still born" calves eyes were obtained from a different abbatoir (Newman Slaughterers Ltd., Buckingham, England), and were stored at -20 ^{0}C until needed, for a period of up to one month. The eyes were enucllated whilst still frozen and the lenses were removed via the posterior approach. A slice 4 mm wide (2 mm either side of the posterior - anterior pole) was taken from the lens using razor blades. The slice was further cut in half in order to expose the area of tissue where the perinuclear region of opacity occurs during the cold cataract phenomenon. The preparations were then immediately placed in the experimental solutions.

The lenses were not subjected to the glycerination process, because Benedek et al. (1979) found that a 50% glycerol solution lowered the temperature at which the cold cataract appears (T_{cat}) by 30 ^{0}C, thus bringing T_{cat} down to well below freezing and making microelectrode experiments at that temperature impossible.

2.2 EXPERIMENTAL SET UP

2.2.1. LIGHT DIFFRACTION

The sarcomere lengths of the muscle preparations were measured using light diffraction from a He/Ne gas laser (N. E. C. Corp. Japan), as described by Naylor et al. (1985). This laser emits photons at a wavelength $\lambda = 0.632$ μm, which is of the same order of magnitude as the sarcomere length repeat.

The power output of the laser is 5 milliwatts and the beam diameter is approximately 1.5 mm. The pattern was measured directly on a screen, as it was not found to be necessary to record it on photographic film. The specimen to screen distance (SSD) was fixed at 50 cm and the distance (δ) in cm between the two first order diffraction maxima measured. The sarcomere length (S) in μm was then detemined from a calibration chart which makes use of the equation

$$S. \sin \theta = n\lambda$$

where θ is the angle between the first order maxima and the direct beam. It was found that δ could be measured to an accuracy of $\pm$ 0.5 cm and thus the sarcomere length was determined to an accuracy of $\pm$ 0.1 μm.

2.2.2. MICROELECTRODE EXPERIMENTAL CHAMBERS

The microelectrode experimental chambers are similar to those described by Bartels et al. (1993). All potential measurements were performed in a petri dish, the bottom of which was filled to a depth of 2-4 mm with a silicone casting resin (Slygard-184 [silicone]; Dow Corning Chemical Co., Midland, MI). The resin is biologically inert and has a consistency of a firm jelly when it solidifies. A small trench (3-4 mm wide and 30-40 mm long) was cut in the resin. For the muscle experiments a small bundle of fibres (5-10) was stretched between the sides and clamped by pushing its ends into cuts made with a razor blade perpendicular to the trench. In all microelectrode experiments involving muscle fibres the sarcomere lengths were kept constant in the range 2.5 - 3.1 μm. Although Bartels & Elliott (1985) report that the measured potentials are independent of sarcomere length, shorter sarcomere lengths were preferred as the A-bands are more visable under high power light microscopy. For the cornea and lens preparations small grooves perpendicular to the main trench were cut to keep the samples in place without damage. In all cases, in order to ensure that casting resin did not exert any physical effect upon the experimental system, all potential measurements were made at the centre of the main trench, at least 1.5 mm from the casting resin.

To control the temperature of the bathing medium, and hence the temperature of the tissue under investigation, a heat exchanger was used. This consisted of two stainless steel tubes 5 mm in diameter, coiled to fit the internal diameter of the petri dishes. The heat exchanger was attached to a Grant (FH15/FC25) water bath flow heater-cooler system (Grant instruments Ltd., Cambridge, England). The temperature of the specimens was determined by using a calibrated Cr/Al thermocouple thermometer (Comark electronics Ltd., Littlehampton, England), with an accuracy of $\pm$ 0.1 ^{0}C.

2.2.3. MICROELECTRODE MEASUREMENTS OF DONNAN POTENTIALS AND PROTEIN CHARGE

The resting membrane potential and action potential of cells has been able to be detected using intracellular microelectrodes with tip diameters ≤ 1 μm as first described by Ling and Gerard (1949). The measurement of a potential difference on impalement of muscle fibres (in which the membrane had been removed) with microelectrodes was reported by many workers in the 1960s and 1970s ; Nayler & Merrilees (1964), Weiss, Lazzara & Hoffman (1967), Colins & Edwards (1971), and Pemrick & Edwards (1974). A similar potential was also observed in extracellular corneal stroma by Goodfellow (1975). These potentials are Donnan potentials due to the fixed electrical charges on the proteins (Collins and Edwards, 1971; Elliott, 1973) and are related to the membrane potential in the case of an intact cell.

Microelectrode techniques described by Naylor (1977) were used to measure the Donnan potentials of the polyelectrolyte tissue under investigation. The microelectrodes were produced by pulling borosilicate glass capillary tubes (Clark Electromedical Instruments, Reading, England) with and inner fibre and an external diameter of 1.5 mm, such electrodes have the advantage that they posses a low surface charge density. The microelectodes were filled with 3 M KCl by capillary action with a syringe, care was taken to avoid air bubbles as they were found to block the flow of the KCl and give anomalous readings. The microelectrode puller was set to give electrodes with typical resistances of 14-25 Ω, which implies that the tip diameters were between 0.1-0.2 μm. The circuit used was the same as that described by Naylor (1978). The microelectrodes were connected to a high impedance direct current amplifier (10^{14} Ω) via a holder with a silver-silver chloride junction (model EH-1S; Transdyne General Corp., Ann Arbor, U.S.A.), which was also filled with 3 M KCl. The output of the amplifier was displayed on a suitable calibrated meter. A 3 M KCl filled calomel reference electrode (Radiometer, Copenhagen, Denmark)

completed the circuit, and a variable millivolt source was available on the low impedance side for calibration before a set of readings was taken.

As well as the phase potential between the tissue and the bathing medium, the amplifier will record two liquid junction potentials, one at the calomel electrode and one at the microelectrode. These do not change during impalement and were simply "backed-off", the back-off potential was normally found to be 32 $\pm$ 0.5 mV. In addition to the liquid junction potentials, the tip of a microelectrode may produce a "tip potential" (Adrian, 1956) which may be $\pm$ 10 mV. This is caused by surface charges on the glass walls of the microelectrodes which may give rise to to an electrical double layer of significant size, compared to the tip size of the electrode (Schanne et al., 1968; Okada and Inonye, 1975). Great care was taken, and the tip potentials were regularly measured by comparison with a broken and blunt microelectrode. Any microelectrodes found to have a tip potential > $\pm$ 1 mV were discarded.

The circuit also contained a resistance meter, which was used to monitor the resistance of the microelectrodes during impalement. Naylor et al. (1985) found that by monitoring the tip resistance it is possible to avoid situations where a large change in resistance occurs due to a partial blockage with a corresponding change in the tip potential, thus giving artifactually high readings. Readings where the resistance varied by >10% were not recorded. It was also found that artifactually high readings occurred on some impalements where the resistance change was <10% due to a mechanical deformation of the microelectrode (e.g. a slight bending of the electrode). In order to avoid this artifact (and in the case of muscle to be able to observe whether the microelectrode was inserted into either the A- or I-bands) high powered light microscopy was used. The experimental chamber was placed on the stage of an inverted microscope (model 405; Carl Zeiss, Inc., New York, U. S. A.), with an overall magnification 400 times. Using both phase contrast and polarization contrast, it was possible to see the position of the microelectrode tip in the A- and I-bands of slightly stretched muscle fibres.

The microelectrodes and the silver-silver chloride junction holder were attached to a three dimensional micromanipulator (model PM-10; LIST-electronic, Darmstadt, Germany), which was mounted onto the side of the stage of the microscope. The micromanipulator allowed the tip of a microelectrode to be placed at a precise point with an accuracy of $\pm$ 0.5 μm. The step motor function allowed the depth of impalement to be determined precisely, this is important as the electrode needs to be far enough inside the tissue so that edge effects on the potential and ion distribution are minimised. Typical impalements without mechanical deformation were 10 μm. In the case of muscle this means that the tip of the microelectrode is several hundred unit cells from the edge of the specimen, given that the unit cell in the filament lattice is of the order of 0.04 μm. The precision of the micromanipulator made it possible to remove mechanically any remnant membrane and sarcoplasmic reticulm (SR) of the chemically skinned frog muscle with the tip of the microelectrode. As the tip of the electrode was removed from the fibre on the first impalement it was possible to see the remnant material attached to the tip, by then traversing the microelectrode parallel to the fibre the material became detached. This was done, as Bartels & Elliott (1985) found that with chemically skinned muscle the SR became negatively charged in the presence of ATP, giving artifactual readings when compared with glycerinated muscle.

2.2.4. X-RAY DIFFRACTION CELLS

The cells and heat exchanger used for low angle X-ray diffraction studies of muscle are shown in Figure 2.1. The specimen was tied with thread on to the central specimen holder, two specimen holders were constructed so that the muscle fibres could be either placed horizontally or vertically in the X-ray beam. The windows were made of mylar, which has a low mass absorption coefficient. In order to reduce the path length of the X-ray beam through the bathing solution, the windows were adjusted to a distance of 1 mm apart. The cell was made water tight with a rubber seal. A small hole was drilled in the top of the cells so that the thermocouple wire of the thermometer could be placed in the bathing solution in order to record its temperature during the experiment.The heat exchanger was connected to the same heater-cooler system described above (section 2.2.2).

2.2.5. X-RAY DIFFRACTION EXPERIMENTS

Most of the X-ray diffraction experiments were conducted at the Science and Engineering Research Council (SERC) high intensity synchrotron radiation source at Daresbury, U.K. An Elliott-automation rotating anode GX 13 laboratory X-ray set was also used in the Oxford labaratory for some experiments.

At the Daresbury synchrotron, electrons are accelerated to 2 GeV by a linear tandem Van de Graaff generator and injected into the synchrotron ring, a quasi-circular 100m orbit in which the relativistic electrons are constrained by a magnetic field. As the electron beam is bent by the magnetic fields holding the electron beam, parasitic synchrotron radiation (which is a continuous spectrum from x-rays to the infra-red regions) is emitted tangentially to the ring. The emitted synchrotron radiation is then collected along beam lines and filtered to the required wavelength by the use of various optical components (eg. mirrors, gratings, monochromators etc.), to give a high intensity focussed beam of a specific wavelength.

The camera set up is simlilar to that described by Bras et al. (1993) and is situated on beam line station 8.2. The wavelength used in the experiments described here was 1.54 Å and the camera length was 3 m. The X-ray diffraction patterns were recorded using a detector (a position sensitive high pressure multi-wire proportional counter) and stored on computer.

The laboratory X-ray set consists of a rotating copper anode which is bombarded by electrons emitted from a filament in the cathode. The characteristic copper Kα X-rays produced had a wavelength of 1.54 Å, and the maximum beam power used was 2.4 Kw. The X-ray diffraction patterns were obtained using both a Franks camera (Franks, 1955) modified by Elliott and Worthington (1963), and a Huxley-Holmes mirror monochromator camera. In all experiments the cameras were aligned to give a vertical line. The specimen to film distances were 27.2 cm and 38.4 cm respectively. All the patterns were recorded on photographic film.

In both cases muscle fibers were either mounted verticaly or horizontaly in the beam, depending on whether the equatorial or meridional reflections were being studied.

2.2.6. X-RAY DIFFRACTION MEASUREMENTS AND CALIBRATIONS

All the calibrations and measurements at the synchrotron were conducted using the Daresbury BSL computer program package, these automatically take into account the decay in the intensity of the beam over time. In order to eliminate the problem of electronic noise in the detector a calibration was carried out by placing a small radioactive beta source at a distance of 0.5m away from the detector for 4 hours. The resulting response of the detector was subtracted from all subsequent patterns. Another source of possible artifacts may arise from diffraction reflections from the mylar windows and the bathing medium. A pattern of experimental cell containing a solution was taken and was also subtracted from all subsequent patterns. The horizontal and vertical positional response of the detector was also calibrated using wet collagen (rat tail tendon). Measurements between diffraction maxima could then be calculated against the known distances between the diffraction maxima of wet collagen, whch has a spacing of 67 nm.

Wet collagen was also used for calibration and focusing of the laboratory X-ray set. Measurement of the diffraction maxima was done using Bragg's law;

$$2d \sin\theta = n\lambda$$

In the low-angle region $\sin\theta$ may be approximated by θ , d is the spacing and λ is the wavelength of the incident radiation.

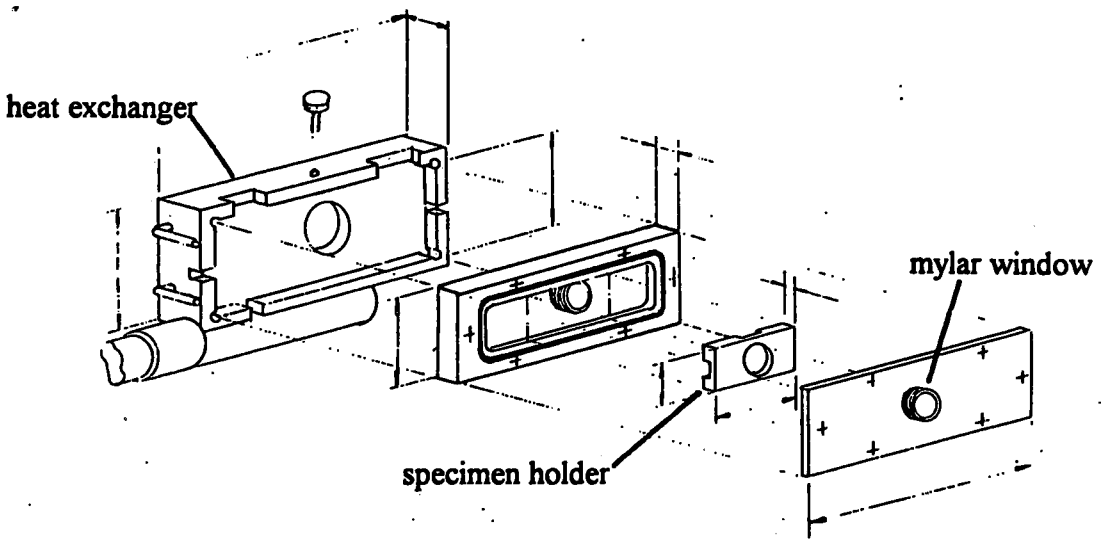

Figure 2.1 Diagram showing the X-ray diffraction cell

2.3 EXPERIMENTAL SOLUTIONS

All the experimental solutions used in the microelectrode and X-ray diffraction experiments are given in Tables 2.3, 2.4, and 2.5. The ionic strength for all the solutions used for the microelectrode investigations were chosen so that they produced a potential large enough to be measured without ambiguity, these are 50% of the physiological concentration. The rigor A solution series is similar to that used by Bartels and Elliott (1985), this is a set of serially diluted ATP-free rigor solutions with decreasing ionic strength. The B rigor solution is the same as that used by Yagi (1992), and differs slightly from the A solution in buffer, ionic strength and pH. For relaxed muscles the solutions were modified to contain suitable amounts of ATP and also EGTA to chelate any residual calcium ions.

The solution used for the bovine corneas is similar to that used by Hodson et al. (1992). In order to avoid hydration of the corneas and thus balance the stromal gel pressure against the osmotic pressure of the bathing medium, non-penetrating polyethylene glycol nominal molecular weight 20 000 Da (PEG 20 K) was added to the solution, following the procedure of Fullwood (1992). The calf lens solution is the same as that used by Benedek et al. (1979).

Solutions	KCl (mM)	$MgCl_2$ (mM)	Buffer (mM)	pH	Ionic strength
A	100	5	20 Phosphate	7	0.141
2 x diluted (A/2)	50	2.5	10 Phosphate	7	0.072
5 x diluted (A/5)	20	1	4 Phosphate	7	0.030
10 x diluted (A/10)	10	0.5	2 Phosphate	7	0.015
B	100	5	10 Immidazole	7.2	0.115

Table 2.3 Table of the Rigor solutions used. All solutions were adjusted with KOH. In all these Tables, the ionic strength is calculated from the Perrin program (section 3.1.1).

KCl (mM)	$MgCl_2$ (mM)	EGTA (mM)	ATP (mM)	Buffer (mM)	pH	Ionic strength
50	2.5	4	2.5	10 Phosphate	7	0.084
50	2.5	4	2.5	5 Histidine	7	0.077

Table 2.4 Table of the relaxing solutions used. All solutions were adjusted with KOH.

Solutions	NaCl (mM)	PEG (20 K)	Buffer (mM)	pH	Ionic strength
Bovine Cornea	30	2.5% (by volume)	10 Histidine	7.4	0.030
Calf Lens	75		9 Phosphate	7.4	0.084

Table 2.5 Table of the solutions used for bovine cornea and calf lens. All solutions were adjusted with NaOH.

2.4 POTENTIAL READINGS AND CHARGE CALCULATIONS

Once Donnan potential readings were taken, the data were plotted as histograms and the means and standard deviations were calculated. In most of the tissues and experimental conditions studied the resultant histogram plots gave a single curve which best fits a normal distribution. However, in most experiments of rigor muscle a bimodal distribution is observed representing the distribution of fixed electrical charge in the A and I-bands, as reported by Naylor et al. (1985) (See Figure 3.1). It was often found that the tails of these two distributions overlapped. In order to determine the overlap boundary between the two distributions, the mid-point crossover value (x) was calculated using the probability density function, and the Z value was then found. The probability that each distribution lies above or below the crossover value, expressed as a percentage, was then determined using probability functions for the normal distribution ie. Pr ($x_I > x$), Pr ($x_A < x$). A worked example is given in Appendix 1.

All values of ionic strength were calculated from a computer program in which the free ion concentrations of each species were determined from the association constants using the iterative method of Perrin and Sayce (1967), and White and Thorson (1972). Once the ionic strength of a given solution was determined and Donnan potential readings taken, the fixed protein charge was calculated from a computer program using the Nernst

equation, The method was taking account of all free ions, both mono- and polyvalent described by Naylor et al. (1985). The results of the concentration of protein charge [Pr] are expressed as mM of univalent charge.

2.5 ERRORS

2.5.1. EXPRESSIONS OF ERROR

Normally the results include the standard deviation (sd) on the mean, where sufficiently large sample size (n) relating to a given condition were obtained. In cases where the sample size is insufficient for detailed statistics (ie. n <3) an estimated error (ee) is given. The estimated error is derived by comparison with the standard deviation found under similar conditions; a figure of at least 2 x the comparable standard deviation is shown.

2.5.2 SOURCES OF ERROR

Human error, instrumental confines and variations in the same biological tissues are likely sources of intrinsic errors. Human errors include minor misjudgements in the estimation of voltmeter readings caused by the parallax effect, and the possibility of the inclusion of apparently artifactual readings. Slight variations in the same biological tissues are inherent in all biological systems and as such are unavoidable. Instrumental limitations include possible systematic errors introduced into the calibration of the X-ray detector and voltmeter, as well as the possibility of errors in measuring small quantities of chemicals on the balance or solutions in measuring cylinders. Given the above considerations it is estimated that the error for microelectrode readings is of the order of 2%; x-ray diffraction spacings 0.4% and intensities 5%.

CHAPTER 3

RESULTS

3.1 MICROELECTRODE RESULTS

3.1.1 EFFECT OF TEMPERATURE IN MUSCLE

Small bundles (5-10 fibres) of glycerinated rabbit psoas muscle were studied in both the relaxed and rigor states over a range of temperatures in order to find out the effect of temperature on the net fixed electrical charge on the contractile proteins, and to see if any changes in the relaxed state coincide with x-ray diffraction data of the temperature-induced disorder transitions observed by Wray (1987), Wakabayashi et al. (1988) and Lowy, Stewart and Popp (1991). The temperature range chosen was from 10 to 35 ^{0}C. Temperatures below 10 ^{0}C proved technically difficult to achieve with the experimental set-up. The bathing solution would often freeze around the heat exchanger, and condensation formed on the under side of the experimental chamber making visibility impossible. The upper limit of 35 ^{0}C was chosen as muscle cells begin to coagulate much above this temperature.

In the following account the potential recorded in the A-band is called E_A, and the potential recorded in the I-band is called E_I. In the temperature range 10 - 25 ^{0}C, it was found that rigor muscle gave two potential peaks corresponding to the A- and I-band potentials, as reported by Bartels & Elliott (1985). Figure 3.1 shows typical experimental data for this temperature range. In relaxed muscle E_I and E_A are the same value resulting in a single potential peak, as Bartels & Elliott observed.

Tables 3.1 and 3.2 give a summary of the Donnan potentials and calculated fixed charge determined in both rigor and relaxed muscle respectively. Both the relaxing and rigor solutions chosen for this experiment were based on 50 mM KCl. This was done so that the potential readings were high enough at room temperature (20 ^{0}C) to detect any change with variation in temperature, which changes lie outside the bounds of experimental error. The experimental data show that in both the rigor and relaxed states the potentials fall sharply with increasing temperature. It should also be noted that the associated calculated charge [Pr] results also decrease. The Nernst equation used to calculate the charge gives an exponential function, however these values lie in the region of the exponential function which may be approximated as a linear function.

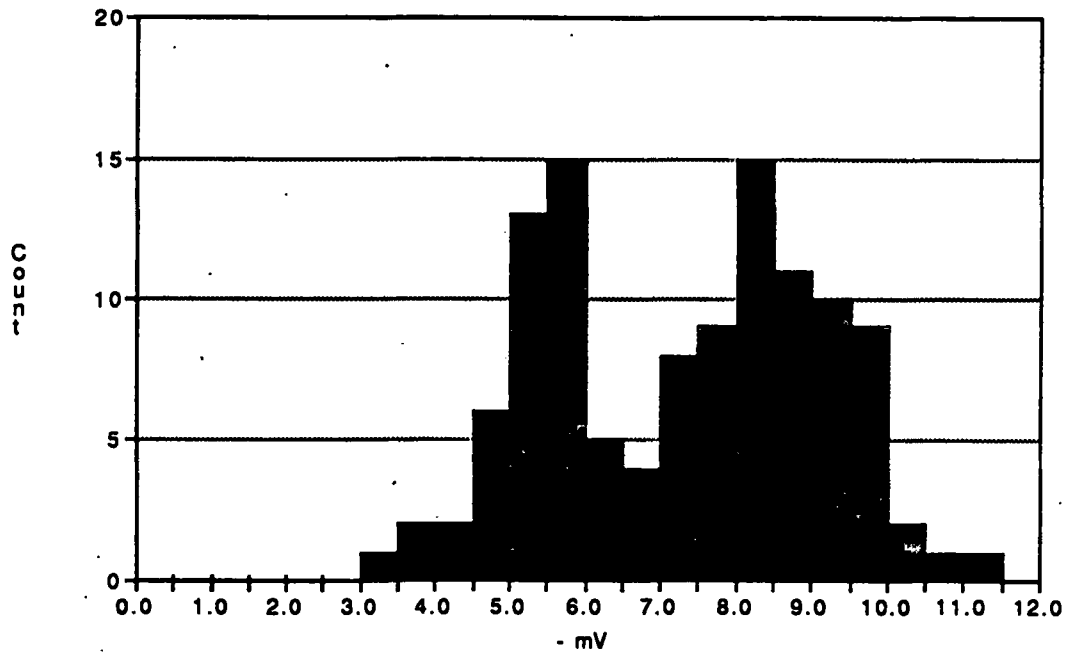

n = 224

Figure 3.1 Histogram of 224 potentials taken in glycerinated rabbit rigor muscle in rigor at 20 ^{0}C.

Temperature	E_A	E_I	$[Pr]_A$	$[Pr]_I$	Midpoint x	$Pr(x_I > x)$	$Pr(x_A < x)$
(^{0}C)	mV	mV	mM	mM	mV	%	%
10	-9.6 ± 0.92 n = 249	5.7 ± 1.19 n = 249	-56 ± 5	-33 ± 7	-7.8	3.75	2.62
20	-8.6 ± 0.94 n = 224	5.4 ± 0.60 n = 224	-50 ± 5	-31 ± 3	-6.7	1.46	2.39
25	-9.1 ± 0.69 n = 226	-5.9 ± 1.01 n = 226	-54 ± 4	-34 ± 5	-7.7	4.01	2.68
27.5	-9.2 ± 0.98 n = 234	-6.0 ± 1.04 n = 234	-54 ± 6	-35 ± 6	-7.6	6.94	5.26
30	-3.3 ± 1.30 n = 234	-3.3 ± 1.30 n = 234	-19 ± 7	-19 ± 7			
32.5	-3.3 ± 0.94 n = 252	-3.3 ± 0.94 n = 252	-19 ± 5	-19 ± 5			
35	-3.5 ± 1.09 n = 716	-3.5 ± 1.09 n = 716	-20 ± 6	-20 ± 6			

Table 3.1 Summary of results from measuring potentials as a function of temperature in rabbit rigor muscle. The solution used was; 50 mM KCl, 2.5 mM $MgCl_2$, 10 mM Phosphate buffer, pH = 7. All potentials and the associated [Pr]s are given as mean and standard deviation, n is the number of readings.

Temperature (^{0}C)	$E_{A\&I}$ mV	$[Pr]_{A\&I}$ mM	n
10	-5.4 ± 1.19	-30 ± 6	226
20	-5.7 ± 1.01	-31 ± 5	236
25	-4.2 ± 1.22	-23 ± 7	247
27.5	-4.7 ± 0.98	-26 ± 3	241
30	-3.8 ± 0.97	-21 ± 5	289
32.5	-3.4 ± 0.43	-19 ± 3	267
35	-3.1 ± 0.52	-17 ± 3	283

Table 3.2 Summary of results from measuring potentials as a function of temperature in rabbit relaxed muscle. The solution used was; 50 mM KCl, 2.5 mM $MgCl_2$, 2 mM EGTA, 2.5 mM Na_2ATP, 10 mM Histidine - HCl buffer, pH = 7. All potentials and the associated [Pr]s are given as mean and standard deviation, n is the number of readings.

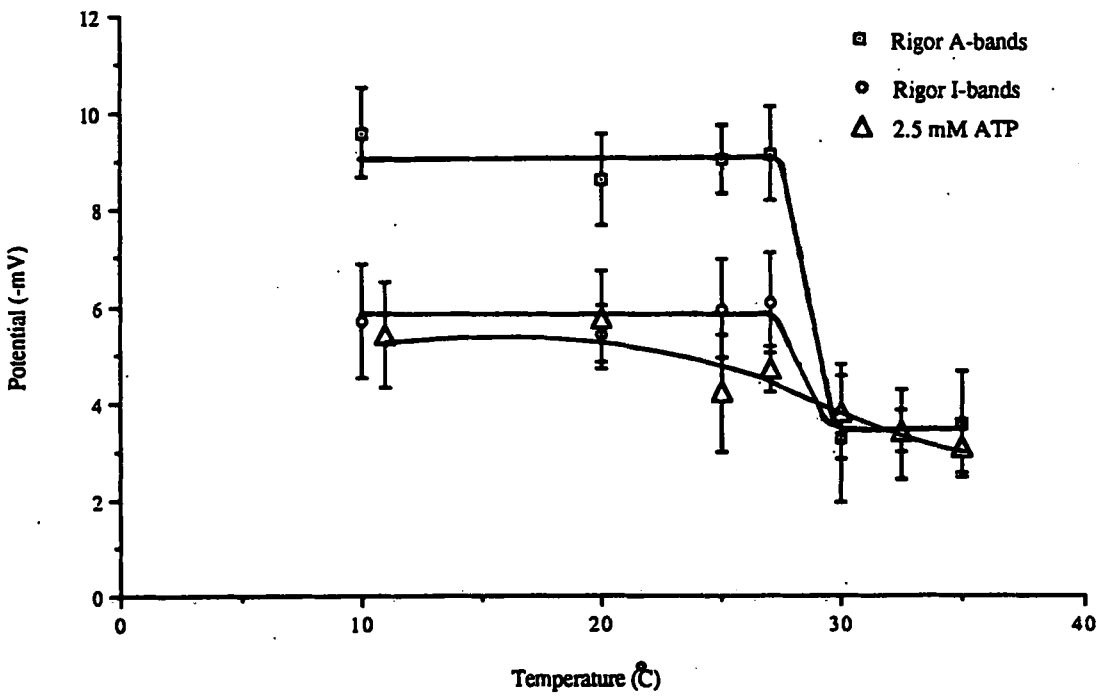

Figure 3.2 Measured Donnan potentials in relaxed and rigor muscle as a function of temperature.

Figure 3.2 shows a plot of the measured potentials in both relaxed and rigor muscle, as a function of temperature. From this figure it can be seen that in rigor muscle the respective values of E_A and E_I are approximately constant, within the bounds of experimental error, in the temperature range of 10 - 27.5 ^{0}C. The mean values are -9.1 mV and -5.8 mV respectively. These results are in good agreement at room temperature (20 ^{0}C) with the potentials reported by Bartels and Elliott (1985), who give E_A and E_I as -8.6 mV and -5.2 mV respectively at this ionic strength. From 30 ^{0}C to 35 ^{0}C both E_A and E_I seem fairly constant over this range. In this temperature range the histograms for rigor muscle show only one potential peak even though the electrodes were observed to impale both A- and I-bands, and thus E_A and E_I are equal with a mean value of -3.4 mV. It should be noted that to avoid confusion only one set of data points for E_A and E_I are plotted in this region. The lines of best fit in both the E_A and E_I data were drawn by eye. The data for rigor muscle taken as a whole shows that the decrease in the potentials with an increase in temperature is a step function, giving a definite transition temperature between 27.5 - 30 ^{0}C

.

In relaxed muscle the potentials of the A- and I-bands also fall off with increasing temperature. E_A and E_I were found to be of equal value at all temperatures, and therefore only one set of data points is plotted. Here, as in rigor muscle, the potentials seem to be constant over two temperature ranges; 10 - 20 ^{0}C and 30 - 35 ^{0}C, with mean values of -5.5 mV and -3.6 mV. However the transition temperature is not as clearly defined as that which occurs in rigor muscle, with the potential values at 25 ^{0}C and 27.5 ^{0}C being less than those at lower temperatures. These two data points make the construction of a line of best fit delineating a clear transition temperature a difficult accomplishment. In order to demonstrate this point figure 3.3 shows the relaxed muscle data plotted on a slightly expanded scale with out a line of best fit. From this graph it may be seen that one of two possibilities may occur, these are; a) that a transition temperature similar to that found in rigor muscle exists and that the data points at 25 ^{0}C and 27.5 ^{0}C are abnormaly low, or b)

that the transition temperature is lower than that in rigor, 20 - 25 ^{0}C. Which-ever is the case it may be said that in relaxed muscle there is a clear decrease in potentials with increase in temperature , and that this phenomenon occurs within the same range (20 - 30 ^{0}C) as the effect that temperature has on the visibility of the myosin layer lines reported in the literature. To demonstrate this an unpaired Student t-test was performed on all the potential readings taken in the ranges of 10 - 20 ^{0}C and compared with all the potential readings taken in the range 30 - 35 ^{0}C. This gave a t-statistic = -35.24 and has a significance much better that 1% ($P << 0.001$, t-test). It is also interesting to note that the residual potentials at and above 30 ^{0}C in both relaxed and rigor muscle are about the same value.

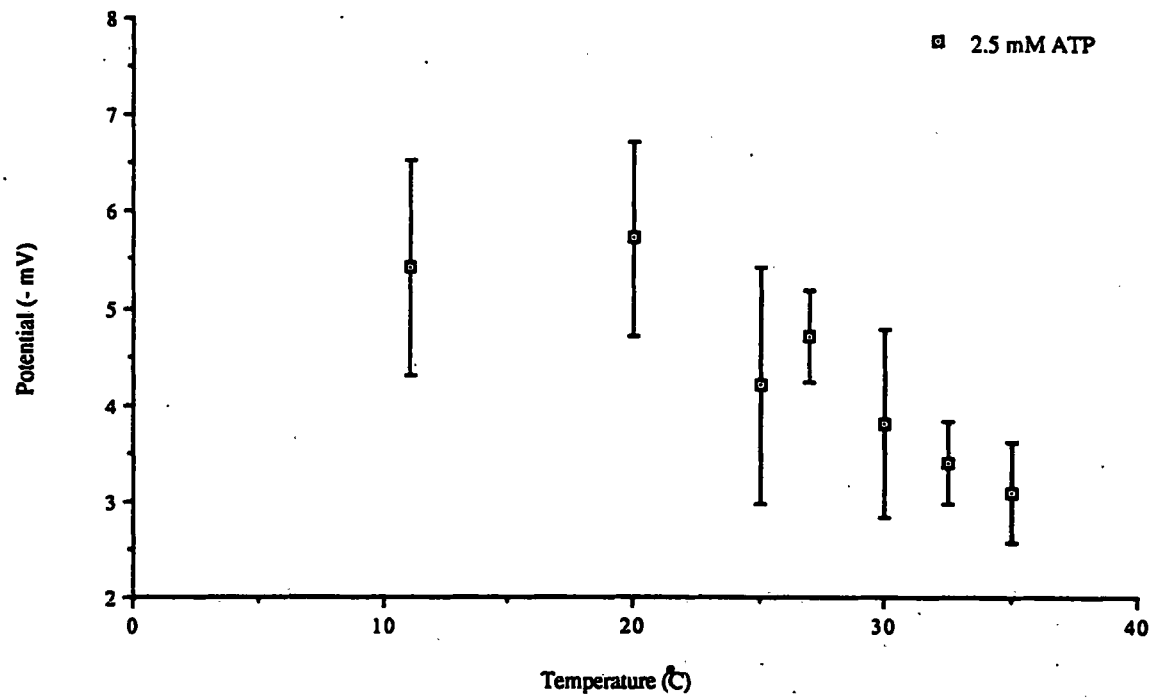

Figure 3.3 Measured Donnan potentials in relaxed muscle as a function of temperature

Temperature (^{0}C)	E mV	[Pr] mM	n
15	-9.7 ± 1.12	-109 ± 12	259
22	-8.2 ± 0.89	-92 ± 8	222
27.5	-5.4 ± 1.32	-68 ± 11	265
30	-4.7 ± 1.05	-61 ± 9	255
35	-3.5 ± 0.76	-52 ± 5	282

Table 3.3 Summary of measured potentials as a function of temperature in bovine corneal stroma. The solution used was; 30 mM NaCl, 2.5 % (by volume) PEG, 10 mM Histidine - HCl buffer, pH = 7.4. All potentials and the associated [Pr]s are given as mean and standard deviation, n is the number of readings.

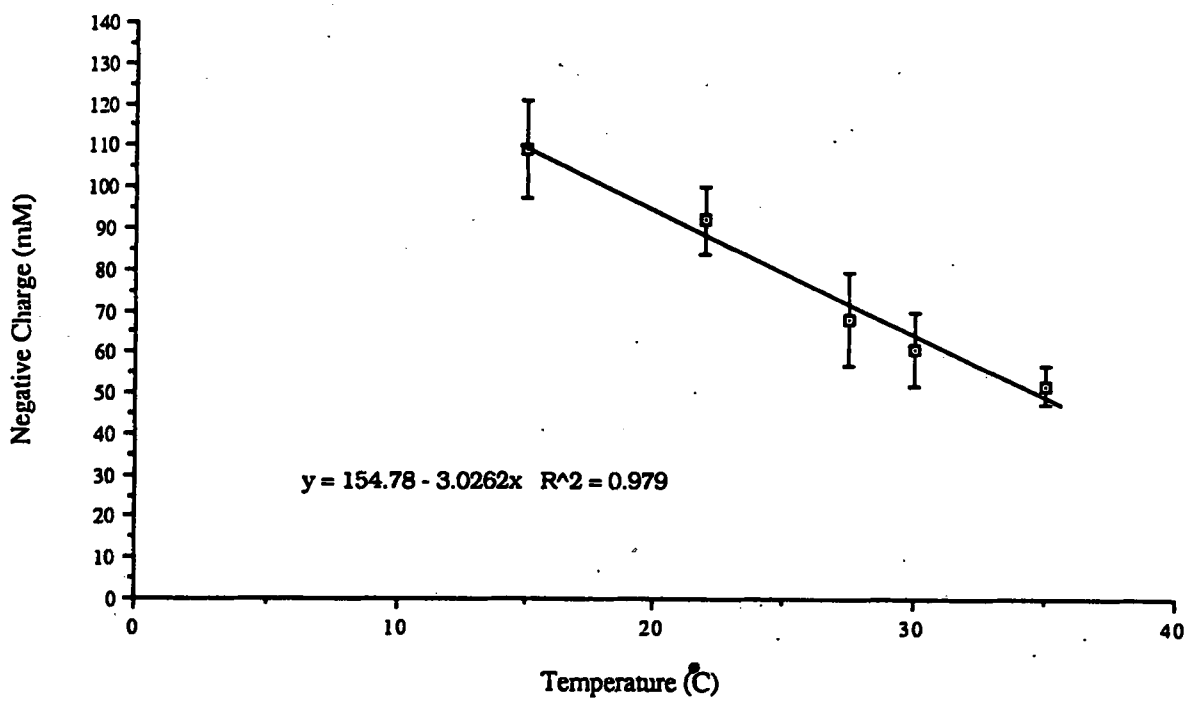

Figure 3.4 Protein fixed charge concentration in corneal stroma, as a function of temperature

3.1.2 EFFECT OF TEMPERATURE IN CORNEA

To see whether the temperature step function effect occurs in other polyelectrolyte tissues, a similar temperature experiment as described above for muscle was conducted on a number of bovine corneal stromas. Only one cornea solution was used and is similar to that used by Hodson et al.(1992),(see section 2.3, Table 2.5). The measured potentials and calculated fixed charge are given in table 3.3 and a plot of the calculated charge as a function of temperature is given in figure 3.4.

As can be seen from figure 3.4 the change in charge with an increase in temperature is constant over the entire range studied. Moreover, the charge decreases linearly with temperature, and has a correlation coefficient which is very close to unity. From table 3.3 it may be seen that the linearity observed between potential and temperature transposes into a linear temperature-charge relation. The Nernst equation used to calculate the fixed charge involves an exponential function, but the experimental data in the range recorded occurs within the linear region of the exponential function.

3.1.3 EFFECT OF TEMPERATURE IN CALF LENS

The concentration of the fraction cryo-protein aggregate γiv-crystallin in calf lens, which is believed to be responsible for the formation of the temperature-dependent reversible cold cataract (Siezen et al. 1985), is < 0.1% by weight. Although this concentration is very low, potential readings were taken above and below the temperature at which the cold cataract appears (T_{cat}). These experiments were conducted to see if there is any change in potentials with respect to opacification. In a solution of 150 mM NaCl, phosphate buffer, pH = 7, T_{cat} was found to be 18.5 ^{0}C. This is in broad agreement with Benedek et al. (1979) who report the value of T_{cat} for the same solution as 17 ^{0}C.

The calf lenses used in this study came from still born calves, in which there is a high synthesis of γiv-crystallin during embryonic development and a steady depletion due to degradation during aging as reported by Papaconstantiou (1965), Slingsby and Croft (1973) and Slingsby and Miller (1983). As the protein concentration is also dependent on the age of the calf, and the ages of the lenses were unknown, potential readings above and below T_{cat} were taken in the same lens nuclei to avoid any ambiguity. Figures 3.5 and 3.6 show histograms of measured potentials at 8 ^{0}C and 30 ^{0}C respectively. Although the mean potentials vary very slightly (-3.2 mV at 8 ^{0}C and -3.4 mV at 30 ^{0}C), the experiment was conducted in twelve separate lens nuclei and no significant change in potentials was found to occur. Each set of readings varied slightly (in the order of ~0.2 mV) but no consistent trend was observed and these slight changes lie well within the bounds of experimental error. The mean value above and below T_{cat} in all the experiments attempted was -3.4 mV.

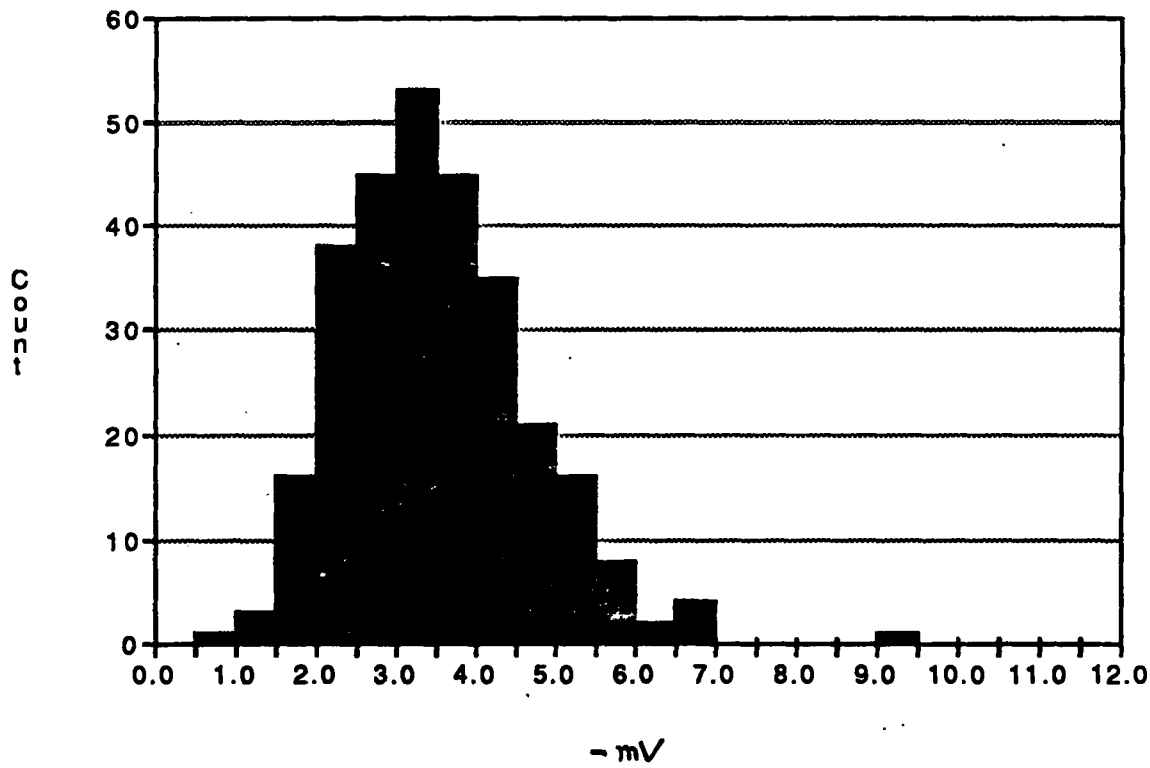

Figure 3.5 Histogram of potentials taken in calf lens nuclei at 8 ^{0}C in a solution of 150 mM NaCL, phosphate buffer, pH = 7.4. Mean potential = -3.2 mV, n = 283

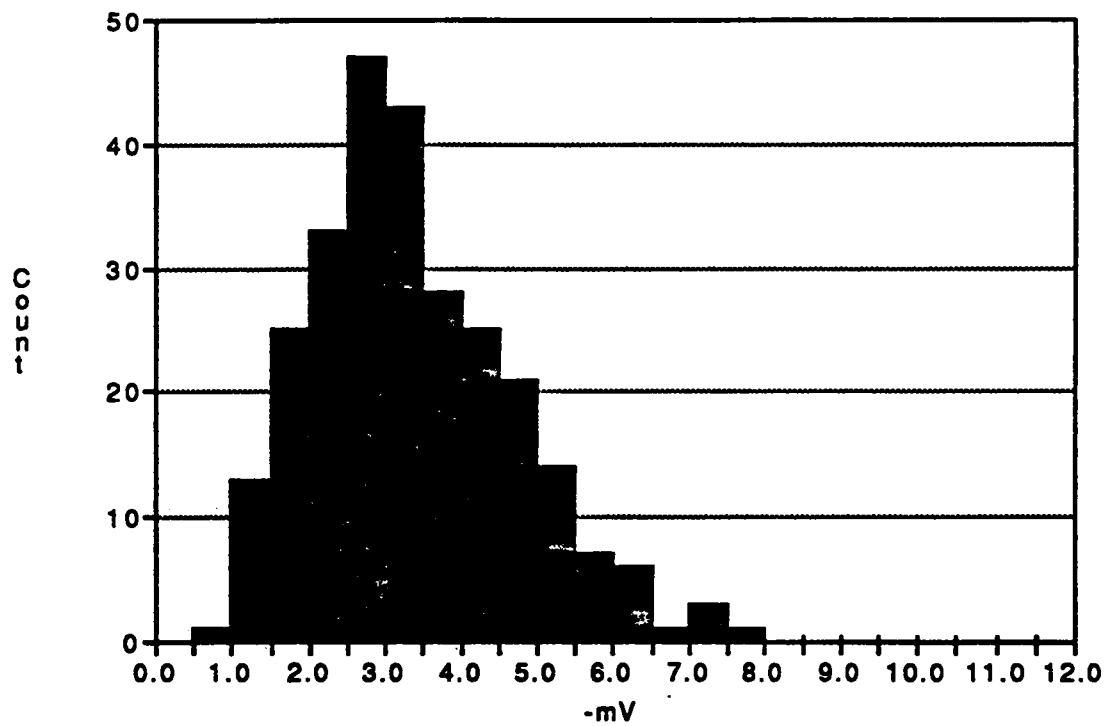

Figure 3.6 Histogram of potentials taken in calf lens nuclei at 30 ^{0}C in a solution of 150 mM NaCL, phosphate buffer, pH = 7.4. Mean potential = -3.4 mV, n = 288.

3.1.4 EFFECT OF N-ETHYLMALEIMIDE IN MUSCLE

The effects of N-Ethylmaleimide (NEM) on the fixed electrical charges on the contractile proteins were investigated to see whether such changes might be linked to the disorder phenomena in muscle treated with NEM, as observed in x-ray diffraction patterns by Yagi (1992). Chemically skinned frog muscle fibres were used at first, in order to closely follow the experimental protocol employed by Yagi (1992). For these sets of experiments Yagi's solutions were used, relaxing see Table 2.2 and Rigor B, see Table 2.3. In both cases 1 mM of NEM was added to the solution. No change in pH was detected in either solution on addition of NEM. Glycerinated rabbit muscle fibres were also used in the same rigor solution to give a comparison to frog muscle.

Tables 3.4 and 3.5 give the measured potentials and calculated charge for chemically skinned frog muscle and glycerinated rabbit muscle respectively. In the relaxed saponin-skinned frog muscle, the I-band and A-band charges were increased about two fold (from -34 $\pm$ 9 mM to -62 $\pm$ 11 mM), an increase of 82% on addition of 1 mM on NEM to the solution. Yagi (1992) observed that the effects of NEM on the pattern were not reversible. To see if the effect of this reagent on charge was also not reversed, relaxed muscles after being treated with NEM were then placed in a rigor solution, being consistent with the protocol of Yagi. Here, two potential peaks were observed as in normal rigor muscle but with an increase in charge in both the I- and A-bands. The I-band charge increased from -25 $\pm$ 4 mM to -37 $\pm$ 6 mM and the A- band from -47 $\pm$ 3 mM to -66 $\pm$ 0.7 mM, an increase of about 70% in each. In the rigor glycerinated rabbit muscle, a similar increase of the same magnitude in the charges of the I- and A- bands was also found. The I-band increased from -25 $\pm$ 4 mM to -35 $\pm$ 5 mM and the A-band from -48 $\pm$ 4 mM to -69 $\pm$ 7 mM, here again the increase was about 70% in each.

CHEMICALLY SKINNED FROG SARTORIUS MUSCLE

	Potential mV	[Pr] mM	n
Relaxed (control)			
I&A-bands	-2.0 ± 0.56	-34 ± 9	295
Relaxed + NEM			
I&A-bands	-3.7 ± 0.68	-62 ± 11	273
Rigor (control)			
I-band	-2.6 ± 0.34	-25 ± 4	319
A-band	-5.1 ± 0.44	-47 ± 3	319
Rigor after Relaxed + NEM			
I-band	-4.0 ± 0.61	-37 ± 6	284
A-band	-7.0 ± 0.64	-66 ± 0.7	284

Table 3.4 Summary of results from measuring potentials in chemically skinned frog muscle in relaxing and rigor solutions, in the presence and absence of NEM. All potentials and the associated [Pr]s are given as mean and standard deviation, n is the number of readings.

GLYCERINATED RABBIT PSOAS MUSCLE

	Potential mV	Charge [Pr]	n
Rigor (control)			
I-band	-2.7 ± 0.45	-25 ± 4	257
A-band	-5.2 ± 0.47	-48 ± 4	257
Rigor + NEM			
I-band	-3.7 ± 0.68	-35 ± 5	292
A-band	-7.3 ± 0.75	-69 ± 7	292

Table 3.5 Summary of results from measuring potentials in glycerinated rabbit psoas muscle in relaxing and rigor solutions, in the presence and absence of NEM. All potentials and the associated [Pr]s are given as mean and standard deviation, n is the number of readings.

3.1.5 CHANGES OF pH WITH TEMPERATURE

In all the microelectrode temperature experiments either phosphate or histidine - HCl buffers were used. A large decrease in pH with increasing temperature would result in lower potentials at higher temperatures, and thus invalidate the results obtained in muscle and cornea. As no data could be found in the literature for the change in pH with increasing temperature for either buffer, a subsidiary experiment was conducted. To see the effect that temperature has on pH of the rigor and relaxing solutions used in the microelectrode muscle experiments , with their respective phosphate and histidine - HCl buffers , approximately the same experimental ranges were used (15 - 35 ^{0}C) and the pH was measured. As before, 2.5 mM ATP was added to the relaxing solution. The pH was measured with a UNIFET pH/mV/^{0}C meter (UNIFET Incorp, San Diego, USA) with an accuracy of $\pm$ 0.01. At room temperature (20 ^{0}C) both solutions were buffered to pH 7 and adjusted with KOH were necessary.

Figure 3.6a shows a plot of pH as a function of temperature for the rigor and relaxing solutions. The pH of the phosphate buffered rigor solution decreases very slightly with increasing temperature, changing.from 7.00 to 6.97 from 20 to 35 ^{0}C. Over the same temperature range, the pH of the relaxing solution (which used a histidine-chloride buffer) decreases much more sharply changing from 7.00 to 6.81. At 15 ^{0}C both solutions were found to have a pH of 7.01.

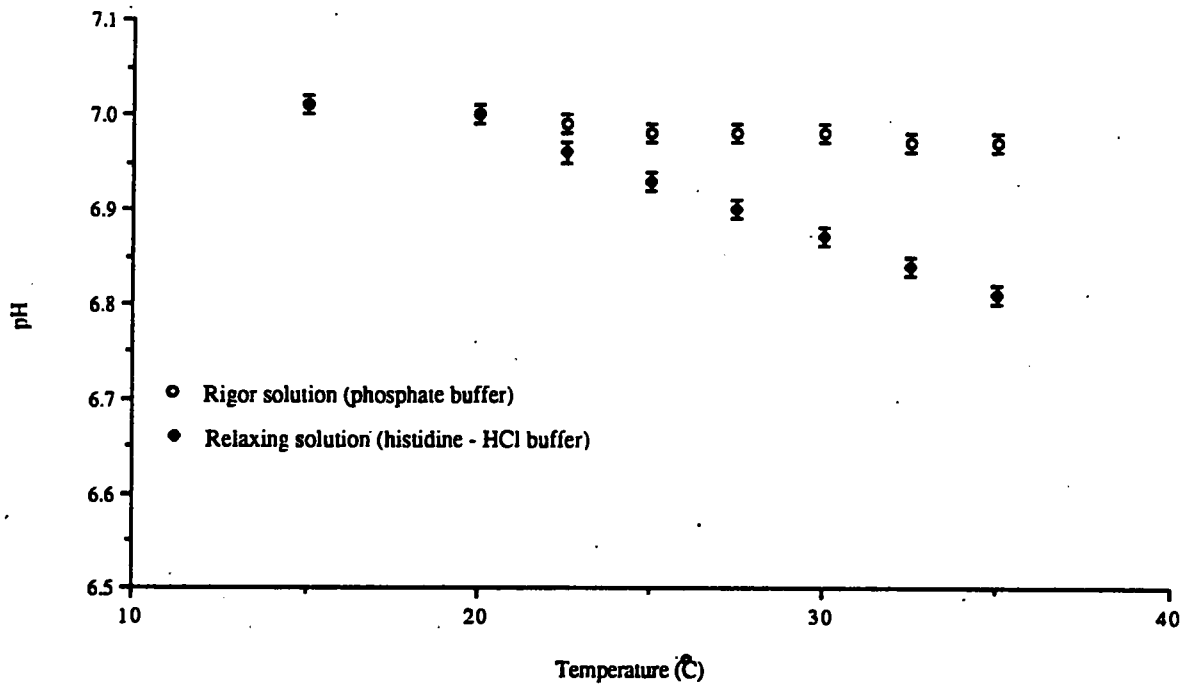

Figure 3.6a The change in pH of the phosphate buffered rigor solution and histidine HCl buffed relaxing solution used in the microelectrode temperature experiments, plotted as a function of temperature.

The change in pH with temperature in the phosphate buffered rigor solution is very slight and falls within the bounds of experimental error, and as such would have no real measurable effect on the value of the potential readings taken over the temperature range studied. Although the decrease of pH in the histidine - HCl buffered relaxing solution is greater than that which occurs in rigor solution, Naylor et al. (1985) report that the measured A-band potential in a 50 mM KCl solution (which is of similar ionic strength to that used in this experiment) does not change significantly until the pH is lowered to about pH 6. To illustrate this point Figure 3.6b shows Figure 5 taken from Naylor et al. (1985), it may be seen that the measured A-band potential is - 9.7 mV at pH 7 and falls to - 7.1 mV at pH 5.7. From interpolation of the line of best fit from this Figure, at pH 6.8 there would seem to be virtually no change in the corresponding potential. As the line of best fit was drawn by eye and may in fact be steeper, it was decided to measure potential readings at 35 ^{0}C in a relaxing solution with a phosphate buffer (Table 2.4), which was buffered to pH 7 at room temperature (20 ^{0}C). Table 3.5a shows the results. When compared to the value obtained at the same temperature in the relaxing solution with the histidine buffer (Table 3.2), the measured potentials are the same. It may therefore be said that within the experimental ranges studied, the minor decreases in pH with increase in temperature found with the histidine - HCl buffer has no measurable effect on the Donnan potentials.

Buffer	Temperature (^{0}C)	$E_{A\&I}$ mV	n
Phosphate	35	-3.12 ± 0.53	59
Histidine-HCl	35	-3.1 ± 0.52	283

Table 3.5a Results from measuring potentials in glycerinated rabbit muscle in a phosphate and histidine-HCl buffed relaxing solution at 35 ^{0}C. pH = 7 at room temperature.

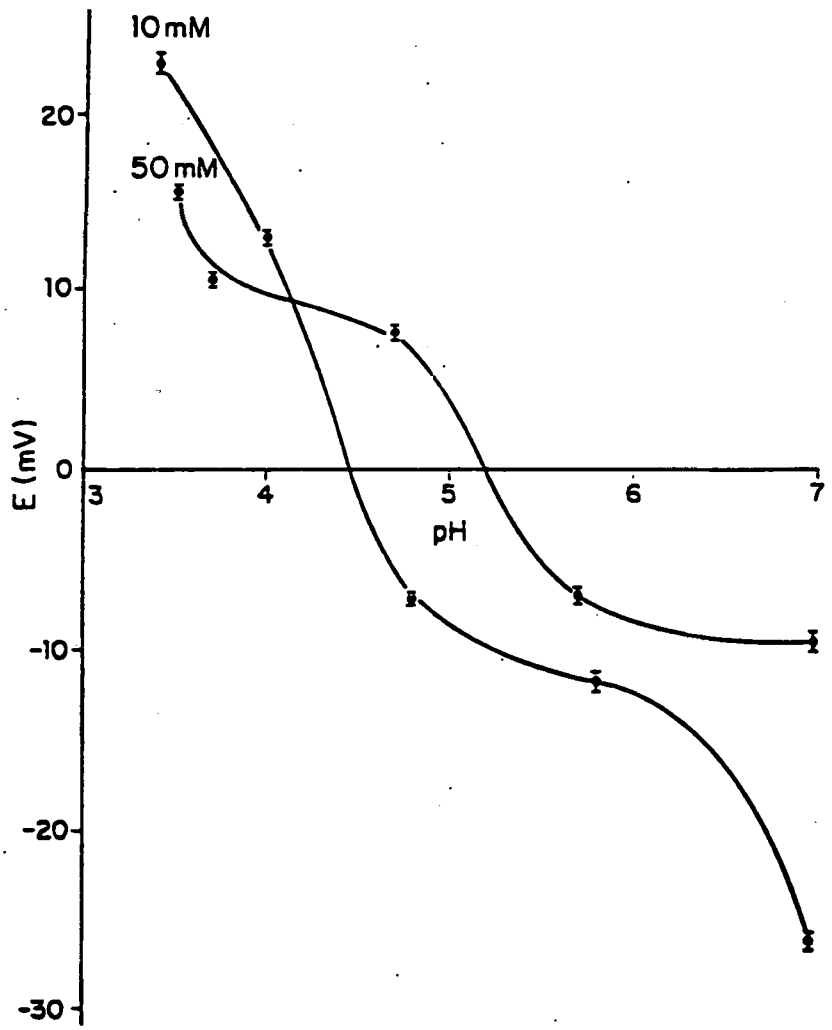

Figure 3.6b The variation of the A-band potential in glycerinated rabbit muscle as a function of pH at two ionic strengths. (After Naylor et al. 1985).

3.2 X-RAY DIFFRACTION RESULTS

3.2.1 EFFECTS OF TEMPERATURE ON MERIDIONAL PATTERNS IN RIGOR MUSCLE

Given that decrease in charge with increasing temperature (see section 3.1.2) seems to occur in the same temperature range at which the temperature dependant disordering effect in relaxed muscle, meridional x-ray patterns were taken in rigor muscle at various temperatures in order to see if the more dramatic change in charge in rigor (see figure 3.2) has any ordering effect on the structure of the muscle lattice. Small strips (2 mm in width) of glycerinated rabbit muscle were placed in the serially diluted A solutions (see Table 2.3) and x-ray patterns taken over the temperature range 10 - 35 ^{0}C. Rest length sarcomeres were used (S = 2.4 - 2.6 μm) in order to obtain meridional patterns with a high degree of sampling along the layer lines. It should be noted that each set of experiments for a given ionic strength over the experimental temperature range were only conducted once (ie n =1), due to the limitations of beam time at the Daresbury synchrotron. Therefore in the results presented for these experiments no quantitative assessment may be made, only a qualitative one.

The only changes observed occured at low ionic strength A/10 (0.015). At higher temperatures it was found that the sharpness (ie the sampling along the layer line) of the first actin layer line (365 Å) increases in the rigor pattern. This sampling is at the 1,1 position of the equatorial pattern. Figures 3.7, 3.8 and 3.9 show the vertical integration along the length of the 365 Å actin layer line from the rigor pattern at low ionic strength at the three different temperature ranges used (the computure program is able to perform either a vertical intergration of a horizontal slit or a horizontal intergration of a vertiacl slit , thus

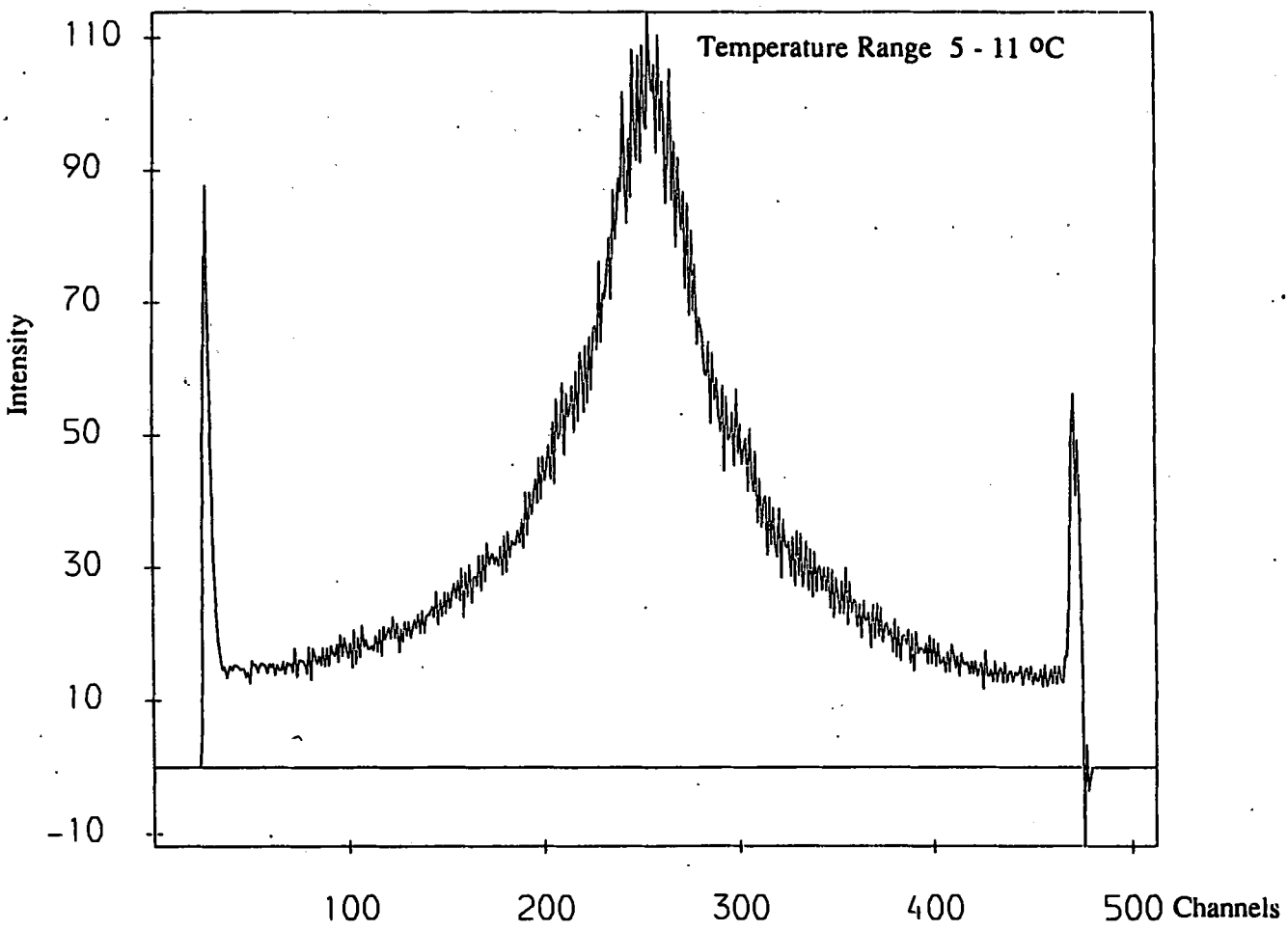

Figure 3.7 Vertical integration of the 365 Å actin layer line of the rigor pattern in the temperature range 5 - 11 ^{0}C, in A/2 solution The y axis units of intensity are arbitrary.

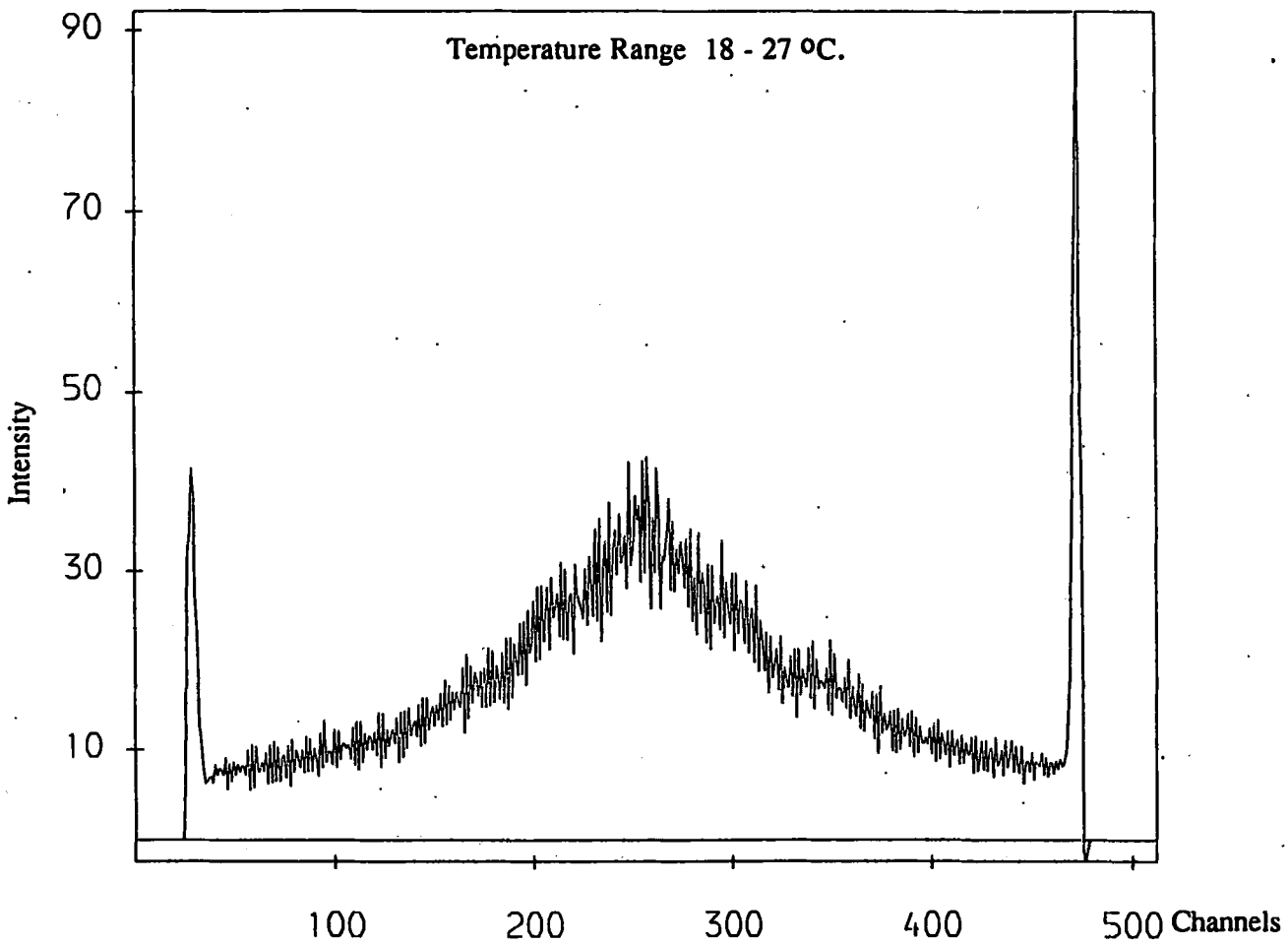

Figure 3.8 Vertical integration of the 365 Å layer line of the rigor pattern in the temperature range 18 - 27 ^{0}C, in A/2 solution The y axis units of intensity are arbitrary.

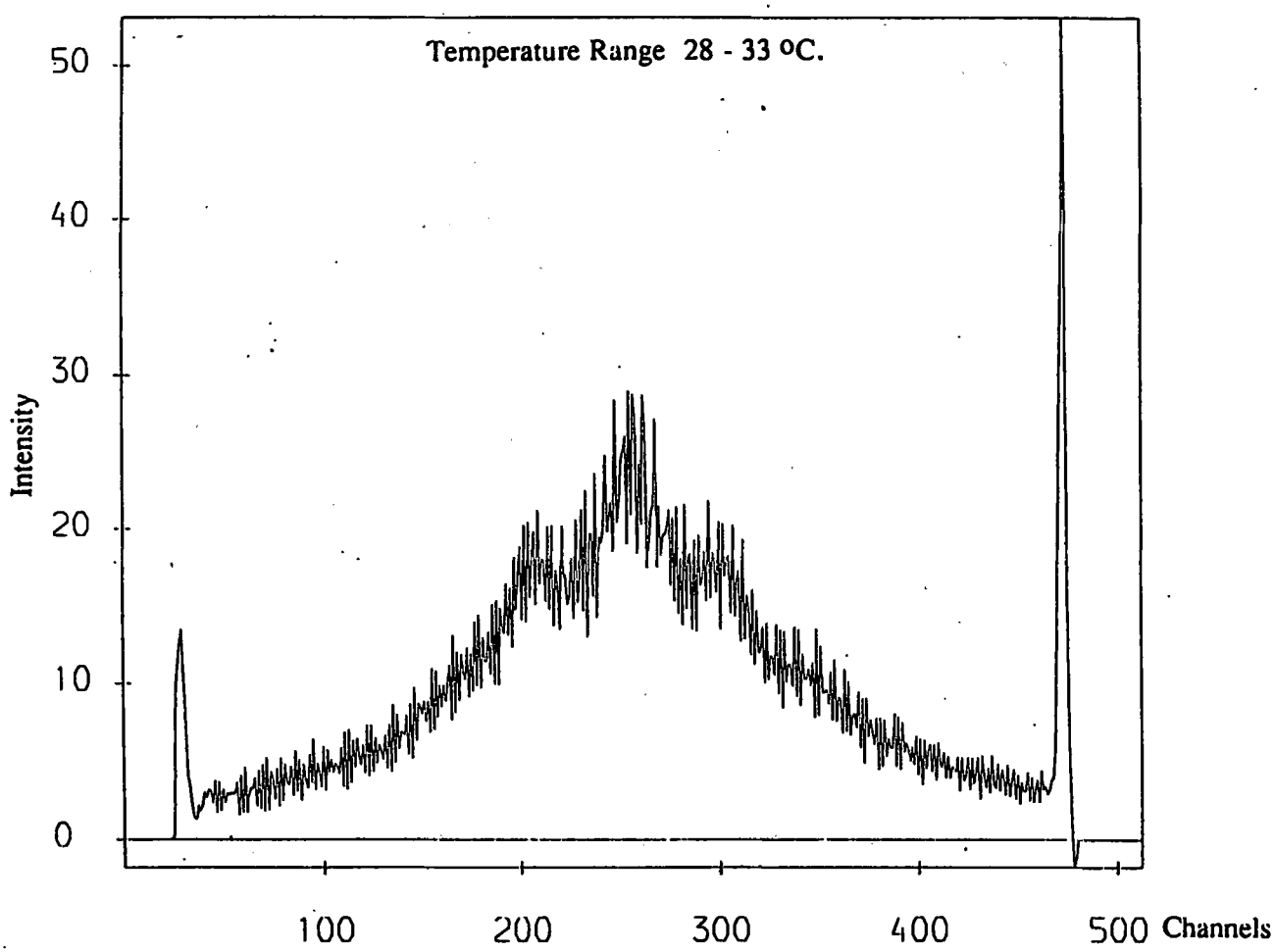

Figure 3.9 Vertical integration of the 365 Å layer line of the rigor pattern in the temperature range 28 - 33 ^{0}C, in A/2 solution The y axis units of intensity are arbitrary

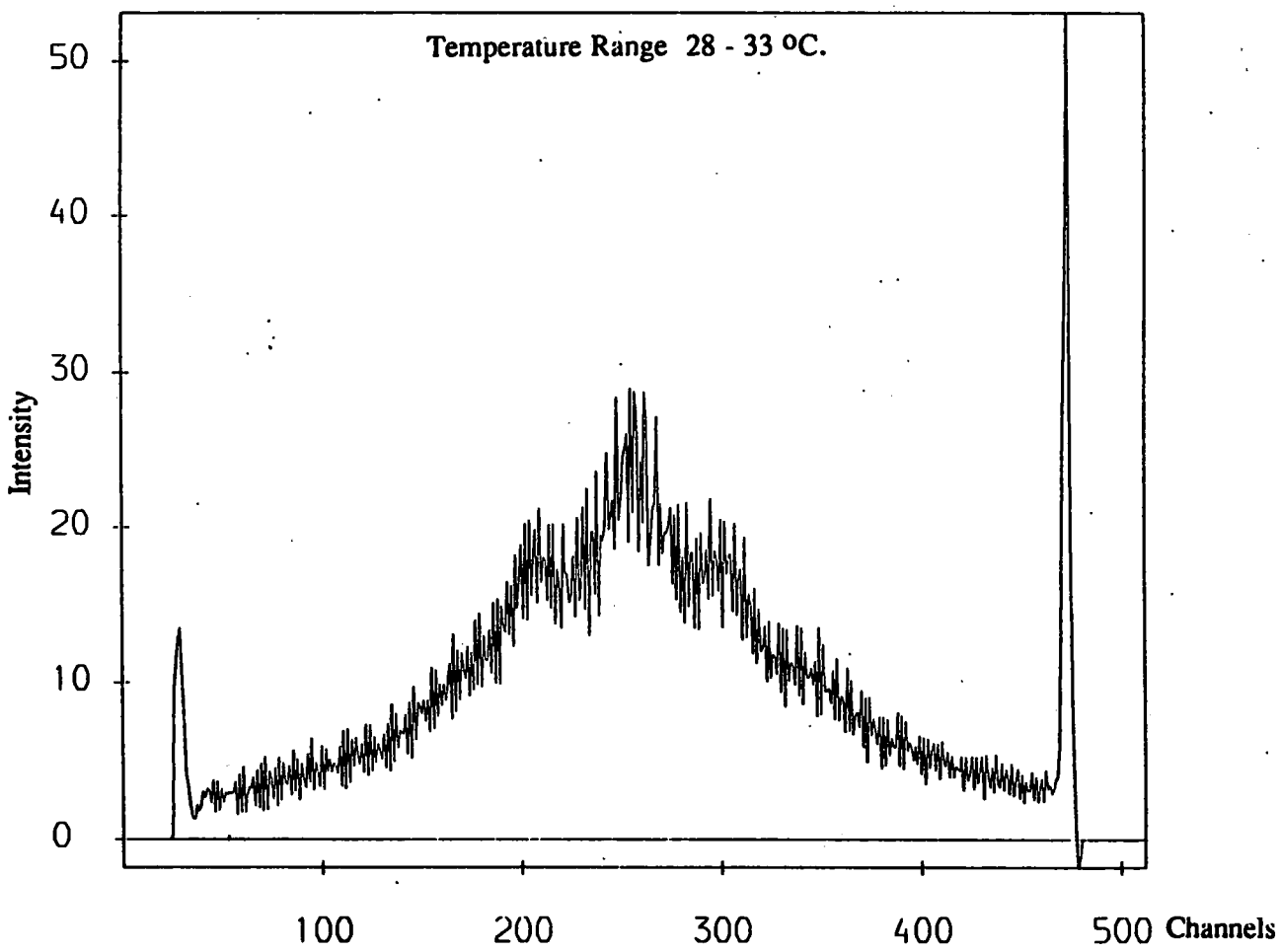

Figure 3.9 Vertical integration of the 365 Å layer line of the rigor pattern in the temperature range 28 - 33 ^{0}C, in A/2 solution The y axis units of intensity are arbitrary

giving a profile of the peaks of intensities being studied). From these figures it can clearly be seen that as the temperature is increased the sharpness of the off-meridional peaks (which occur in the region of channels 200 and 300) on the layer line also increases.

Horizontal integrations of vertical slits were performed axially along the meridional patterns and the spacings and intensities of the reflections were measured. At all temperature ranges studied no spacing changes were found. However, there was found to be a change in the intensity of the 144 Å myosin reflection with increasing temperature. Unlike Huxley's relative intensity ratio $I_{1,1}/I_{1,0}$ (section 3.2.2) no protocol exists for measuring the relative intensity of the 144 Å reflection. It was therefore decided to divide the measured peak height of the 144 Å reflection by that of the 220 Å actin axial reflection, and thus create a relative intensity ratio I_{144}/I_{220}.

Table 3.6 shows the I_{144}/I_{220} intensity ratios for the temperature ranges studied. It may be seen that a definite trend exists with I_{144}/I_{220} increasing with increasing temperature, and that the largest increase between the 18-27 ^{0}C and 28-33 ^{0}C. This corresponds to the definite temperature transition identified with potential measurements.

Temperature	5-11 ^{0}C	18-27 ^{0}C	28-33 ^{0}C
I_{144}/I_{220}	1.75	1.86	2.20

Table 3.6 Relative intesities I_{144}/I_{220} at different temperatures in rigor muscle.

3.2.2 EFFECTS OF LOW LEVELS OF ATP AND SODIUM PYROPHOSPHATE ON EQUATORIAL X-RAY PATTERNS IN RABBIT MUSCLE

Titrations of ATP and sodium pyrophosphate (PPi), from 50 μM to 10 mM, were conducted on small bundles of glycerinated rabbit muscle fibres and the equatorial reflections were studied. This was done in order to see if there are any spacing or intensity changes of the equatorial reflections accompanying the dramatic lowering of charge on the muscle lattice and myosin gels when only small amounts (micromolar to 0.1mM) of ATP or PPi are added to a rigor solution (A/2, Table 2.3), as reported by Bartels et al.(1993) (section 4.3). Only the 1,0 and 1,1 equatorial reflections were studied, these correspond to the two planes of the hexagonal filament lattice. The spacing of the 1,0 reflection, d(1,0), was taken to define the dimension of the filament lattice and is given in Ångstroms (Å). The relative intensities of the two reflections were determined by performing a vertical integration of a horizontal slit across the equatorial and measuring the peak heights, after a background had been fitted. Figure 3.10 gives a typical example of a vertical integration of the 1,1 and 1,0 equatorial peaks.. The ratio of the two intensities was found by cutting the traces of peaks out of card and weighing them. In some cases the position of the beamstop obscured part of the 1,0 peaks. In these cases the traces of the missing part of the peaks were estimated assuming symmetry. Some patterns displayed large negative intensities close the the beamstop, Wim Bras of the Daresbury laboratory (Private communication) says that this sometimes occurs due to over subtraction of the back ground caused by errors in the normalisation in the computor programe. Bras also states that this only affects very weak intensity data.

For these experiments long sarcomere lengths (S > 3.4 μm) close to zero overlap were used in order to investigate any myosin - myosin interaction. Elliott, Bartels and Hughes (1985) report that the spacing between the muscle filaments is sensitive to the myosin charge, and at such long sarcomere lengths the situation is not complicated by

A/2 Solution + [Ligand]	ATP (+ 4 mM EGTA) Ionic strength for ATP / EGTA	PPi Ionic strength for PPi
50 μM	0.0685	0.0575
0.1 mM	0.0687	0.0577
0.2 mM		0.0579
0.5 mM	0.0698	0.0585
1.0 mM	0.0711	0.0596
2.5 mM		0.0726
5.0 mM		0.0777
10 mM	0.1329	0.107

Table 3.7 Ionic strengths of solutions used in the PPi and ATP titrations. ATP and PPi were added to the rigor solution A/2 and adjusted to pH = 7 with KOH. In the case of ATP, 4 mM EGTA was added to chelate calcium ions

actin-myosin interactions. It should also be noted that the charge on the myosin filaments is not dependent on sarcomere length, Naylor et al.(1985). Table 3.6 gives concentrations of ATP and PPi, and the ionic strengths of the solutions used. These solutions are the same as those used by Bartels et al (1993) in which the charge measurements were conducted.

The ATP titration of relaxed muscle was first attempted using the GX 13 laboratory X-ray set. A typical exposure time required for equatorial reflections using the GX 13 is in the order of 20 minutes, and it was found that at low levels of ATP the substrate is hydrolised rapidly by the enzyme so the muscle returns quickly to the rigor state. Thus it was not possible to be certain of the state of the specimen when trying to perform this experiment by diffusing in very low levels of ATP. In an attempt to resolve this problem the same experiment was conducted at the Daresbury synchrotron radiation source, where a typical exposure time required for equatorial reflections is in the order of 30 seconds. However, even with a much shorter exposure time it was found that muscle was partially returning to the rigor state with low concentrations of ATP. Although the data are presented here it should be noted that the lattice spacing and intensity ratios are equivocal and the data are only presented in order to illustrate the problems of this experiment. It should also be noted the experiment was only performed once, ie. n =1, due to the problems encountered. Additional intermediate concentrations of ATP than shown here were investigated, but these data have been omitted, as the equatorial intensities in these samples showed clearly that they had passed into the rigor state.

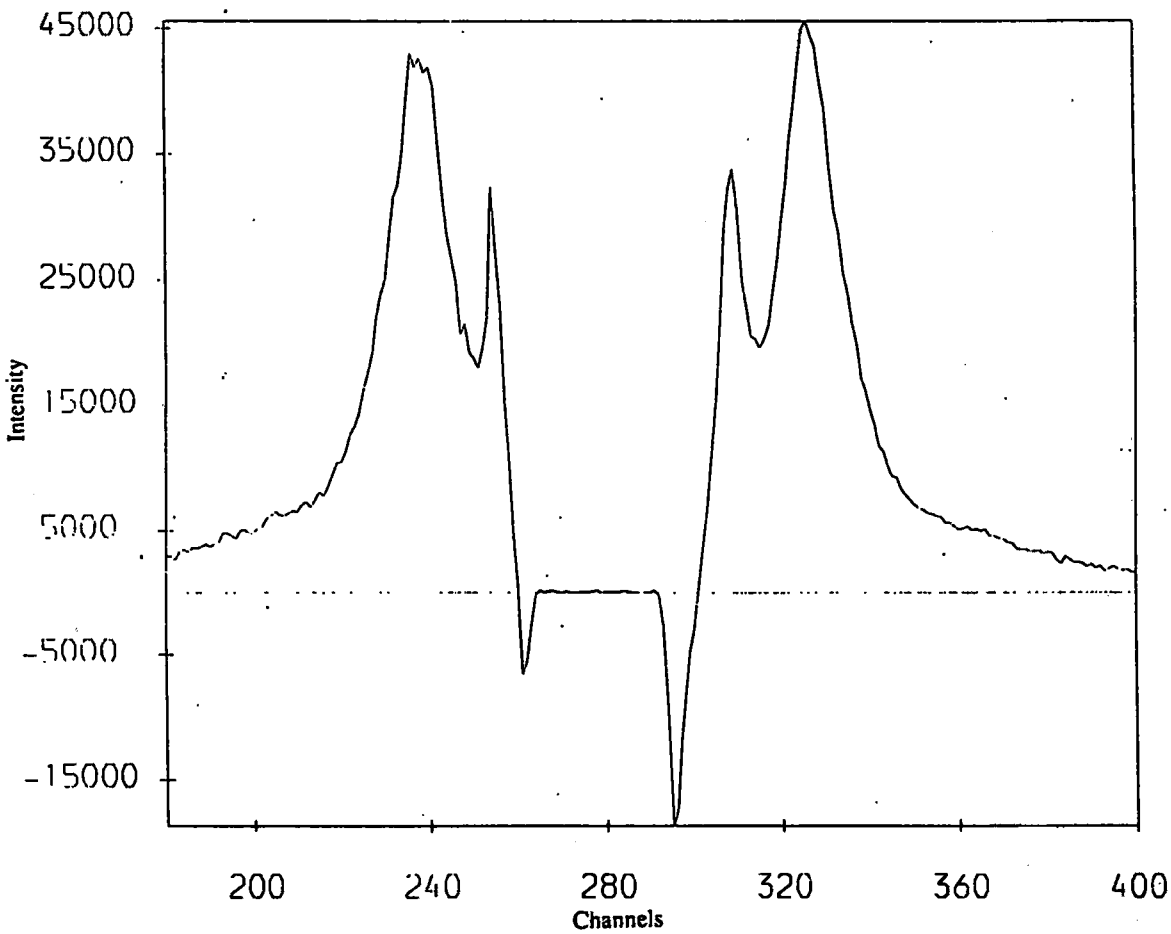

Figure 3.10 A horizontal integration of the equatorial 1,1 and 1,0 peaks of glycerinated rabbit muscle in A/2 solution + 1mM PPi. The y axis units of intensity are arbitrary. In this example the scatter from the back-stop has been removed completly, by the data processing program.

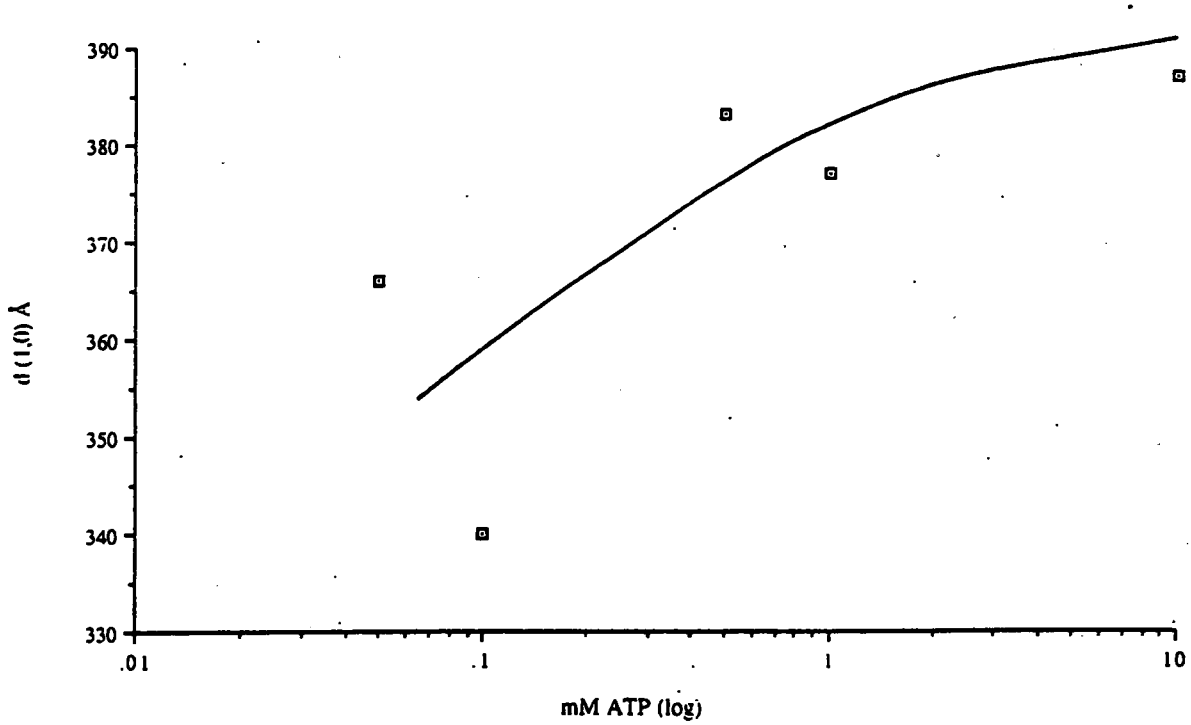

Figure 3.11 Lattice spacing, d (1,0), taken form the equatorial pattern of glycerinated rabbit muscle in A/2 solution + ATP and 4 mM EGTA, plotted as a function of ATP concentration.

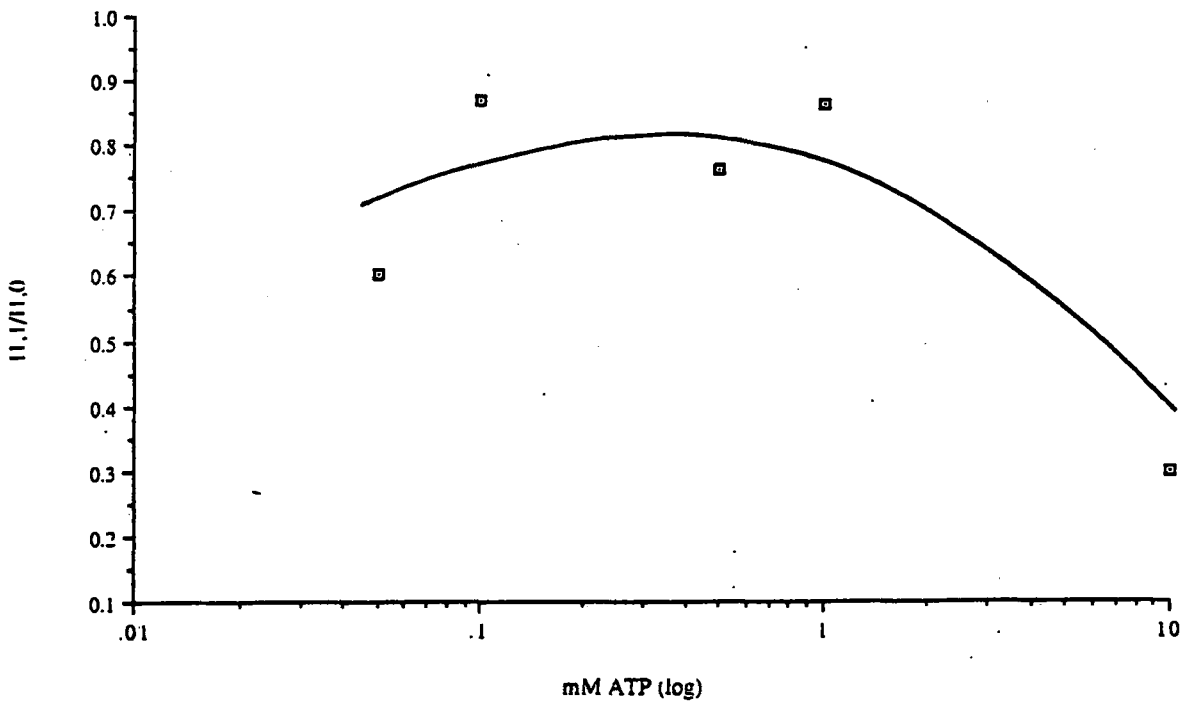

Figure 3.12 Relative intensities of the equatorial pattern ,$I_{1,1}/I_{1,0}$,of glycerinated rabbit muscle in A/2 solution + ATP and 4 mM EGTA, plotted as a function of ATP concentration.

Figure 3.11 shows a plot of the lattice spacing, d (1,0) of the equatorial reflections, as a function of ATP concentration. The line of best fit is drawn by eye, as are all lines of best fit presented in this Section.There appears to be an increase in the lattice spacing with an increasing concentration of ATP, with a minimum value of 366 Å at 50 μM and a maximum value of 387 Å at 10 mM. The lattice spacing value at 0.1 mM ATP (340 Å) illustrates the problem with the data. It may be that this is a spurious point and that in fact the line of best fit is more horizontal that that shown.

Figure 3.12 shows a plot of the relative intensity ratios ,$I_{1,1}/I_{1,0}$, as a function of ATP concentration. As the concentration increases the ratio rises to maximum values between 0.1 and 1 mM ATP (between 0.76 - 0.87) and then falls off sharply at 10 mM ATP (0.30).

Due to the problems encountered with the use of small amounts of ATP, it was decided to concentrate on using the ATP analog PPi, as this also known to lower the charge on the myosin filaments (see above) and would not introduced the problems outlined above.

Two successful experimental runs, hereafter called A & B, were completed using PPi. Two separate muscle specimens were used with S = 3.4 and 3.7 μm respectively. Due to computing problems at the Daresbury laboratory beyond the author's control the data for 0.1 and 2.5 mM PPi concentrations in run A were lost. However it is felt that this does not affect the overall pattern of the results presented here. Figure 3.13 shows a plot of d (1,0) as a function of PPi concentration for runs A and B, the rigor values (about 380 Å) are plotted on the y - axis. Although there is some variation in d (1,0) between runs A and B at nearly all the concentrations studied, a clear trend may be identified. Here it may be seen that on addition of between 0.1 μM and 1 mM of PPi to the rigor solution the lattice spacing increases to between 430 to 450 Å, where it is at a maximum at about 200 μM. On increasing concentration of PPi there is a linear decrease of the lattice spacing, and at 10 mM the value is at about the same as in rigor.

Figure 3.14 a) shows the relative intensity ratios, $I_{1,1}/I_{1,0}$, for runs A and B plotted as a function of PPi concentration. Here again, the rigor values are plotted on the y - axis and there is difference between the values given of A and B but a clear trend exists. On addition of PPi to the rigor solution the value of $I_{1,1}/I_{1,0}$ increases rapidly until it reaches a maximum value (about 1.4) between 200 to 500 μM, before falling off rapidly and reaching approximately the same value as that of rigor (about 0.7) at 10 mM. Thus a clear bell-shaped curve may be identified. The intensity data from the ATP titration (see Figure 3.12) were also plotted on the same graph (Figure 3.14 b)in order to determine if the same trend could be identified. As can be seen, although the actual values are lower and the data points are fewer a similar trend would seem to exist. If indeed there were more data points it may be that a much more pronounced bell shaped curve similar to that identified in Figure 3.14 exists for the ATP intensity data.

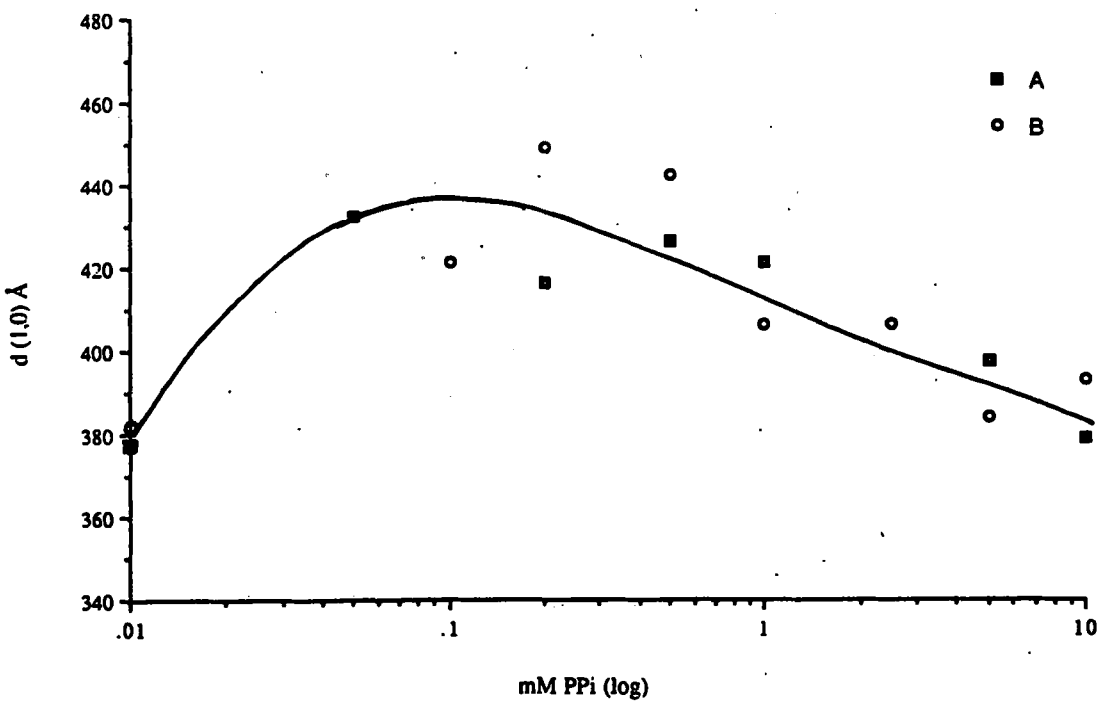

Figure 3.13 Lattice spacing, d (1,0), taken form the equatorial pattern of glycernated rabbit muscle in A/2 solution plotted as a function of PPi concentration

a)

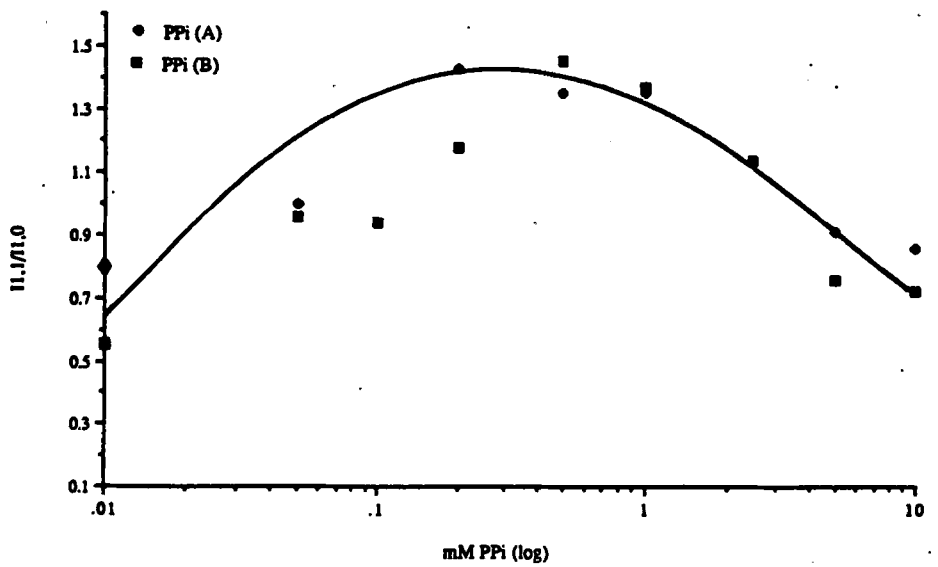

b)

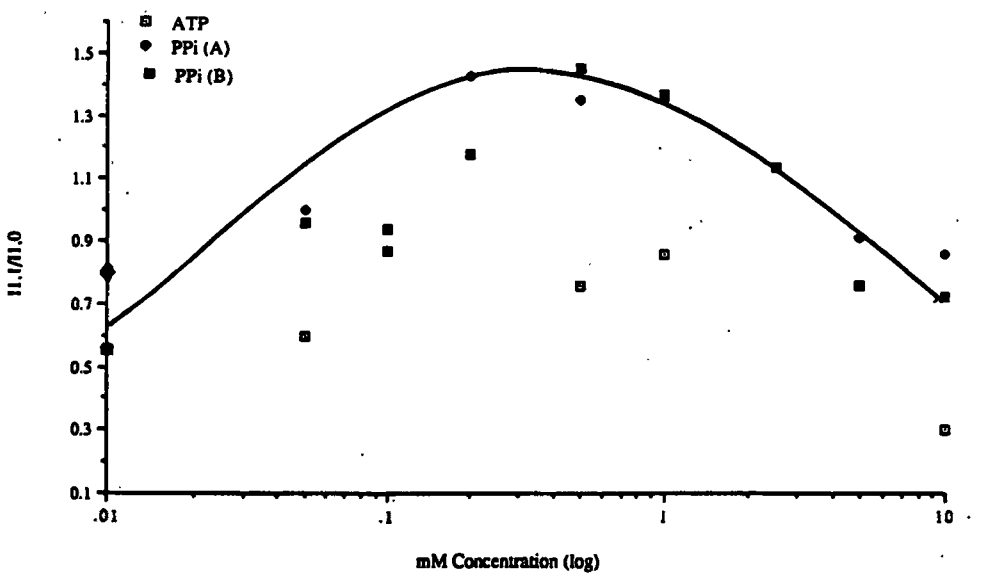

Figure 3.14 a) Relative intensities of the equatorial pattern, $I_{1,1}/I_{1,0}$,of glycerinated rabbit muscle in A/2 solution plotted as a function of PPI concentration. b) For a comparison the intensity data from the ATP titration are plotted on the same graph)

3.2.3 EFFECTS OF PPI ON MERIDIONAL PATTERNS IN RIGOR MUSCLE

A titration of PPi on the meridional X-ray pattern of rigor muscle was conducted in order to determine if effects occur to the spacings of the meridional reflections or their intensities, as was found on the equatorial reflections (section 3.2.2). Small bundles of glycernated rabbit psoas muscle were used with sarcomeres at rest length (S = 2.4 - 2.6 μm), in order to obtain meridional patterns with a high degree of sampling along the layer lines. The solutions used were the same as those given in Table 3.6, and the concentration range was from rigor (no PPi) up to 10 mM PPi..

Vertical integrations were performed axially along the meridional patterns and the spacings and intensities of the reflections were measured. Figures 3.15 and 3.16 show two such integrations in rigor (A/2 solution) and A/2 + 50 μM PPi respectively. At all concentrations studied no spacing changes were found. However as can be seen from these figures there is a change in the intensity of the 144 Å myosin reflection on addition of PPi. The relative intensity ratio I144/I220 was used as before (section 3.2.1).

Figure 3.17 shows the I144/I220 intensity ratio plotted as a function of PPi concentration, with the rigor value plotted on the y - axis. It may be seen that a definite trend exists with I144/I220 reaching a maximum value of 2.63 on the addition of 50 μM PPi

and decreasing steadily on increasing concentration.

Here again due to limitations of beam time allocation at the Daresbury laboratory the experiment was only performed once. Two data points were lost as poor patterns were obtained at 100 and 200 μM PPi because of badly diffracting specimens. However, unlike the ATP equatorial titration, it is felt that the data are good in that the trend identified is similar to the discovered with the PPi equatorial titration. The intensity ratio rises to a

maximum from the rigor value at μM concentrations of PPi and falls off at higher concentrations, with the value of the intensity ratio at 10 mM PPi approache that of the value in rigor.

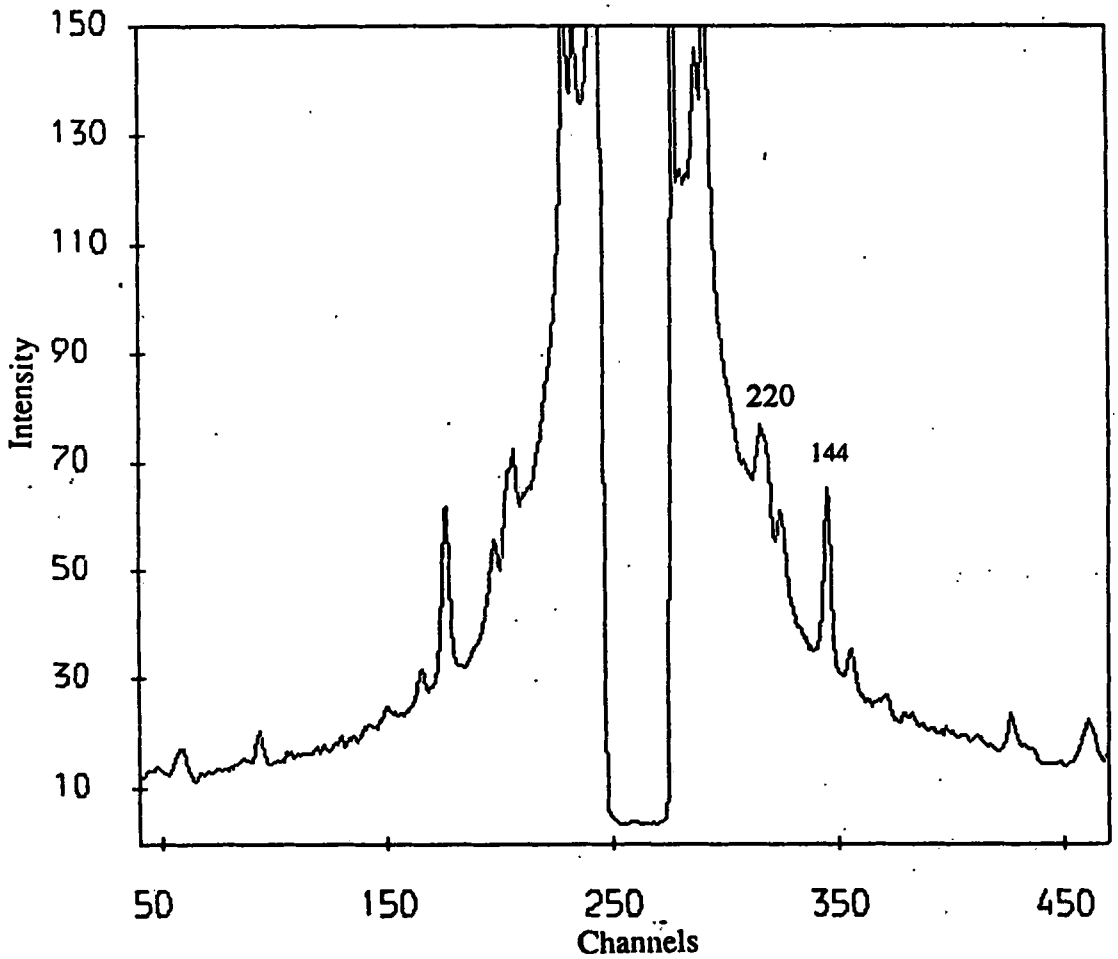

Figure 3.15 An axial vertical integration taken from the meridional pattern of glycernated rabbit muscle in A/2 solution. The y axis units of intensity are arbitrary.

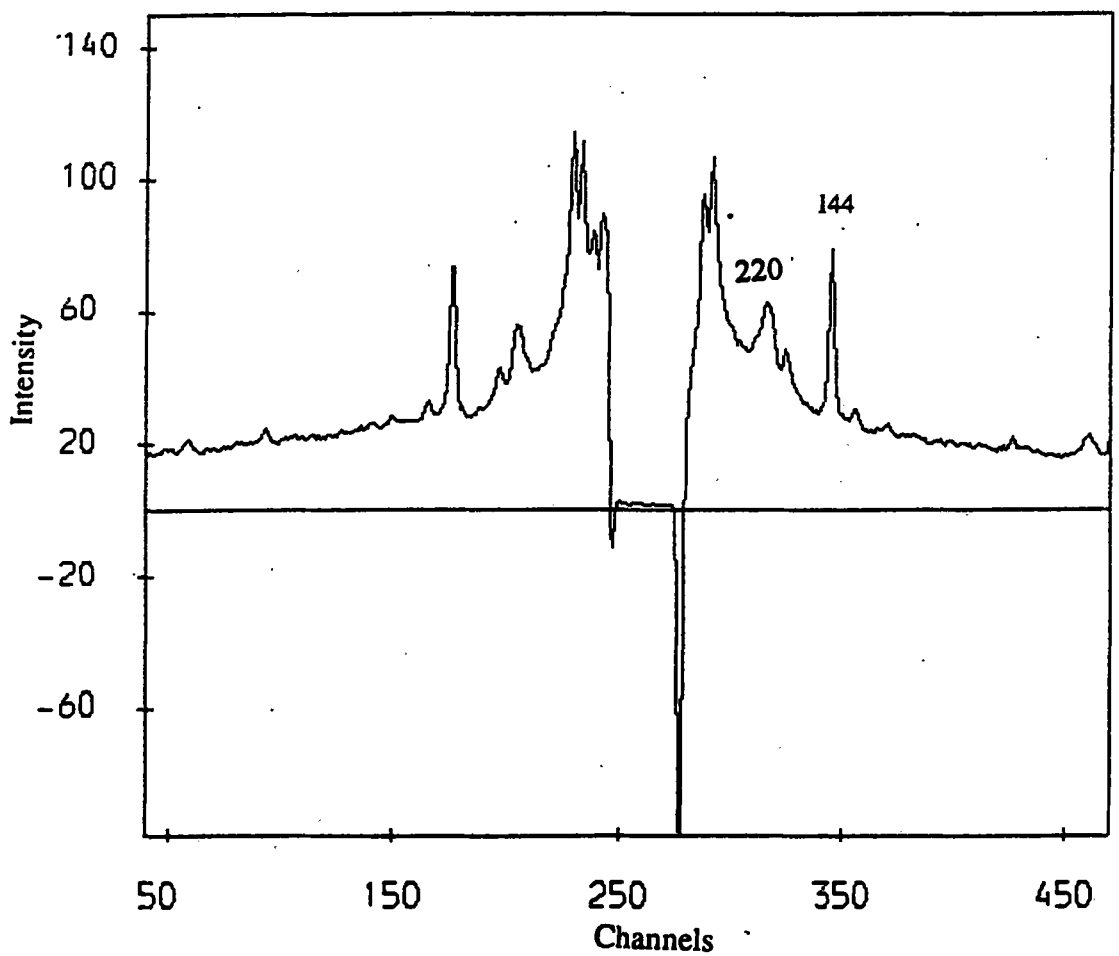

Figure 3.16 An axial vertical integration taken from the meridional pattern of glycernated rabbit muscle in A/2 solution + 50 μM PPi. The y axis units of intensity are arbitrary.

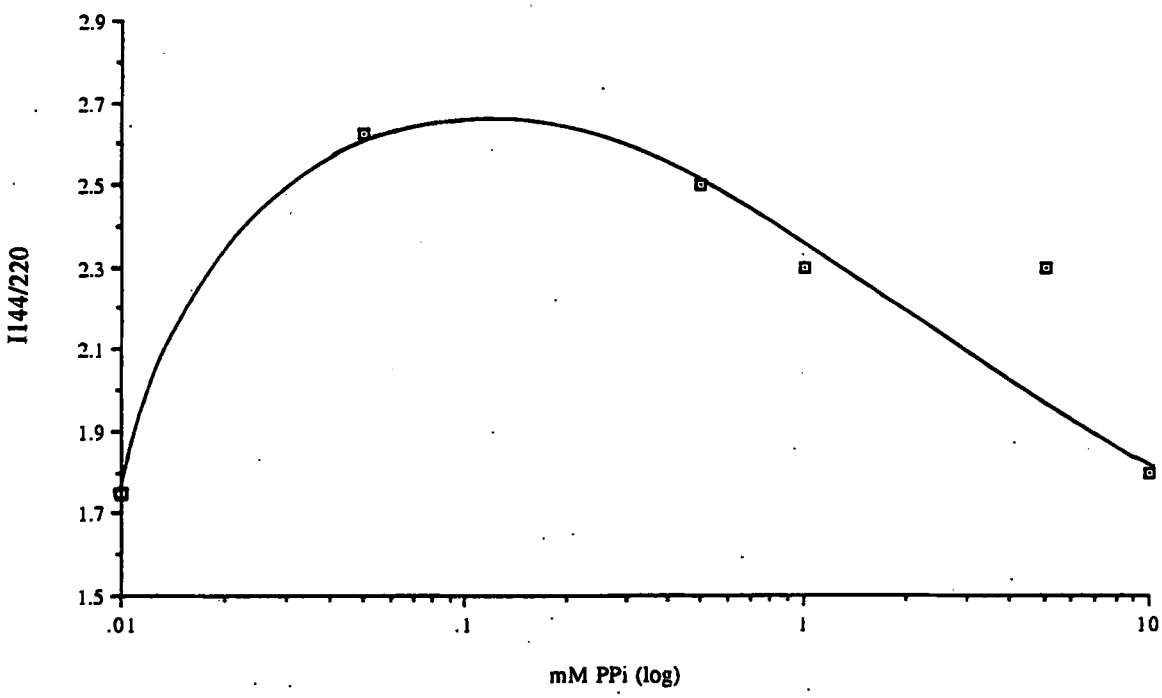

Figure 3.17 The relative intensity ratio, I144/I220, from the meridional pattern of glycerinated rabbit muscle in A/2 solution plotted as a function of PPi concentration.

CHAPTER 4

DISCUSSION

4.1 THE TEMPERATURE DATA

4.1.1 ION BINDING MODELS IN MUSCLE AND CORNEA

The decrease in the measured potentials with increasing temperature observed in rigor and relaxed muscle (section 3.1.2) and in corneal stroma (section 3.1.3), may be explained in terms of the ion binding (or ion association) models proposed by G.F. Elliott, Elliott (1973), Elliott (1980), Elliott et al.(1980), Elliott, Bartels & Hughes (1985), Bartels & Elliott (1985) and Bartels et al. (1993).

In the case of muscle, Bartels & Elliott (1985) observed a 40% increase in the A-band potential from the relaxed to the rigor state at room temperature (compare the results in section 3.1.2). This increase occured in both glycerinated rabbit muscle and chemically skinned rat muscle in solutions of different ionic strengths. This effect was independent of sarcomere length. In the relaxed state the associated calculated charge was given as 80 - 90 electrons per molecule (e/molecule) and 112 - 126 e/molecule in rigor, an increase of 32 - 36 e. This increase in charge was too large to be explained in terms of the binding of two ATP ligands (6-8 e) to the myosin molecule. Moreover, these ligands are known to be bound to myosin in the relaxed state, and released as the muscle passes in to contraction or the (ATP-free) rigor state. It was stated by the authors that the consequence of this effect would be in the reverse direction to that observed, and that the charge reversal must be amplified in some way. As the increased charge in rigor was not dependent on sarcomere length, and therefore independent of filament overlap, the actin-myosin cross linking would

seem to have no relation to the effect. They speculated that the ion-binding properties of myosin molecules might be modified as a result of some initiating event between the relaxed and rigor states, thus giving rise to the observed change in charge.

Bartels and Elliott (1985) then tried to establish where in the A-band the charge amplification takes place and by which mechanism it is initiated. As myosin is the main constituent of the thick filament in the A-band, the authors postulated that it is likely that the charge amplification occurs on the myosin molecules themselves. Further evidence for this comes from fluorescence labelling studies of Scordilis et al. (1975) and Scordilis (1976, unpublished). In these studies synthetic thin filaments (polymerized G-actin) and synthetic thick filaments (aggregated myosin) were used. The synthetic thick filaments were also cleaved with the enzymes trypsin and papain into their S1 head, S2 rod and LMM constituent parts. The fluorescence of the electrofluorochrome CC-6 was used as an indicator of the Donnan potential measured in glycerol-extracted muscle with microelectrodes. Scordilis found that on addition of ATP the fluorescence decreased by 30 % only on the S2 portion of the myosin molecule. As this observation closely correlates with the observed decrease in charge in the A-bands of relaxed muscle, it would seem likely that the S2 portion of myosin is the site where the charge amplification takes place.

As muscle passes from the rigor to the relaxed state, the implication is that the binding of ATP to myosin causes either the release of cations or the absorption of anions . A possible ion-binding mechanism which may explain the charge amplification, depends upon the theoretical model of H. A. Saroff (Loeb & Saroff, 1964 , Saroff, 1973) for chloride binding to ribonuclease. Saroff suggested that anions are hydrogen-bonded to clusters of charged side chains along the peptide chain. In the case of ribonuclease, Loeb and Saroff suggested a cluster of three positive charges (protonated amino groups) with two carboxyl groups close enough to form hydrogen bonds. The chloride competes with the carboxylate ions to form hydrogen-bonds with the three amino groups and one carboxyl group in a tetrahedral array. Elliott et al. (1985) proposed that the sites at which such interactions occur should be called "Saroff sites", and suggested that similar Saroff sites

occur in the myosin filament, either between the myosin rods of different myosin molecules or between the two polypeptide chains of a single myosin molecule (Figure 4.1). Whichever happens to be the case Bartels & Elliott (1985) argue that mechanical stress transmitted along the shafts of the molecules or between the two chains in a single molecule, may make small variations in the structure of the intermolecular (or interchain) Saroff sites. Saroff (1973) also suggested that these sites are linked, thus implying that the ion binding may be cooperative in nature.

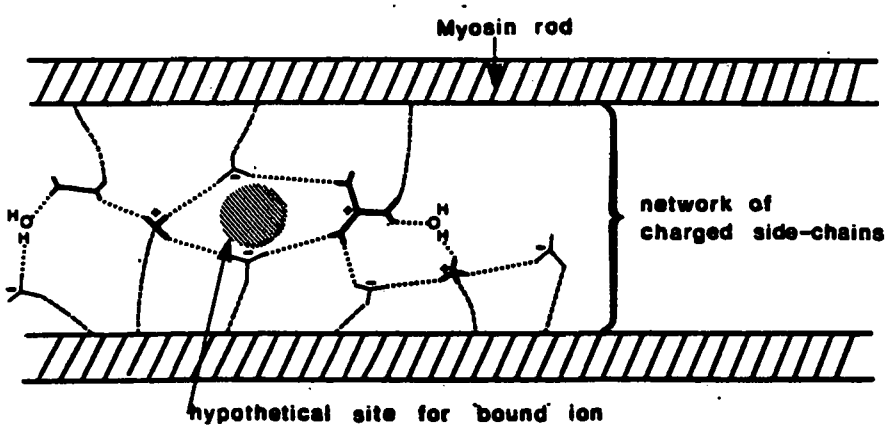

Figure 4.1 A schematic diagram of a hypothetical Saroff site, the vertical scale has been exaggerated to show the network. (After Bartels & Elliott, 1985).

As to the question of the charge effect between the rigor and relaxed states being due to either the release of cations or the absorption of anions, Collins & Edwards (1971) Naylor et al. (1985) and Bartels & Elliott (1985) all report that the measured potentials in glycerinated and chemically skinned skeletal muscle become more negative as the ionic strength of the bathing solution is decreased, both physiological states. For example, Bartels & Elliott (1985) using glycerinated rat muscle report E_A and E_I as -5.3 and -2.7 mV for rigor muscle in a 100 mM KCl solution, and E_A and E_I as -27.1 and -20.1 mV in a 10 mM KCl solution. Scordilis (1976, unpublished) also demonstrated that the fluorescence of a CC-6 containing synthetic myosin filament suspension changed linearly with the magnitude of the Donnan potential as the ionic strength of the bathing medium was changed.The decrease in fixed charge concentration with decreasing ionic strength would mean that more cations would be bound with the lowering of ionic strength. This seems unlikely and is more probable that it is anions that are bound due to the process of Mass Action..

Further evidence for the absorption of anions to proteins comes from the radioactive isotope labelling studies in corneal stroma of Hodson et al. (1992). Hodson et al. (1992) used the radioisotope $Na^{36}Cl$ in order to investigate the anomalous Donnan-osmotic swelling pressure phenomenon in corneal stroma. This was done by measuring the amount of activity before and after the corneas had been bathed in a $Na^{36}Cl$ solution and then calculating the intrastromal chloride. The authors report that the intrastromal chloride was consistently higher than that predicted by Donnan theory and conclude that the "missing" chloride ion concentration (the loss of activity which can not be attributed to the decay of the radioisotope) provided positive support for the hypothesis of Elliott (1980) and Elliott et al. (1980). In these papers Elliott suggests that a fraction of the intrastromal chloride ions bind to the corneal stromal matrix and in doing so provides the NaCl-dependent increase in fixed negative charge. The chloride-binding and resulting increase in charge are partly

responsible for the driving force for swelling, the swelling pressure.Given the evidence of Hodson et al.(1992), it would seem likely that the increase in negative charge concentration in muscle between the relaxed and rigor states may also be due to the absorption of anions. As yet it is not clear which anion or anions is responsible for the charge effects observed in muscle. Bartels et al. (1993) suggest the phosphate ion as an obvious candidate due to its importance in muscle during the hydrolysis of ATP. The chloride ion is also a possibility, for which there is some evidence. Millman & Irving (1988) measured the lattice spacing of chemically skinned frog muscle which had been osmoticaly shrunk from X-ray equatorial patterns. This was done in order to investigate the nature of the electrostaic forces acting on the filaments. They found that the lattice spacing in a chloride relaxing solution was on average 1.7 ± 0.4 nm larger than that in a relaxing solution based on K-acetate of the same ionic strength. The authors comment that the increase may be due to changes in filament charge, possibly because of chloride binding. Here the physical characteristics of the chloride and K-acetate ions are different. Chloride are small inorganic ions, wereas K-acetate are large organic ions. It is probably difference in size which results in differential binding. Bridgman, Elliott & Bartels (unpublished results) measured the fixed charge concentration in the A-bands of muscle fibres, in acetate- and chloride-based rigor solutions of the same ionic strength. The protein charge in the acetate-based rigor solution was found to be one half of the charge in a similar solution based on chloride. This suggests that the larger organic ions do not absorb so strongly on to the Saroff sites as does the smaller inorganic chloride ion.

In corneal stroma the constituent proteins and their structure differ from that found in muscle. In corneal stroma (Hodson et al., 1992) the cation exchange ability of the connective tissue creates a Donnan-osmotic swelling pressure and a Donnan electrical potential, these generate passive swelling called gel pressure (Hodson, 1971, Hodson et al. 1992). In their 1992 paper Hodson et al. confirm the gel pressure arise from the fixed negative charges of the stromal matrix had two contributions, one is from the anionic sulphonic and carboxylic acid groups of the glycosaminoglycans and the other is a charge

resulting from the transient binding of free chloride ions to a ligand. Each contribution to the charge is 45 and 55% respectively. Although the proteins to which chloride bind have as yet not been formally identified, it has been established that the collagen molecules are not responsible. Hodson et al. (1992) found that by treating corneal stroma with 4 M-guanidine hydrochloride the intrastromal charge had been dramatically reduced with no evidence of chloride-binding and concluded that nearly all the chloride binding ligand had been extracted. All of the Type 1 collagen remained in the tissue after guanidine extraction and therefore could not be the major chloride binding ligand. This evidence would suggest that the site at which ion binding is taking place may be the glycoproteins. In this system, the chloride-binding protein Hodson et al. (1992) suggest has an important physiological role, as it acts to buffer the tissue swelling pressure against changes in the ionic medium that is in contact with the eyeball.

Both muscle and cornea belong to a group of systems identified by Elliott (1968). Such systems are formed from arrays of filaments or fibrils, which are polyelectrolytic in nature and therefore bear a net electrical charge at physiological pH. In muscle these are the myosin and actin containing filaments, and in corneal stroma the collagen fibrils. Surrounding these cylindrical charged filaments or fibrils there exist electrical fields (Elliott, 1968, Millman & Nickel, 1980, Elliott & Bartels, 1982 and Naylor, 1982) which give rise to electrical double layer forces (See also for example, Alexandrowitz & Katchalsky, 1963). Each filament or fibril has an electrically effective surface and a potential well exists between the neighbouring cylinders, the depth of which has been calculated to be about 50-100 mV in muscle (Elliott & Bartels, 1982, Elliott, 1992). Swelling is characteristic of such systems and the electrostatic repulsion between the filaments or fibrils is the driving force of the swelling. In some systems there may be cross-links between the charged cylinders (eg rigor muscle) which will alter the gradient and shape of the potential well, the swelling pressure of the system is directly related to the potential difference between the depth of the potential well in the lattice and the bathing medium surrounding it (Elliott & Bartels, 1982). The elastic properties and tensile strength of the cross-links are also important in

determining the extent of swelling.

One may hypothesize that in such systems the anions are hydrogen-bonded to the electrically-effective surfaces of the binding proteins and as such are governed by Boltzmann's theorem, and thus as the temperature of the bathing medium is increased the weakly-bound anions are released. At lower temperatures such systems are prone to ion absorption that will increase the charge, because the anions will then have less thermal energy to escape from the absorption sites.

4.1.2 ANION RELEASE WITH INCREASING TEMPERATURE IN MUSCLE

The decrease in charge observed with increase in temperature in muscle (Figure 3.2) is consistent with the ion binding (or ion association) models proposed by Elliott (section 4.1.2).

In relaxed muscle, since the temperature reduction of the A-band potential in the relaxed state appears to coincide with the appearance of the myosin layer lines (see below), it seems likely that the two observations are connected, and that the layer lines appear when the charge falls. The weakening of the layer lines suggests that the myosin heads are disordered and that they may lie some way from the filament backbone (Offer, 1987). However, there is some disagreement between several of the X-ray laboratories that are concerned with the layer line effect as to the precise temperature at which the layer lines start to disappear. The layer line data in the literature, taken as a whole, suggests that the myosin layer lines in relaxed rabbit muscle are well developed at 25 ^{0}C, this is agreed by all authors (Wray 1987, Wakabayashi et al., 1986, Lowy et al., 1991 and Poole & Popp [unpublished]) The data of Lowy et al. (1991), which are published in greatest detail, show that in all the three muscles they examined, the maximum layer line pattern was not established until the temperature reached 18 ^{0}C. Clearly more X-ray data are needed to establish the exact temperature transition.

Although the temperature transition in the charge-measurement data in relaxed muscle is not as clearly defined as in rigor muscle (section 3.1.2), the effective temperature range is very similar (between about 20-25 ^{0}C) to the X-ray data. This indicates that in relaxed muscle the ion binding process is a cooperative one, thus being consistent with the ideas of Saroff. It may be postulated that as the bound ions are released the mechanical stress transmitted along the shafts of the myosin molecules is also reduced. The reduced charge also restores order to the filament lattice as the heads move back towards the

backbone. This mechanism may also explain the disappearance of the myosin layer lines. From a thermodynamic point of view one would assume that if there was an input of thermal energy into a system, there would be increasing disorder. For example, in the case of the relaxed filament lattice one might expect an increase in the Brownian motion of the myosin heads with increasing temperature. This might result in weaker myosin layer lines of the X-ray pattern. This is not the phenomenon that is observed however. It would seem that the input of thermal energy is used to remove bound anions which at lower temperatures do not posse enough thermal energy to escape from the Saroff sites, and that excess charge acts as a disordering agent in relaxed muscle.

In rigor muscle the charge-measurement data indicate that ions bound to the myosin molecules are released between 27.5 - 30 ^{0}C. This temperature transition is more clearly defined than in relaxed muscle and gives a better indication that the anion binding process is a cooperative one, in that the Saroff sites are linked. Given the ordering of the A-band lattice with increasing temperature and the accompanying drop in charge in relaxed muscle, one might have expected a corresponding increase in the ordering of the A-band lattice in rigor. In the single experiment that was possible because of beam time limitations, a slight increase in order of the meridional pattern was observed at low ionic strength (section 3.2.1), with an increase in the sharpness of the off meridional peaks of the 365 Å actin layer line and an increase in the intensity of the axial 144Å myosin reflection as indicated by the I_{144}/I_{220} ratio. However, the experiment was only performed once and this raises two possibilities. Firstly it may be that the effect is artifactual. If this is indeed the case, then it may be argued that although there is a decrease in charge, the mechanical effect generated by the cross linking between actin and myosin in the rigor state is much greater than any effect generated as a consequence of the release of bound anions with increasing temperature. Secondly, if the observed change is not an artifact, then one may ask why is there only a change at low ionic strength ? Here there are a number of possibilities which will only be considered briefly. At low ionic strength there are less ions in solution in proportion to the protein concentration, and it may be that a specific species of

anion has a different binding affinity at different ionic strengths. It may also be that two different species of anions have different binding affinities, one being released at low ionic strength and the other at the higher ionic strength. Whichever happens to be the case, the release of anions will lower the net fixed electrical charge on the proteins, as occurs at higher ionic strength.

The axial spot of the 365 Å actin layer line is generally supposed to give the true repeat of the actin double helix (Haselgrove & Rodger, 1980, Squire, 1981). As the off-meridional peaks are seen to sharpen with temperature, this indicates that the order of the actin filaments is increased as the charge falls. As many of the myosin heads are attached to the actin filaments in rigor, it may be that the fall in charge releases the mechanical stress on the S2 portion and changes the conformation of the heads. This in turn might also release a certain amount of stress on the actin filaments, thus increasing their order. Much more work would be needed to establish this hypoyhisis firmly, however.

The trend of the I_{144}/I_{220} ratio is consistent in nature with the trend of the measured potentials, both as a function of temperature. The maximum change in intensity from 1.86 to 2.20 occurs between the temperature ranges 18-27 ^{0}C and 28-33 ^{0}C respectively. This coincides with the temperature transition (27.5 to 30 ^{0}C) at which the potentials fall in rigor. The retention of the 144 Å myosin layer line in rigor muscle is not fully understood, although its presence is thought to indicate either a maintained backbone structure (Haslegrove, 1975), or a continued axial repeat for some or all of the detached myosin heads (Huxley & Brown, 1967). Here again the increase in temperature is increasing the ordering of either the maintained backbone structure or the heads, since the intensity of this reflection increases. If the intensity of this reflection is due to the order of the detached heads, again it may be that as the bound anions on the S2 portion are released the orientation of the free myosin heads change with the accompanying release of mechanical stress. Here again, much more work is needed.

In both relaxed and rigor muscle one may speculate that the increase in negative charge may itself cause the disordering of the muscle lattice through electrostatic charge interaction. This may occur as well as the setting up of mechanical stress between Saroff sites outlined above. The electrical double layer forces surrounding both the actin and myosin filaments are repulsive forces (the charge on the myosin filament being about three times greater than that of actin). These repulsive forces are balanced by net attractive forces. The attractive forces are comprised from two main components, firstly the weak intermolecular dipole-dipole interactions of Van der Waals forces which gives rise to net attraction between neighbouring filaments (Elliott, Bartels & Hughes, 1985). Secondly the elastic forces generated mainly by the M-line transverse connections which hold neighbouring filaments in axial register and determine their azimuthal orientations relative to one another (Knight & Trinick, 1987). There are also elastic forces from the actin and α-actinin proteins of the Z-line which is known to be dynamic during contraction (Squire et al., 1987). It is the balance between these two opposing sets of forces which gives the muscle lattice its stability. The extra charge seen below 20 -25 ^{0}C in relaxed muscle and below 27.5 to 30 ^{0}C in rigor muscle will increase the negative potential at the myosin filament surface and thus contribute to extra longitudinal electrical double layer forces between the filaments. This alters the balance between the attractive and repulsive forces which could destabilise the lattice causing disorder.

4.1.3 ANION RELEASE WITH INCREASING TEMPERATURE IN CORNEA

The nature of the decrease in charge with increasing temperature (Figure 3.4) in corneal stroma is different to that which occurs in muscle. The linearity between charge and temperature and the fact that there are only two mono-valent ions (Na, Cl) in the bathing medium would seem to indicate that the anion binding is simpler and non-cooperative. However, the basic process is probably similar in that the chloride ions are hydrogen-bonded onto networks of charged side chains of the binding proteins and released from these sites when they gain enough thermal energy.

The detailed structure of corneal stroma is still not known. Models broadly fall into two categories, firstly there are those in which the charged glycosaminoglycans surround the collagen fibrils (Hodson & Meenan, 1969, Myers et al. 1973). Here the protyoglycans and glycoproteins are attached to the collagen fibrils and project out from them.These models are consistent with charged cylinder ideas (section 4.2.1). The chloride ions bind to the electrically effective surface of the charged cylinders. As the highly charged glycosaminoglycans project out from the fibrils, the electrically effective surface will be further away from the surface of the cylinders than in muscle. As a result the potential gradient between the cylinders is probably not as steep as that which exists in muscle. The protein to which the chloride ions bind and thus the exact site of this component of the fixed stromal charge is unknown. Recent attempts to isolate this chloride binding ligand in human and bovine stroma have been made by Guggenheim & Hodson (1994 a) and Guggenheim & Hodson (1994 b). By separating extracted proteoglycans and non-proteoglycan stromal proteins the authors found that the non-proteoglycan fraction showed an elevated concentration of chloride binding when both fractions were labelled with ^{36}Cl. However, the non-proteoglycan fraction contained up to fifteen or more proteins, and studies are currently being conducted to try and further isolate this protein.

The second group of models are ones in which the collagen fibrils are cross-linked by the proteoglycan chains (Hart & Farrell, 1969, Scott , 1991). In the theoretical Hart & Farrel (1969) model the collagen fibrils are linked radially by the two proteoglycan chains at regular intervals along the backbone of the fibrils. The chains are positioned at 60^0 intervals around the circumference of the fibrils. It is proposed that these chains stretch during swelling and that the magnitude of the stretching increases with the degree of swelling. The model proposed by Scott (1991) differs in that various species of proteoglycans form two types of duplex. It is proposed that with the first type the chondroitin sulphate and dermertan sulphate proteoglycan protein cores are bound to the periphery of the collagen fibril and that the chains from neighbouring fibrils then duplex together. The result is a linear array, tangential to the fibrils which could link a set of collagen fibrils at large separation. The second type of duplex is shorter, here the keratan sulphate proteoglycans span the gap between the equator of the fibrils. It is proposed that both types of duplex dissociate rapidly in response to swelling pressure. Moreover, this change is reversible so that the duplexes are able to form rapidly once the tension or pressure is released. There is some evidence of cross-linking from micrographs of swollen corneas (Meek, Personal communication). It has often been observed that the collagen fibrils do not swell in a uniform manner, this is thought in part to be due to the tissue only being able to swell in the thickness direction. Often the swelling is asymmetric and from X-ray data the increase in spacing of the fibrils is not enough to account for the amount of swelling of the whole tissue. From a number of micrographs it may be seen that there are small numbers of rows of collagen fibrils in close proximity in the thickness direction, thus implying that these fibrils are linked.

Elliott et al. (1980) argue that it is difficult to interpret the extent of the swelling phenomenon if there is very strong mechanical cross-linking between the collagen fibrils. It may be that the fibrils are indeed weakly cross-linked as implied by the evidence above, and that these cross-links are needed to maintain the critical separations between the fibrils. However instead of a strong mechanical bond between the fibrils it may be that the cross-

links are weak and break when swelling occurs. Why some of the linkages remain after swelling has taken place is not clear. If indeed there are weak cross-links, the charge cylinder models would still be valid as a first approximation (section 4.2). The fixed charges on the glycosaminoglycans and chloride ions surrounding each fibril would still repel each other, setting up an electrical double layer.

Hodson et al. (1992) calculate the value of the overall fixed stromal charge under normal physiological conditions as 40 mM, consisting of a 45% proteoglycan contribution of 18 mM and a 55% chloride binding contribution of 22 mM. Under normal physiological conditions the concentration of NaCl is 154 mM. They also report measured potential values of -3mV and -10.5 mV for stroma in solutions of 154 mM NaCl and 30 mM NaCl respectively, at room temperature (18 ^{0}C). The value of -10.5 mV in the 30 mM NaCl solution at 20 ^{0}C is in reasonable agreement with our observed value of -9.7 mV at 15 ^{0}C in 50 mM NaCl with the corresponding charge [Pr] = 109 $\pm$ 12 mM (Table 3.3, Figure 3.4). This experiment was conducted in a solution of low ionic strength in order to obtain large enough potentials to avoid ambiguity, and as such the calculated charge will also be greater. As the temperature is increased to 35 ^{0}C and the chloride ions are released, the charge has fallen to [Pr] = 52 $\pm$ 5 mM. This is a decrease of 47.7%, this is likely to represent the loss of chloride binding contribution to the overall fixed stromal charge as it is very close to the 55% calculated by Hodson et al. (1992). Although the decrease in charge is not exactly 55%, the figure lies within the bounds of experimental error as defined by the standard deviations of the calculated charges at 15 and 35 ^{0}C.

The decrease in the net fixed charge gives a negative temperature coeffcient (α'_p) to the swelling pressure. This is in agreement with the theoretical studies of Brenner and Parsegian (1976), and Kwok and Klyce (1990) who have shown that the anomalous temperature coefficient, measured by Hara & Maurice's (1972), can be explained on Donnan theory so long as the corneal stromal fixed electrical charge also has a negative temperature coefficient. This provides a mechanism for Hara & Maurice's (1972)

observations, which cannot be taken as a reason to doubt the dominance of the Donnan swelling pressure, as Hara and Maurice supposed.

4.1.4 COLD CATARACT EFFECT IN CALF LENS

The formation of the cold cataract is believed to be due to an isoelectric effect of one of the constituent lens crystallin proteins. The evidence for this is that T_{cat} is able to be altered by either a change in the cytoplasmic pH or by changing the ionic strength of the bathing medium. For example, Hammer & Benedek (1982/1983) report that a change in one pH unit shifts T_{cat} by 4 ^{0}C and Benedek et al. (1979) report a change in T_{cat} from 33^{0}C to 12 ^{0}C in bathing solutions based on 600 mM and 100 mM NaCl respectively.

By isolating the soluble fraction of the lens protein γiv-crystallin and measuring its light scattering properties above and below T_{cat} Siezen et al. (1985) discovered that there are two distinct populations of protein aggregates that cryoprecipitate below T_{cat}.This was done at various protein concentrations in which T_{cat} varied accordingly. At all concentrations and corresponding temperatures the two cryoprecipitated protein aggregate populations were found to have mean hydrodynamic radii of 90 Å and 20,000 Å below T_{cat}. These populations of aggregates and disaggregates were found to be reversible on temperature cycling. These protein aggregates scatter light differently in the solution and hence the lens nucleus of young mammals. It has been established that it is the phase separation of the population of the larger scatterers of γiv-crystallin that is responsible for the observed opacification in cold cataract (Benedek et al., 1979). This is because their mean size is comparable to the wavelength of light.

The concentration of calf lens γiv-crystallin in the nucleus is 26 g/litre, some 6.5% of the total concentration of crystallin proteins in the nucleus, 400 g/litre. The concentration of the larger scatterers with mean radii of about 20,000 Å is given as <0.1 % protein by weight (Siezen.et al.1985). The lack of any observed change in the measured potentials above and below T_{cat} in our experiments (section 3.1.4) indicates that any change in their Donnan charge concentration is too low to be detected by the microelectrode techniques

(section 2.2.3). In this polyelectrolyte system, the spatially-averaged change in the fixed charge that occurs due to phase separation of the 20,000 Å protein is too small to be detected by the tip of the electrode. The tip of the electrode only records a simple Donnan average potential of all the proteins (Elliott & Bartels 1982), and therefore is unable to detect small highly localised changes in relation to the rest of the proteins. It seems clear that this is the expanation of the failure to see any temperature effect around the transition temperature for cold cataract. It is of interest that a very dramatic physical effect in the lens occurs because of change in so small a fraction of the total protein.

4.2 CHEMICALLY-INDUCED DISORDERING OF THE MUSCLE LATTICE

Yagi (1992) described the effect of NEM on the X-ray observed structure of chemically skinned frog muscle. He found that on addition of 1 mM NEM to relaxed muscle the lattice became disordered, notably the myosin layer lines at both full overlap (S = 2.2 μM) and zero overlap (S = 4.4 μM) became weak. The intensity of the first myosin layer line at 429 Å decreased by 87%, and the myosin layer lines at 216 Å and 144 Å also decreased by 75% and 32% respectively. These effects were found to be irreversible. In the same study it was also found that on removal of ATP after the NEM treatment (rigor muscle, S = 2.2 μM), an increased sampling of the actin layer lines was observed but the myosin layer lines did not reappear. The 365 Å actin layer line was clearly sampled at the row-lines defined by the hexagonal filament lattice. Yagi's hypothesis was that this reagent is specific for the reactive sulfhydryl (SH) cysteine residues of the myosin S1 head, and possibly those of the thin filaments Thus, NEM caused structural changes to occur which result in a change in the helical order of the myosin heads around the thick filament backbone.

It is also known that NEM will interact with lysine and histidine residues (Mahler & Cordes, 1971, Table 7.4; Brewer & Riehm, 1967). Such reactions (alkylations) will probably change the net negative electrical charge on the proteins because both lysine and histidine are positively charged under physiological conditions, with pKs of 6.8 and 10.2 respectively. NEM could therefore change the pKs of these positively charged groups which might in turn increase the net negative charge of the proteins.

In our microelectrode studies under near identical conditions to that of Yagi (Table 3.4) it was found that the fixed charge in both the A- and I- bands increased after treatment with NEM. This occured in relaxed muscle and rigor muscle that had been previously been relaxed muscle treated with NEM. These observations suggest strongly that charge changes are responsible for the order-disorder state of the muscle, rather than the effect that Yagi postulates. Thus the weakening of the myosin layer lines caused by the disordering of the helical array of the myosin heads around the backbone of the filament is due to charge interaction, as discussed in section 4.2.1.

The increase in charge of the A- and I-bands in rigor, in both chemically skinned frog and glycerinated rabbit muscle (Table 3.5), is consistent with NEM increasing the net negative charge by deionizing some of the lysine and histidine residues. Yagi's observation of increased sampling of the actin layer lines may be explained in terms of the A- band bowing model of Ward (1987). From micrograph and X-ray diffraction studies, Ward observed that in normal rigor muscle (without NEM) the A-band bows and often assumes an elliptical shape. The degree of bowing changes with the pH of the bathing solution and with sarcomere length. On rasing the pH it was found from equatorial X-ray patterns and micrographs that the A-band lattice swells and bows. Ward argued that as the pH is raised the charge on the filaments increases, and so the electrostatic repulsion increased, and that although there is increased strain on the acto-myosin cross links this was overridden by the increase in electrostatic repulsion, as indicated by the swelling of the lattice. He observed a similar effect with decreasing S, here the explanation for the increased bowing was that as S decreased there was more of the thin filament within the A-band. This increased the electrostatic repulsion and hence the degree of bowing.

It is known from X-ray patterns of normal muscle that the intensities of the actin reflections increase, (particularly the 59 Å and 365 Å reflections) as the muscle goes into rigor. This is taken to be due to the labelling of the myosin heads on the thin filament as the cross links are formed (Squire, 1981). From Ward's experiments one may speculate that

the bowing of the cross-linked A-band causes the actin filaments in the I-band to be pulled mechanically into better register, thus increasing their order. In the case of rigor muscle treated with NEM the charge was found to be greater than in normal rigor, an increase of about 70 % in both the A- and the I-band of both muscle preparations studied (section 3.1.6). The further resulting electrostatic repulsion between the filaments may well increase the bowing of the A-band, and hence increase the strain on the thin filaments in the I-band. Although there is an increase of the charge in the I-band, which will result in a larger electrostatic repulsion between the thin filaments, this might be overridden by the greater force generated from the higher charge in the cross-linked A-band. The increased strain on the thin filaments could increase the ordering of the I-band lattice and result in the increased sampling of the actin layer lines observed by Yagi.

The conclusion of our experiment with NEM is that it seems to be a rather promiscuous reagent, and it is clear that caution should be taken in ascribing the effects of this ligand to a specific interaction with SH groups, in situations where the net electrical charge on molecules or assemblies of molecules may also be important.

4.3 ATP AND PPI TITRATIONS AND CHARGE DECREASE IN MUSCLE

The experiments of Scordilis et al. (1975) and Scordilis (1976, unpublished) used fluorescence labelling to identify myosin as the protein where the charge decrease on addition of ATP (section 4.2) might well take place. Direct Donnan potential measurements with microelectrodes on isolated whole myosin molecules or the constituent parts were made by Bartels et al. (1993), who isolated myosin from rabbit back and leg muscle and manufactured thread-like gels of whole myosin, myosin rod and LMM (See also Cooke et al., 1987). Titrations of ATP, ADP and PPi were performed in these gels and also in the A-bands of glycerinated rabbit muscle. Figure 4.4 shows a summary of the results of the measurements taken in whole myosin gels. The data are taken from Bartels et al. (1993) and plotted here on a semi-log scale with the charge expressed as e/molecule; the line of best fit is fitted to both sets of data points (ATP and PPi) and drawn by eye. It was found that the charge decreased to a minimum value at concentrations of ATP and PPi between 0.1 μM and 1 mM, and that the maximal charge drop occurs at about 100-200 μM. The values of charge for both ATP and PPi were indistinguishable within the experimental error. At concentrations greater than between 1-2.5 mM a subsequent small charge increase is seen . It is interesting to note that the net negative charge is about 115 e in the absence of ATP and about 80 e in its presence. This is an increase of about 44%, which corresponds to the increase seen in whole muscle between the relaxed and rigor states. This effect was observed in the whole myosin gels, myosin rod gels and the A-bands of glyceranated rabbit muscle, but not in the LMM gels. As the S2 portion of myosin is common to both whole myosin and myosin rod, it seems likely that it is at this location that the charge effect occurs, which is in general agreement with the observations

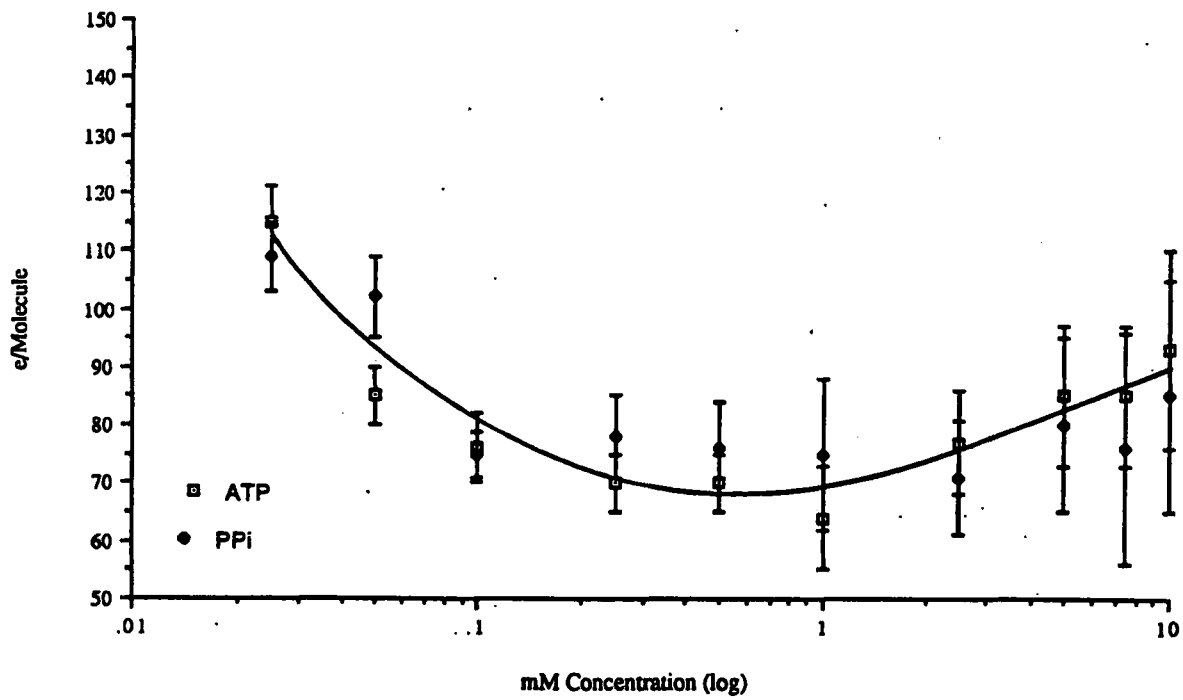

Figure 4.2 The change in fixed negative charge with ATP and PPi concentration for whole myosin gels. The data are taken from Bartels et al (1993) and plotted on a semi-log scale.

of Scordilis (1975). The experiments of Bartels et al. (1993) show that ADP does not initiate the same fall in negative charge, and the authors argued that it appears to be the terminal PPi part of the ATP molecule which caused the decrease, since PPi showed the same effect as the ATP on the electrical charge of the myosin molecule. This effect is probably stoichiometric as there are 240 μM S1 myosin heads per A-band (Bagshaw, 1993) and about the same concentration in the gels, and 100-200 μM ATP or PPi is where the maximal fall in charge occurs. Bartels et al. (1993) suggested that the stoichiometic ATP and PPi saturation effect on the charge indicates a definite ATP initiating site as opposed to ATP-binding or absorption onto a large number of Saroff sites. The obvious initiating site is on the S1 head. However the results from the rod gels indicates that there must also be another initiation site (or sites) on the rod or S2 for the charge reversal and charge amplification. The authors suggest that this may well be the secondary ATP binding site reported by Bowen & Evans (1968) and also Harrington & Himmelfarb (1972). As the initial stoichiometric effect of low levels of ATP and PPi is reversed by much higher concentrations, Bartels et al. (1993) suggested that under these conditions ATP was bound non-specifically on to the myosin filaments. Probably at higher concentrations the ATP and PPi compete for the Saroff sites.

The spacing and intensity data for the equatorial X-ray patterns taken at different concentrations of PPi (section 3.2.2) show remarkably similar but inverse trends when compared to the myosin charges measured in the A-bands of rabbit muscle and in gels (Figure 4.2). Both the d(1,0) spacing data and the $I_{1,1}/I_{1,0}$ intensity data of Figures 3.13 and 3.14 give an inverse of the bell shaped curve of the PPi charge data. However, the curves are not simply identically inverse, Figure 4.3 gives a comparison of all three figures. There will be error in measurement, especially because only two successful experimental runs of the PPi titration were conducted and that some concentrations were not investigated. The I_{144}/I_{220} intensity ratio of the meridional pattern (Figure 3.17) does not show the same degree of similarity, probably due to the paucity of data, but does show some similarity as the maximum value is at micromolar concentration, with a decrease at

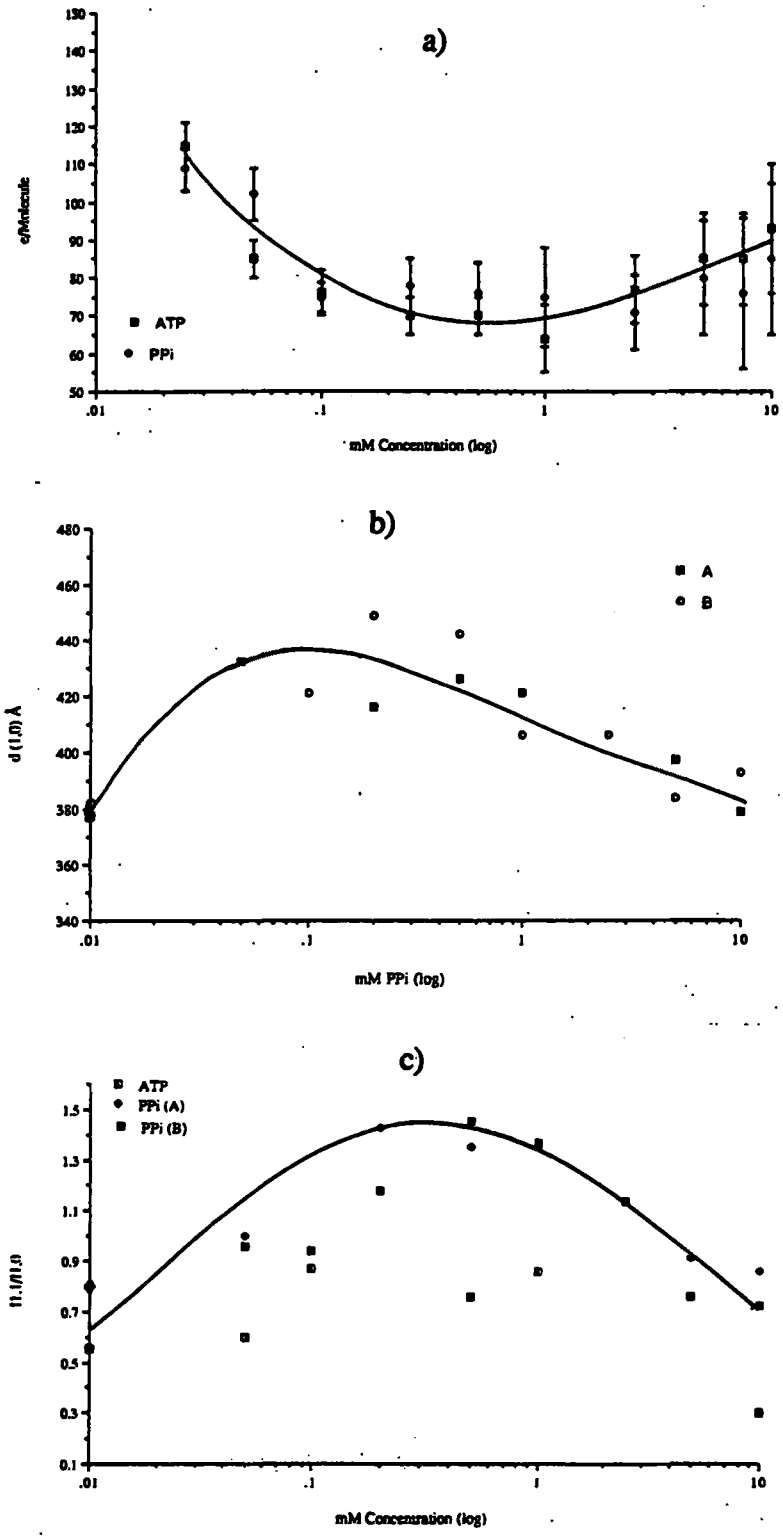

Figure 4.3 a) Figure 4.2 b) Figure 3.13 c) Figure 3.14

higher concentrations. The d (1,0) spacing and the $I_{1,1}/I_{1,0}$ intensity both show the rising phases of their curves and maximum values are similar to the sharp drop of the myosin net negative charge, the maximum values in all three cases being at about 200-300 μM before steadily decreasing. Given that the maximum values of the X-ray data all seem to coincide with myosin charge data at about 200-300 μM PPi and the degree of similarity of their curves, it is proposed that the two phenomenon are connected.Firstly it is important to consider some features of existing models of charge in relation to the behaviour of the muscle lattice.

4.3.1 CHARGE MODELS AND SWELLING OF THE MUSCLE LATTICE

In a recent model of muscle contraction, Elliott & Worthington (1994) postulate that as myosin can exist in two states of differing electrical charge, the discharging of myosin when attached to the thin filament generates a mechanical snap-back and a consequent impulsive mechanical force. This is the power stroke which causes contraction. Figure 4.4 gives a diagrammatic summary of the model. One of the main features of the model is the site at which charging occurs. Since the crystallographic structure of S1 has been resolved (Rayment et al.1993) Elliott & Worthington, following Bartels et al. (1993), suggest that the site of the charging up occurs in the region where the long α helix which extends from the S1 and continues into the S2 region. This is because at the extremities of the neck of S1 there are two myosin light chains which are wrapped in tandem around the α helix. It is well known that these chains are at sites that can be electrostatically modified by such ions as calcium or covalently bonded phosphate. The main points of the model are 1) the rise of sarcoplasmic calcium initiates the cycle 2) When the myosin head is locked in the binding site of the actin filament, the products of hydrolysis are released. At this time the neck region charges up slowly and the myosin tail curves inwards under the influence of the radial potential gradient. In order to satisfy the binding requirements in the limited space, the charged tail will be constrained to curl up in the field. 3) When the tail is fully charged in an actomyosin complex ATP binds to the enzymatic site. When this occurs the myosin tail discharges and snaps back, resulting in the contractile impulse. 4) After the ATP binding and discharge the myosin head is released from the actin-binding site, with ATP in place in the active site of S1, but with the tail of the molecule not yet charged. 5) the cycle repeats.

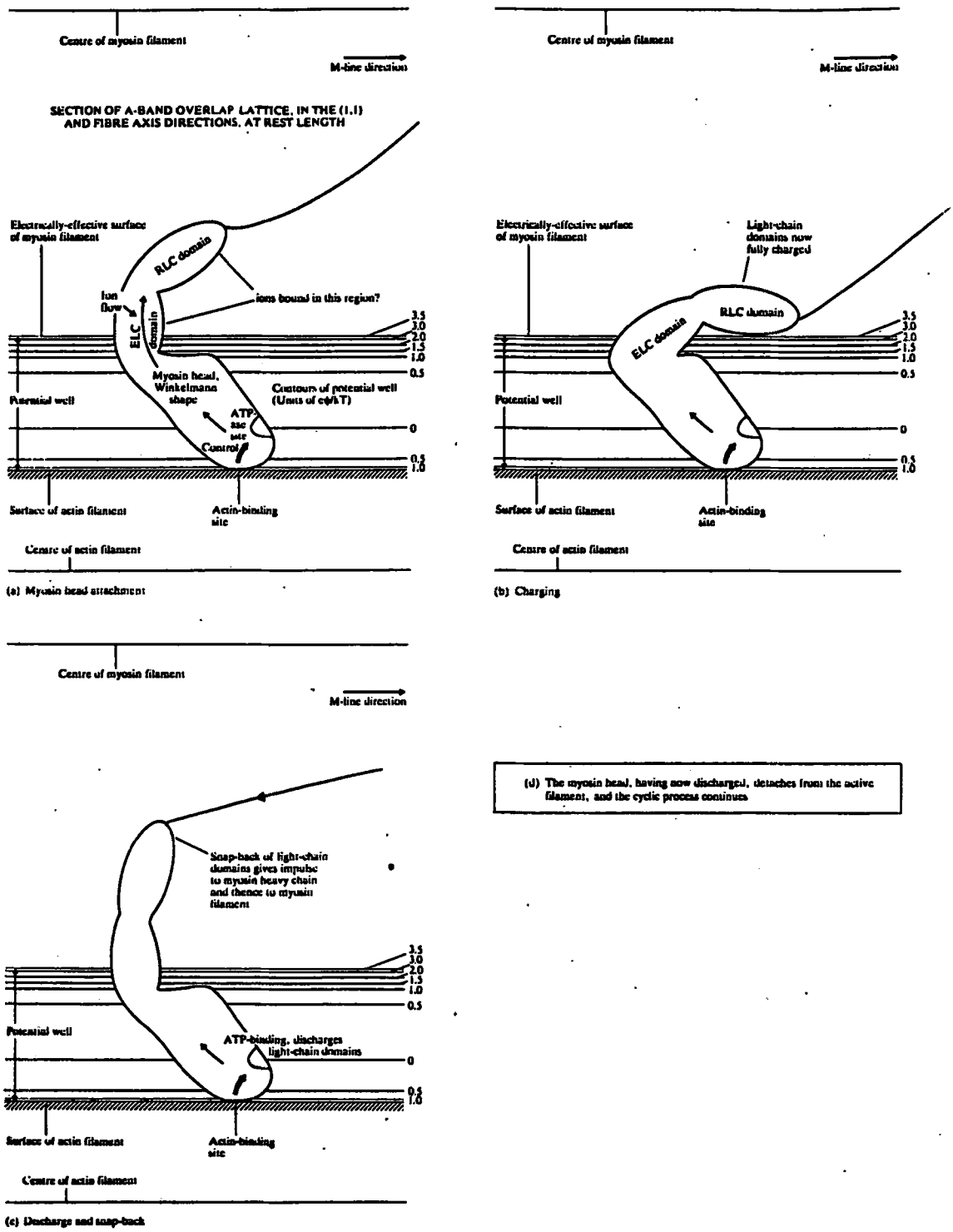

Figure 4.4 A diagramatic representation of stages in the operation of an electrical model of muscle contraction (After Elliott & Worthington, 1994)

If this model proves correct, one may give a tentative explanation for some of the data gathered in this thesis. Although it would seem that the X-ray data and the charge on the myosin molecule are indeed connected, the behaviour of the, $I_{1,1}/I_{1,0}$, I_{144}/I_{220} intensities and the d(1,0) are not fully understood in terms of charge. The explanation given here is a tentative one, put forward as a working hypothesis only.

The two runs of the equatorial experiments were carried out with specimens very close to or above zero overlap, S = 3.4 and 3.7 μm, to investigate myosin - myosin interaction. Although in the presence of PPi the muscle is in rigor, very few actomyosin cross links will form at S = 3.4 μm and none at S = 3.7 μm. As the spacing and intensity data for both runs A and B lie very close together, the specimen where S = 3.4 will be considered to be at zero overlap for the purposes of this discussion. Millman & Nickel (1980) calculated that when overlap occurs electrostatic forces between neighbouring thick and thin filaments were much greater than the electrostatic forces between pairs of thick filaments, because the thick filaments were closer to the thin filaments than to other thick filaments. Therefore at zero overlap the electrostatic forces in the A- band arise only from repulsion between thick filaments. From osmotic shrinking studies of the muscle lattice, Millman & Irving (1988) also suggested that at the high surface charges found in muscle, the lattice spacing was more dependent on the position of the charge than on the amount. It was also suggested that as in ionic solutions the electrostatic forces fall off rapidly with distance, the charge and the charge diameter are effectively those of the outer-most charges on the filament. The authors proposed that the outer-most charge which produces repulsion lies near the centre of the S1 head when not attached to the thin filaments; in the rigor state the effective charge must shift away from the ends of the S1. They supposed this because the net charge on the thick filament increases in rigor, this would imply an increase in repulsive force as the S1 head moves towards the thin filament which does not occur.

The d(1,0) spacing data shown in Figure 3.13 indicate that on addition of PPi the

thick filaments in the A-band move away from each other, thus swelling the lattice. The maximum spacing coincides with the maximal charge drop on the thick filament. The increase in concentration of PPi causes the charge to increase and the thick filaments to move closer together. At the same time the $I_{1,1}/I_{1,0}$ data (Figure 3.14) might indicate that there is a movement of mass from the 1,0 plane towards the 1,1 plane at stoichiometric concentrations of PPi, and that this trend is reversed at higher concentrations. As there are no thin filaments in the A-band the potential well may be deeper than when overlap occurs. However if it is assumed that in the high charge state that the myosin tail is curled up against the backbone in the absence of ATP, one may postulate that on the addition of PPi the molecule discharges, the α helical part snaps back and thus the head moves away from the backbone of the myosin filament. The tail is fully discharged as concentration of PPi reaches 100 - 200 μM. At this stage it may be that the stoichiometric amounts of PPi are bound at the ATP enzymatic site on the S1 head and to the second ATP-binding site on the rod or S2. As the molecule is discharged and the heads project away from the backbone, steric constraints force the filaments apart. At the same time there could be azimuthal movement of the S1 heads from the 1,0 plane towards the 1,1 plane, as they are in a low charge state and not as constrained by the greater electrostatic forces when overlap occurs. At much higher concentrations, the PPi is bound non-specifically on to the myosin filament and starts to compete for the Saroff sites. As the charge rises the myosin tail starts to curve inwards and thus the filaments start move closer together and the heads move from the 1,1 plane back to the 1,0 plane.

In the model given above the filament spacing increase is not due to electrostatic repulsion. This is a consequence of the low charge at such concentrations of PPi, and the low electrostatic repulsion at zero overlap calculated by Millman & Nickel (1980). It would seem possible that at zero overlap, and at stoichiometric concentrations of PPi and presumably ATP, it is the discharging of the myosin molecule which characterises the swelling of the muscle lattice and not the charge radius as suggested by Millman & Irving (1988). However, it must be emphasised that their ideas were drawn from a totally

different set of experimental conditions in which the muscle lattice had been subjected to pressures of up to 1,000 Torr, where the charge radius is clearly important in determining the lattice spacing. Their muscles were also relaxed with 5 mM ATP, a concentration at which there is a higher charge that at stoichiometric amounts.

The site of the charging up of the myosin molecule is critical to the snap-back model of Elliott & Worthington (1994). Given the crystallographic evidence of Rayment et al. (1993) this site would probably be at the neck region of the S1 head with some portion of the S2 myosin rod continuous with the long α helix at the C terminal end of the S1 chain. This is in broad agreement with the observations of Scordilis (1976, unpublished) and Bartels et al. (1993). How this effects the model of Millman & Irving (1988) is not yet clear.

The similar trend of the I_{144}/I_{220} ratio at rest length from the meridional patterns indicate that a similar process is taking place as with the PPi equatorial titrations. Here though the S1 heads are attached to the actin filaments and the charge change is the same as before. This could lower the charge and causes the the myosin tail to discharge, as described above. This in turn then changes the orientation of the heads attached to the thin filaments and would result in a better helical order of those heads which are unattached. It is intresting to note that the I_{144}/I_{220} ratio from the temperature experiments also increased as the charge decreased (Table 3.6), and it would seem that charge plays and important role in the order of the S1 heads. Unfortunately in both cases the equatorials were unable to be measured at the same time due to the size of the beam stop. This information may well have given an insight to any changes d(1,0) and $I_{1,1}/I_{1,0}$ which may accompanying the change in the I_{144}/I_{220}.

4.3.2 MICROMOLAR AMOUNTS OF ATP AND TENSION IN MUSCLE

A search of the literature suggests that micromolar concentrations of ATP generate some interesting effects in tension development in muscle fibres. These possibly give an insight into the interaction of actin and myosin and hence the origin of the contractile force.

It has been reported in the literature that low levels of substrate can generate tension in the absence of calcium. In vitro it has long been known that ATP dissociates actin from myosin in solution. In vivo at micromolar concentrations of ATP the situation is more complex. For example Reuben et al.(1971) reported that with skinned crayfish muscle fibres in the absence of calcium tension was produced, up to 50% of the fibre capacity, with ATP in the concentration range 1-100 μM. The fibres were in the rigor state before the addition of the substrate and the bathing solution was continuously pumped through the experimental chamber. At higher concentrations the tension was reduced, thus giving a bell-shaped curve. The rising shape of this bell shaped curve corresponds in the concentration range to the fall in charge of the myosin molecule as reported by Bartels et al. (1993) (Figure 4.2). Goldman et al. (1982) also reported a similar effect in the absence of calcium. Here micromolar amounts of caged ATP were released into single skinned rabbit psoas fibres in the rigor state. At concentrations below 300 μM it was observed that there was an initial tension rise before relaxation. The tension transient lasted in the order of 50 milliseconds. The authors explain these observations in terms of the reattachment of detached cross-bridges. However, from their model Elliott & Worthington (1994) argued that at low ATP concentrations the myosin discharge, snap-back and tension production occurs before the substrate concentration becomes sufficient for the dissociation of actin and myosin produced by ATP to overwhelm the effect of ATP in producing visible tension.

The above model is also able to explain the large increase in isometric tension observed at low levels of substrate. Ferenczi et al. (1984) reported that at micromolar

concentrations of ATP the contractile force is at its maximum in skinned frog fibres. Figure 4.5 shows the data from Figure 5 of Ferenczi et al. (1984) replotted on a semi-log scale. The y axis is given as a ratio of relative isometric tension. The isometric tension at 5 mM ATP is used as the standard (solid square) and the rigor values are plotted on the y axis. The line of best fit is drawn by eye. From this Figure it may be seen that it is similar to the PPi titration curves (Figures 3.13, 3.14 &3.17) and the myosin charge curve (Figure 4.2) of Bartels et al. (1993) in that the maximum isometric tension occurs at about 20-100 μM ATP with a steady decrease at higher concentrations. Again this would seem to indicate that charge is important in the amount of tension produced during contraction.

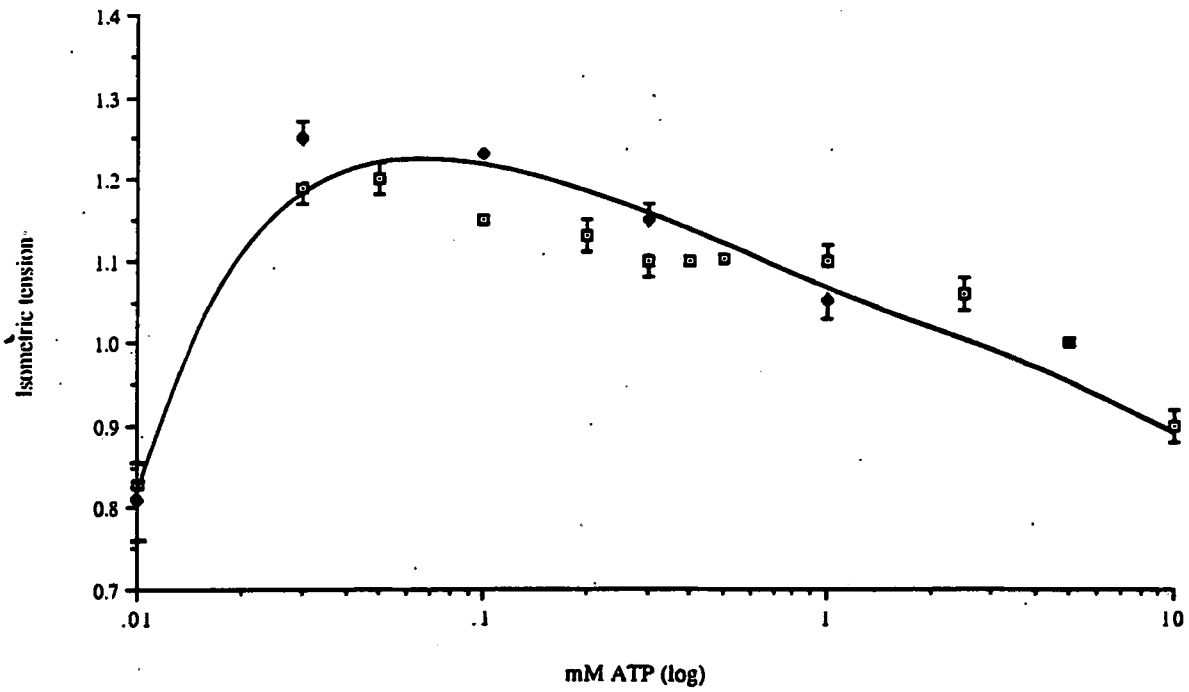

Figure 4.5 The change in relative isometric tension with increasing concentration of ATP in skinned frog muscle. The tension produced at 5 mM ATP is taken as the standard (solid square). The data are taken from Ferenczi et al (1984) and plotted on a semi-log scale

CHAPTER 5

CONCLUSION

5.1 CONCLUSION

It has been shown that concurrent use othe the techniques of microelectrode studies and low-angle X-ray diffraction give a powerful insight into the electrical properties of the polyelectrolyte tissues, muscle, cornea and lens. Using these methods useful information can be gained about the net fixed electrical charges on such proteins, and about changes of charge when such systems are perturbed.

The protein charges have been determined in muscle, cornea and lens under a variety of different experimental conditions. In the case of muscle, from microelectrode experiments it has been shown that in both the relaxed and rigor states the fixed negative charge decreases with increasing temperature. This is interpreted in terms of thermal energy causing the release of bound anions from the charged surfaces of the muscle proteins. This phenomenon is correlated with temperature-induced order-disorder transitions observed from X-ray patterns in the relaxed muscle lattice. In rigor muscle the X-ray observed change in the ordering of the lattice with increasing temperature may be artifactual since beam-time limitations precluded further observations, clearly this experiment needs to be repeated. If there is no increase in the ordering of the rigor muscle lattice with increasing temperature, then one can conclude that the mechanical effects generated by the actomyosin cross links are greater than any effects which arise from ion binding and from the electrical properties of the filaments.

In corneal stroma it has also been shown that the fixed stromal charge decreases with increasing temperature. The amount that the charge decreases is consistent with that

portion of the stromal charge which is believed to be due to chloride ions immobilized on to the stromal matrix. It also gives support to the hypothesis that the fall in swelling pressure at temperatures between 22- 37 ^{0}C, and hence the negative temperature coefficient of the swelling pressure (α'_p), is caused by the release of bound chloride ions. Thus the swelling pressure may be explained in terms of Donnan theory alone. An attempt was made to observe any changes in the corneal equatorial reflections with increasing temperature at the Daresbury laboratory, but the failure of the experimental heating system at the time prevented the experiment from being performed.

In calf lens the microelectrode techniques did not detect the putative isoelectric effect of the aggregation of the cryoprotein γiv-crystallin below T_{cat}. The low concentration of this cryoprotein gives a natural explanation of this observation.

The reagent NEM was found to increase the fixed charge on the muscle lattice, this may be caused by the alkylation of the lysine and histidine residues. NEM induces disordering of the muscle lattice and and we postulate that the excess charge is the agent which gives rise to this disordering.

Micromolar amounts of PPi added to zero-overlap muscle in rigor were found to give maximum d(1,0) spacings and $I_{1,1}/I_{1,0}$ intensity ratios from X-ray equatorial reflections, and maximum I_{144}/I_{220} intensity ratios from meridional reflections in muscle at rest length. These results are interpreted in terms of the fall in charge on the myosin molecule at stoichiometric concentrations of PPi. This is correlated with the observations that such small concentrations ATP can produce tension in rigor muscle in the absence of calcium, and can also produce maximum contractile force in the presence of calcium.

5.2 FUTURE WORK

The X-ray equatorial experiments of muscle with micromolar amounts of ATP clearly need to be repeated. The ATP $I_{1,1}/I_{1,0}$ intensity ratio of Figure 3.14 b) seems to show that the trend is similar to that which occurs with the (unhydrolysed) PPi. One might expect the spacing and intensity results from both to be rather similar, given the identical fall in charge that occurs with both at micromolar concentrations. In order to avoid the effects encountered due to the rapid hydrolysation of the substrate, either caged ATP or continuous flow of the bathing medium techniques should be employed. It is proposed that either chemically skinned whole frog muscle or mechanically skinned frog muscle fibres be used, as many workers (eg, Squire, 1981) report that it is very difficult to induce a fully "relaxed" state indistinguishable from that in live relaxed muscle by the addition of ATP to glycerinated vertebrate skeletal muscle.

It is possible to design an experiment which would test the difference between the models of Elliott & Worthington (1994) and Goldman et al. (1982) as to the behaviour of the cross bridges during tension development in rigor muscle at very low levels of ATP, in the absence of calcium. (section 4.3.2). Small bundles mechanically skinned fibres would be mounted in an experimental cell and attached to a force transducer and piezoelectric length controller .This would then be be placed in an X-ray beam so that the equatorial pattern could be recorded. Rigor solution would first be pumped into the chamber to ensure the fibres were in the rigor state. Micromolar concentrations of caged ATP (and EGTA to chelate the calcium ions) would then be pumped in, and a Xenon flashlamp would be used to release the ATP. The rise in tension and the equatorial patterns would be recorded. It would be necessary to study the spacings and intensities in a time-resolved manner, and measure the tension generated at the same time. The interesting initial tension rise in these experiments would coincide with micromolar levels of free ATP, and the total time scale of

the experiment would be about one second. Given that at most synchrotrons the equatorial X-ray pattern from a few fibres of muscle can be seen in a few milliseconds, an initial time resolution of ten 100ms slots would give useful information.

The attachment/detachment of the actin-myosin cross-links would manifest itself in the $I_{1,1}/I_{1,0}$ intensity ratio in the equatorial diffraction pattern, and probably also in the equatorial spacing. This is because the maximum spacing data with PPi coincides with the maximal charge fall of the myosin molecule (Figure 3.13).

REFERENCES

Adrian, R. H. (1956). *J. Physiol.* **133**, 631- 658

Alexandrowitz, Z. & Katchalsky, A. (1963). *J. Polymer Sci.* **A1**, 3231-3260

Asakura, S., Taniguchi, M. & Oosawa, F. (1963) *J. Mol. Biol.* **7**, 55-69

Bagshaw, C. R. (1993) *Muscle Contraction*, 2 nd Edition, Chapman and Hall, New York

Bartels, E. M., Cooke, P. H., Elliott, G. F & Hughes, R. A. (1993). *Biochim. Biophys. Acta,* **1157**, 63-79

Bartels, E. M. & Elliott, G. F. (1985). *Biophys. J.* **48**, 61-76

Benedek, G. B., Clark, J. I., Serrallach, E. N., Young, C. Y., Mengel, L., Sauke, T., Bagg, A. & Benedek, K.(1979) *Phil. Trans. R. Soc. Lond.* **A293**, 329-340

Berman, E. R. (1991) *Biochemistry of the Eye*, Plenum press, New York

Bernal J. D. & Fankuchen I. (1941) *J. Gen. Physiol.*. **25**, 111-146

Bjork, I. (1970) *Exp. Eye Res.* **9**, 152-157

Bras, W. et al. (1993) *Nuc. Inst. Meth. Phys. Res.* **A326**, 587-591

Brenner, S. L. & Parsegian, V. A. (1976). *Exp. Eye Res.* **22**, 95-99

Brewer, C. F. & Riehm, J. P. (1967) *Analyt. Biochem.* **18**, 248-255

Bowen, W. J. & Evans, T. C. (1968) *Eur. J. Biochem.* **5**, 507-512

Buckley, R. J. (1987) *Clinical Opthalmology*, Ed, Miller, S, I. O. P. Publishing Ltd. Bristol

Clark, J. I. & Benedek, G. B. (1980) *Biochem. Biophys. Res. Commun.* **95**, 287-292

Clark, J. I., Delaye, M., Hammer, P. & Mengel, L. (1982) *Curr. Eye Res.* **1**, 695-704

Collins, E. W. & Edwards, C. (1971). *Am. J. Physiol.*. **221**, 1130-1133

Cooke, P. H., Bartels, E. M., Elliott, G. F. & Hughes, R. A. (1987) *Biophys. J.* **51**, 947-957

Elliott, G. F. & Worthington, C. R. (1963). *J. Ultrastructure Res.* **9**, 166-170

Elliott, G. F., Lowy, J. & Worthington, C. R. (1963). *J. Mol. Biol.* **6**, 295-305

Elliott, G. F. (1968). *J. theor. Biol.* **21**, 71-87

Elliott, G. F. (1973). *J. Mechanochem. Cell Motil.* **2**, 83-89

Elliott, G. F. (1980). *Biophys. J.* **32**, 95-97

Elliott, G. F. & Bartels, E. M. (1982). *Biophys. J.* **38**, 195-199

Elliott, G. F., Goodfellow, H. M. & Woolgar, A. R. (1980) *J. Physiol.* **298**, 453- 470

Elliott, G. F. (1985). OU Teaching Unit, S324 unit 12, Ed Thomas, J. , Open University Press, Milton Keynes, UK.

Elliott, G. F., Bartels, E. M. & Hughes, R. A. (1985). *Electrical double layers in Biology*, Ed. Blank M., Plenum Publishing Corp., New York, pp 277-285

Elliott, G. F. (1992). *Muscle Res. Cell Motility* **13**, 232

Elliott, G. F. & Worthington, C. R. (1994) *Biochim. Biophys. Acta,* (in press)

Farrell, R. A. & Hart, R. (1969). *Bull. Math. Biophys.* **31**, 727-759

Ferenczi, M. A., Goldman, Y. E. & Simmons, R. M. (1984) *J. Physiol.* **350**, 519-543

Franks, A., (1955). *Proc. Phys. Soc. (London).* **B68**, 1054

Fullwood, N. (1992). Ph.D. Thesis, Open University, Milton Keynes

Goldman, Y. E., Hibberd, M. G. Mc Cray, J. A. & Trentham, D, R. (1982) *Nature*, **300**, 701-705

Goodfellow, J. M. (1975). Ph.D. Thesis, Open University, Milton Keynes

Guggenheim J. A. & Hodson S. A. (1994 a). *J. Physiol.* **475P**, P91

Guggenheim J. A. & Hodson S. A. (1994 b). *Invest. Ophth. and Vis. Sci.* **35**, No 4, P1992

Hammer, P. & Benedek, G. B. (1982/1983) *Current Eye Res.* **2**, No.12, 809-814

Hanson, J. & Huxley, H. E. (1955). *Stymp. Lond. Soc. Exp. Biol..* **9**, 228

Hara, T. & Maurice, D. M. (1972) *Exp. Eye Res.*, **14**, 40-48

Harrington, W. F. & Himmelfarb, S. (1972) *Biochemistry*, **11**, 2945-2952

Harrington, W. F. (1979) *The Proteins iv*, third edition, Eds, Neurath, H. & Hill, R. L., Academic Press, New York.

Haselgrove, J. C. (1975). *J. Mol. Biol.* **92**, 113-143

Haselgrove, J. C. & Rodger, C. D. (1980) *J. Muscle Res. Cell Motility* **1**, 371-390

Hodson, S. A. & Meenan, A. (1969). *Separatum Experimentia* **25**, 1305

Hodson, S. A. (1971). *J. theor. Biol.* **33**, 419-427

Hodson, S. A., Kaila, D., Hammond, S, Rebello, G.,. & Al-Omari, Y. (1992). *J. Physiol..* **450**, 89-103

Huxley, A. F. & Niedergerke, R. (1954) *Nature*, **173**,971-973

Huxley, H. E. & Hanson, J. (1954) *Nature*, **173**,973-976

Huxley, H. E. & Brown, W. (1967). *J. Mol. Biol.* **30**, 383-434

Huxley, H. E. (1968). *J. Mol. Biol.* **37**, 507-520

Knight, P. & Trinick, J. (1987). *Fibrous Protein Structure*, Eds., Squire, J. M. and Vibert, P. J., Academic press, London, pp 247-281

Kwok, L. S. & Klyce, S. D. (1990). *Biophys. J.* **57**, 657-662

Ling, G. & Gerard, R. W. (1949). *J. Cell Comp. Physiol.*. **34**, 382

Loeb, G. I. & Saroff, H. A. (1964). *Biochemistry*. **3**, 1819-1826

Lowy, J. Popp, D. & Stewart, D. D. (1991) *Biophys. J.* **60**, 812-824

Mahler, H. R. & Cordes, E. H. (1971) *Biological Chemisty*, 2 nd edition, Harper and Row, New York

Meek, K. (1994) Personal comunication.

Millman, B. M. & Nickel, B. G. (1980). *Biolphys. J.* **32**, 49-63

Millman, B. M. & Irving, T. C. (1988). *Biophys. J.* **54**, 437-447

Myers, D. B., Highton, T. C. & Rayns, D. G. (1973). *J. Ultrastruct. Res.* **42**, 87-92

Nayler, W. G. & Merrellees, N. C. R. (1964). *J. Cell Biol.* **22**, 533-550

Naylor, G. R. S (1975). PhD. Thesis, Open University, Milton Keynes

Naylor, G. R. S. (1978). *Pfluegers Arch. Eur. J. Physiol.* **378**, 107-110

Naylor, G. R. S. (1982) *Biophys. J.* **38**, 201-204

Naylor, G. R. S, Bartels, E. M., Bridgman, T. D. & Elliott, G. F. (1985). *Biophys. J.* **48**, 47-59

Offer, G. (1987). *Fibrous Protein Structure*, Eds., Squire, J. M. and Vibert, P. J., Academic press, London, pp 307-356

Okada, Y. & Inonye, A. (1975). *Experimenta.* , **31**, 545

Oosawa, F. (1971) *Polyelectrolytes*, Marcel Dekker, Inc., New York

Papaconstantinou, J. (1965). *Biochimi. Biophys. Acta,* **107**, 81-90

Pemrick, S. M. & Edwards, C. (1974). *J. Gen. Physiol..* **64**, 551-567

Perrin, D. D. & Sayce, I, G. (1967). *Talanta.* **14**, 833-842

Rayment, I. et. al. (1993) *Science*, **261**, 50-58

Rome, E. (1972). *J. Mol. Biol..* **65**, 331-345

Reuben, J. P., Brandt, P. W., Berman, M. & Grundfest, H. (1971) *J. Gen. Physiol..* **57**, 385-407

Saroff, H. A (1973). *Biopolymers.* **12**, 559-610

Schanne, O. F., Lavallee, M., Laprade, R. & Gagne, S. (1968). *Proc. I. E. E. E.*, **56**, 1072-1082

Scordilis, S. P., Tedeshi, H. & Edwards, C. (1975). *Proc. Natl. Acad. Sci. USA.* **72**, 1325-1329

Scordilis, S. P.(1976). Unpublished manuscript communicated to G. F. Elliott

Scott, J. E. (1991). *Biochem. Soc. Trans.* **19**, 877-881

Sharp, D. W. A. (1988) *Dictionary of Chemistry*, Fifth Edition, Longman Group Ltd.,

Siezen, R. J., Fisch, M. R., Slingsby, C.& Benedek, G. B. (1985). *Proc. Natl. Acad. Sci. USA.*, **82**, 1701-1705

Slayter H. S. & Lowey S. (1967) *Proc. Natl. Acad. Sci. USA.* **58**, 1611-1618

Slingsby, C. & Croft, L. R. (1973). *Exp. Eye Res.* **17**, 369-376

Slingsby, C. & Miller, L. R. (1983). *Exp. Eye Res.* **37**, 517-530

Squire, J. M., Luther, P. K. & Trinick, J. (1987). *Fibrous Protein Structure*, Eds., Squire, J. M. and Vibert, P. J., Academic press, London, pp 423-448

Squire, J. M. (1981) *The Structural Basis of Muscle Contraction*, Plenum Publishing Corp., New York

Szent-Gyorgyi, A. (1951). *Chemistry of Muscular Contraction.*, Academic Press, New York:

Verwey E. J. W. & Overbeek J. Th. G. (1948) *Theory of the stability of Lyophobic Colloids.* Elsevier Publishing Co., New York

Wakabayashi, T. et. al (1988). *Ad. in Exp. Med. and Biol.* **226**, 39-46

Ward, R. J. (1987) PhD. Thesis, Open University, Milton Keynes

Weiss, M. R., Lazzara, R..& Hoffman, B. F. (1967). *Nature* , **215**, 1305

White, D. C. S. & Thorson, J. (1972) *J. Gen. Physiol.*. **60**, 307-3336

Wray, J. S. (1987). *J. Muscle Res. Cell Motility* **8**, 62

Yagi, N. (1992). *J. Muscle Res. Cell Motility* **13**, 457-463

APPENDIX 1

STATISTICAL METHODS

In this example to try and establish the cross over point (x) between the A- and I-band distributions the data are taken from rigor muscle at 10 ^{0}C.

I-band distribution, mean = 5·695 , sd = 1·193

A-band distribution, mean = 9·596 , sd = 0·915

The cross-over point occurs where the two distribution curves intersect, ie where the right hand side of the two equations y = f (x) are simultaneously equal. For the normal distribution, f(x) is the mathematical expression describing the normal shape and is called the "probability density function". For the normal distribution, this is given by

$$y = f(x) = \frac{1}{\sigma \cdot \sqrt{2\pi}} \cdot e^{-\frac{1}{2}\left(\frac{x-\mu}{\sigma}\right)^2}$$

Where x = cross-over
μ = mean
σ = sd

$$= \frac{1}{\sigma \cdot \sqrt{2\pi}} \cdot e^{-\frac{1}{2}Z^2} \quad \text{where} \quad Z = \frac{x-\mu}{\sigma}$$

Equating $f(x_s) = f(x_A)$

$$\frac{1}{1.193\sqrt{2\pi}} \cdot e^{-\frac{1}{2}\left(\frac{x_B - 5.695}{1.193}\right)^2} = \frac{1}{0.915\sqrt{2\pi}} \cdot e^{-\frac{1}{2}\left(\frac{x_A - 9.596}{0.915}\right)^2}$$

$$\frac{0.915}{1.193} = \frac{e^{-\frac{1}{2}(Z_A)^2}}{e^{-\frac{1}{2}(Z_I)^2}} = e^{\left(-\frac{1}{2}Z_A^2\right)+\left(-\frac{1}{2}Z_I^2\right)} = e^{-\frac{1}{2}\left(Z_A^2 - Z_I^2\right)}$$

$$\ln 0.76697 = -\frac{1}{2}\left(Z_A^2 - Z_I^2\right) = -0.26530$$

$$Z_A^2 - Z_I^2 = 0.53061$$

Difference of two squares factorisation

$$(Z_A + Z_I)(Z_A - Z_I) = 0.53061$$

$$\left(\frac{x_A - 9.596}{0.915} + \frac{x_I - 5.695}{1.193}\right)\left(\frac{x_A - 9.596}{0.915} - \frac{x_I - 5.695}{1.193}\right) = 0.53061$$

But $x_A = x_I$ at Cross-over $= x$

$$\left(\frac{1.193\,(x-9.596)+0.915\,(x-5.695)}{1.193\times 0.915}\right)\left(\frac{1.193\,(x-9.596)-0.915\,(x-5.695)}{1.193\times 0.915}\right)=0.53061$$

$$\frac{1.193x-11.448+0.915x-5.210}{1.092}\times\frac{1.193x-11.448-0.915x+5.210}{1.092}=0.53061$$

$$\frac{2.108x-16.658}{1.092}\times\frac{0.278x-6.238}{1.092}=0.53061$$

$$(2.108x-16.658)(0.278x-6.238)=0.53061\cdot(1.092)^2$$

$$0.586x^2-17.781x+103.912=0.6327$$

$$0.586x^2-17.781x+103.279=0$$

Solve by formula $x=\dfrac{-b\pm\sqrt{b^2-4ac}}{2a}$

$$x=\frac{17.781\pm\sqrt{316.153-242.085}}{1.172}$$

$$=\frac{17.781\pm 8.606}{1.172}=\cancel{22.51}\ \text{(Inadmissable)}\ \text{or}\ \underline{\underline{7.82}}$$

ie Cross-over point between the two distributions occurs at $-7.82\,mV$

To find the probability that each distribution lies above or below the cross-over value.

I distribution

$$Z = \frac{7.82 - 5.695}{1.193} = 1.78$$

$$P_r(x_I > 7.82) = 1 - P_r(Z < 1.78)$$

$$= 1 - 0.9625 = 0.0375 \quad \text{ie } \underline{3.75\%}$$

A distribution

$$Z = \frac{7.82 - 9.596}{0.915} = 1.94$$

$$P_r(x_A < 7.82) = 1 - P_r(Z < 1.94)$$

$$= 1 - 0.9738 = 0.0262 \quad \text{ie } \underline{2.62\%}$$

APPENDIX 2

450P Journal of Physiology (1993). 459. 450P

A physical mechanism for the anomalous thermal dependence of swelling of bovine cornea, with an application to rabbit muscle X-ray diffraction patterns

G.F. Elliott and J. Regini

Open University Oxford Research Unit, Boars Hill, Oxford OX1 5HR

Kwok & Klyce (1990), extending the analysis of Hodson (1971) and Elliott *et al.* (1980), have shown that the anomalous negative temperature coefficient for corneal swelling, measured by Hara & Maurice (1972), can be explained on Donnan theory so long as the corneal stromal fixed electrical charge also has a negative temperature coefficient.

In cornea, a substantial part of the fixed net negative charge on the proteins arises from immobilized anions (probably largely chloride ions) trapped in potential wells or otherwise fixed to the protein surfaces (Elliott, 1980; Elliott *et al.* 1980). Hodson *et al.* (1992) have confirmed that transient chloride binding is a large contributory factor to corneal stromal swelling in the ox in the physiological regime, showing that the model described here is reasonable. An increase in temperature will decrease the amount of anionic immobilization, by the operation of Boltzmann's theorem. Thus there will be a decrease in the fixed charge, giving a negative temperature coefficient to the swelling pressure. This provides a mechanism for Hara & Maurice's (1972) observations, which cannot be taken as a reason to doubt the dominance of the Donnan swelling pressure, as Hara & Maurice supposed.

In muscle, another polyelectrolyte system, order–disorder effects are seen in the myosin layer-line X-ray diffraction data (Wray, 1987; Lowy *et al.* 1992) that can also be understood if the fixed electric charge decreases as the temperature increases. The mechanism may well be the same in both cases, supposing that the higher fixed charge has a disordering effect upon the muscle X-ray pattern, as postulated by Elliott (1992).

To test this mechanism in the muscle case we measured the A-band Donnan potential (which depends on the A-band fixed charge, Bartels & Elliott, 1985) as a function of temperature. The A-band potential falls dramatically as the temperature is increased in the critical range in rabbit psoas, both in rigor and relaxed muscle. The effect maps on the X-ray data in the same muscle (Lowy *et al.* 1992). In corneal stroma the Donnan potential falls linearly in the temperature range 15–35 °C.

REFERENCES

Bartels, E.M. & Elliott, G.F. (1985). *Biophys. J.* **48**, 61–76.
Elliott, G.F. (1980). *Biophys. J.* **32**, 95–97.
Elliott, G.F. (1992). *J. Muscle Cell Motil.* **13**, 232.
Elliott, G.F., Goodfellow, J.M. & Woolgar, A.E. (1980). *J. Physiol.* **298**, 453–470.
Hara, T. & Maurice, D.M. (1972). *Exp. Eye Res.* **14**, 40–48.
Hodson, S. (1971). *J. Theoret. Biol.* **33**, 419–427.
Hodson, S., Kalia, D., Hammond, S., Rebello, G. & Al-Omari, Y. (1992). *J. Physiol.* **450**. 89–103.
Kwok, S. & Klyce, S.D. (1990). *Biophys. J.* **57**, 657–662.
Lowy, J., Popp, D. & Stewart, A.A. (1991). *Biophys. J.* **60**, 812–824.
Wray, J.S. (1987). *J. Muscle Cell Motil.* **8**, 62.

J. Physiol. (1994), **475. P, 78**

Order–disorder phenomena induced by *N*-ethyl maleimide in skinned frog sartorius muscle

J. Regini and G.F. Elliott

Open University Oxford Research Unit, Oxford OX1 5HR

Yagi (1992) described the effect of *N*-ethyl maleimide (NEM) on the X-ray observed structure of chemically skinned frog skeletal muscles. Yagi's hypothesis is that this reagent is specific for the reactive SH groups of the myosin head (S1). However NEM will also interact with lysine and histidine residues (Mahler & Cordes, 1971, Table 7·4; Brewer & Riehm, 1967). Such reactions (alkylations) will change the net (negative) electrical charge on the protein, because they affect the pKs of these positively charged groups. These changes may affect the order–disorder state of the muscle fibre by charge interactions (Elliott, 1992; Elliott & Regini, 1993) rather than by the effect that Yagi postulates.

We therefore measured the net electrical charge in the A- and I-bands of skinned frog sartorius muscles at room temperature, 20 °C, following as closely as possible the procedures used by Yagi (1992) and using the micro-electrode technique developed by Bartels & Elliott (1985). The results of our experiments are shown in Table 1. In the relaxed saponin-skinned frog sartorius muscle, the A-band and I-band charges are increased about twofold (by 82 %) by 1 mM NEM (as used by Yagi). We also observe a 40 % increase with NEM in the charge in the A-band in Yagi's rigor solutions.

Table 1. The A- and I- band Donnan potentials (identical in relaxed muscle) measured in Yagi's relaxing solutions, at pH 7·0 with and without 1 mM NEM, and the calculated fixed-charge concentrations for proteins (standard deviations shown, $P < 0{\cdot}001$, *t* test)

Relax	$E = -2{\cdot}0 \pm 0{\cdot}6$ mV ($n = 319$)	$[Pr^-] = 34 \pm 9$ mM
Relax + NEM	$E = -3{\cdot}7 \pm 0{\cdot}7$ mV ($n = 273$)	$[Pr^-] = 62 \pm 11$ mM

The order–disorder effects observed by Yagi, notably the disappearance of the myosin layer lines in relaxed muscle treated with NEM, may result from the disordering effect of the extra charge (Elliott, 1992). Regini & Elliott (1993) reported that the net charge could be reduced by increasing the temperature; this increases the visibility of these layer lines. NEM seems to be a rather promiscuous reagent, and one should use caution in ascribing the effects of this ligand to a specific interaction with SH groups in situations where the net electrical charge on molecules or assemblies of molecules may also be important.

REFERENCES

Bartels, E.M. & Elliott, G.F. (1985). *Biophys. J.* **48**, 61–76.
Brewer, C.F. & Riehm, J.P. (1967). *Analyt. Biochem.* **18**, 248–255.
Elliott, G.F. (1992). *J. Muscle Cell Motil.* **13**, 232.
Elliott, G.F. & Regini, J.W. (1993). *J. Physiol.* **459**, 450*P*.
Mahler, H.R. & Cordes, E.H. (1971). *Biological Chemistry*, 2nd edition. Harper and Row, New York.
Regini, J.W. & Elliott, G.F. (1993). *J. Muscle Cell Motil.* **14**, 260.
Yagi, N. (1992). *J. Muscle Cell Motil.* **13**, 457–463.

Biophys. J. (1993), **64**, 2, A270

W-Pos118

CHLORIDE BINDING AND DONNAN SWELLING

((*Gerald Elliott **Stuart Hodson and *Justyn Regini))
*The Open University, ORU, Oxford, OX1 5HR and **Vision Sciences, UWCC, Cardiff, CF1 3XF, UK.

In corneal stroma, the cation exchange capacity of the connective tissue creates a Donnan-osmotic swelling pressure and a Donnan electrical potential. These generate passive swelling. The exchange capacity has two contributions: (1) the charged carboxylic and sulfonic acid groups of glycosaminoglycans and (2) a charge resulting from the transient binding of free chloride ions to a ligand. Chloride binding shows first order kinetics and provides most of the stromal cation exchange capacity under physiological conditions. Chloride binding has the consequence of stabilising Donnan swelling on exposure of the cornea to solutions of varying tonicity, and it explains the well documented negative temperature coefficient of stromal swelling. It is suggested that a similar phenomenon explains the temperature-dependent disappearance of the myosin layer lines in the X-ray diffraction pattern of relaxed rabbit muscle, and may also be relevant to cold-cataract in eye lens.